REPORT DOCUMENTATION PAGE

Form Approved
OMB No. 0704-0188

1. REPORT DATE *(DD-MM-YYYY)*	**2. REPORT TYPE**	**3. DATES COVERED** *(From - To)*
29-09-2010	Final Technical	01-02-2007 – 31-08-2010

4. TITLE AND SUBTITLE

(U) (YIP) Experimental Study of the Oxidation, Ignition, and Soot Formation Characteristics of Jet Fuel

5a. CONTRACT NUMBER

5b. GRANT NUMBER
FA9550-07-1-0114

5c. PROGRAM ELEMENT NUMBER
61102F

6. AUTHOR(S)

Matthew Oehlschlaeger

5d. PROJECT NUMBER
4113

5e. TASK NUMBER
YX

5f. WORK UNIT NUMBER

7. PERFORMING ORGANIZATION NAME(S) AND ADDRESS(ES)

Rensselaer Polytechnic Institute
Mechancial, Aerospace and Nuclear Engineering Dept
Troy NY 12180-3590

8. PERFORMING ORGANIZATION REPORT NUMBER

9. SPONSORING / MONITORING AGENCY NAME(S) AND ADDRESS(ES)

Air Force Office of Scientific Research
875 North Randolph Street
Suite 325, Room 3112
Arlington VA 22203-1768

10. SPONSOR/MONITOR'S ACRONYM(S)

11. SPONSOR/MONITOR'S REPORT NUMBER(S)

12. DISTRIBUTION / AVAILABILITY STATEMENT

Approved for public release. Distribution is unlimited.

13. SUPPLEMENTARY NOTES

14. ABSTRACT

The objective of the present research program was to develop a database of kinetic targets, in the form of ignition delay times, for jet fuel representative hydrocarbons, jet fuels, and jet fuel surrogate mixtures, with a focus on gas turbine main combustor conditions (i.e., elevated pressures with air as the oxidizer). Shock tube autoignition studies for 16 hydrocarbons provided quantitative targets for the development of kinetic oxidation models and information regarding the structure-reactivity dependencies for fuel components. Measurements for two jet fuel samples provided real fuel reactivity for a large range of temperatures of interest to gas turbines (650-1200 K at 20 atm) and show that the JP-8 additive package has no discernible influence on fuel reactivity. Studies of two three- and a four-component surrogate mixtures designed to mimic jet fuel reactivity through matching the derived cetane number (DCN) exhibit reactivity very close to that of the jet fuel samples, indicating that there is potential in using DCN to formulate surrogates.

15. SUBJECT TERMS

Ignition, oxidation, shock tube, jet fuel, Jet A, JP-8, surrogate, n-alkane, iso-alkane, cyclo-alkane, aromatic

16. SECURITY CLASSIFICATION OF:			**17. LIMITATION OF ABSTRACT**	**18. NUMBER OF PAGES**	**19a. NAME OF RESPONSIBLE PERSON**
a. REPORT	**b. ABSTRACT**	**c. THIS PAGE**			Julian Tishkoff
Unclassified	Unclassified	Unclassified	UL	61	**19b. TELEPHONE NUMBER** *(include area code)* 703-696-8478

Experimental Study of the Oxidation, Ignition, and Soot Formation Characteristics of Jet Fuel

Prepared Under
Grant # FA9550-07-1-0114

Final report submitted by:
Matthew Oehlschlaeger, Ph.D. (PI)
Rensselaer Polytechnic Institute
Mechanical, Aerospace, and Nuclear Engineering Department
110 8th St.
Troy, NY 12180

Submitted to:
Dr. Julian Tishkoff
Air Force Office of Scientific Research
875 N. Randolph St.
Suite 325, Rm 3112
Arlington, VA 22203-1768

For the period:
February 1, 2007 – August 31, 2010

Contents

1. Executive Summary

The autoignition of hydrocarbon compounds relevant to jet fuels and alternatives (Fischer-Tropsch, oil-sands, coal-to-liquid, hydrotreated renewable jet fuels), two benchmark jet fuel samples, and two jet fuel surrogate mixtures were studied in a newly constructed high-pressure heated shock tube at Rensselaer Polytechnic Institute. Measurements were made at conditions relevant to combustion in gas turbine combustors: temperatures of 650-1400 K and pressures of 7-60 atm for fuel/air mixtures with equivalence ratios of 0.25-1.5. The ignition delay time measurements provide: 1) data for real jet fuels that can be useful for the design/development of combustors, 2) kinetic targets for the development and assessment of oxidation models for compounds for which data in the literature is sparsely available, 3) an assessment of the influence of organic structure on reactivity, and 4) data needed for the development and assessment of surrogate mixtures for jet fuels and their detailed kinetic models.

Measurements for neat hydrocarbon components were made for n-heptane, n-decane, n-dodecane, n-tetradecane, iso-octane, iso-cetane, cyclopentane, cyclohexane, methylcyclohexane, ethylcyclohexane, decalin, toluene, o-, m-, and p-xylene, ethylbenzene, and α-methylnaphthalene. These measurements quantitatively illustrate several interesting structure-reactivity relationships including: 1) for large n-alkanes, an increase in chain length has little influence on high- to moderate-temperature reactivity at elevated pressures; 2) cyclohexane is more reactive than cyclopentane due to the energetic requirements for opening of the strained C_5 cyclopentane ring; 3) an increase in side chain length causes an increase in reactivity for both substituted aromatics and cyclohexanes; and 4) adjacent (ortho) substitutions in aromatics cause increased reactivity due to the potential for side-chain interactions. Additionally, measurements for iso-octane with air and O_2/Ar bath gases demonstrate the importance of diluents on autoignition phenomena in shock tubes.

Measurements for jet fuels and jet fuel surrogate mixtures illustrate that simple surrogates (three and four components) chosen such that they match the hydrogen-carbon ratio (H/C), derived cetane number, and aromatic fraction can be used to mimic jet fuel reactivity for a large range of temperatures (650-1200 K) at elevated pressures. Finally, measurements for jet fuel samples illustrate that the addition of the JP-8 additive package has no discernible influence on fuel reactivity.

1.1 Objectives

- Develop a heated high-pressure shock tube facility for the study of low-boiling point fuels.
- Characterize the autoignition of neat hydrocarbon components found in and of relevance to jet fuels at gas turbine relevant conditions (elevated pressures with air as the oxidizer) for the assessment, development, and validation of kinetic models and to provide insight into the relative influence organic structure has on hydrocarbon reactivity.
- Characterize the autoignition of benchmark jet fuels at gas turbine relevant conditions.
- Develop and evaluate jet fuel surrogate mixtures with reactivity mimicking that of specific jet fuels.

1.2 Introduction

Future advances in the development of combustion-based aero-engines will rely on the ability of engineers to predict performance quantitatively using detailed computational simulations. One aspect of importance in these simulations is the description of the chemical conversion of fuel and oxidizer to products. These simulations generally characterize chemical reactions using detailed models containing the appropriate elementary reactions and thermochemical parameters. Because the combustion of jet fuels in aero-engines is a complex process that involves accurate modeling of the coupled chemical and transport processes, kinetic models typically are validated using data from controlled experiments where transport processes are not significantly sensitive or experiments in which the flow field is well characterized. Experiments utilizing shock tubes, flow reactors, rapid compression machines, and flames traditionally have been performed to develop and validate these kinetic models. In this project, the investigation of the oxidation and autoignition of jet fuels, surrogates, and components at engine-relevant conditions was undertaken using the shock tube technique. The shock tube technique provides a well-defined nearly uniform temperature and pressure environment at conditions of interest to aero-propulsion devices, and experimental observables generally are isolated from sensitivity to transport phenomena.

Commercial and military jet fuels are typically mixtures of hundreds to thousands of distinct hydrocarbons and currently are too difficult to model as a whole. As such, various researchers have proposed surrogates, which are mixtures of a small number of hydrocarbon molecules that are designed to mimic the physical and/or chemical properties of the real fuel; however, for even the relatively simple combustion of a single hydrocarbon component, models require the inclusion of hundreds of species and thousands of reactions. The surrogate mixtures are proposed to reduce the chemical complexity of the distillate mixture to just a few major molecules representative of those found within the real fuel. The kinetics of the surrogate components must be well understood to provide accurate modeling of the surrogate oxidation and ignition, which may be useful, if the surrogate is formulated properly, in modeling the performance of a combustor operating on the compositionally complex jet fuel.

Given the importance of combustion chemistry and transport in the modeling of combustion systems, there are challenges associated in modeling both phenomena. Due to the complexities of modeling the highly turbulent multi-phase reacting flows that occur in combustors, it is important to develop experiments that separate transport phenomena from chemical reaction, in order to provide data that can be interpreted reasonably. Experimentally measured ignition delay times are one important data set used to validate fuel combustion models, generally with minimal transport interference. Since the correct prediction of the time required for a fuel/oxidizer mixture to autoignite is critical in the design of combustors, a model must be able to predict ignition delay reasonably (up to interpretation and depending on application).

1.3 Current Study

Kerosene-based jet fuels contain a variety of compounds whose carbon makeup typically spans between eight and sixteen carbon atoms. The current study focuses on compounds that are found in or are representative of those found in kerosene-based jet fuels, which are comprised mostly of n-alkanes, iso-alkanes, cycloalkanes, and aromatics, as shown in Figure 1.1. The current study provides ignition delay time validation targets and kinetic insight for selected larger hydrocarbon fuels, as well as simple surrogate mixtures designed to mimic the global reactivity of specific jet fuels. See Figure 1.2 and Tables 1.1 and 1.2 for details of the hydrocarbon components, surrogate mixtures, and jet fuels studied. These data are needed for the development of kinetic models and surrogate representations of jet fuel. Additionally, little to no kinetic data were available in the literature for many of the selected compounds prior to this study.

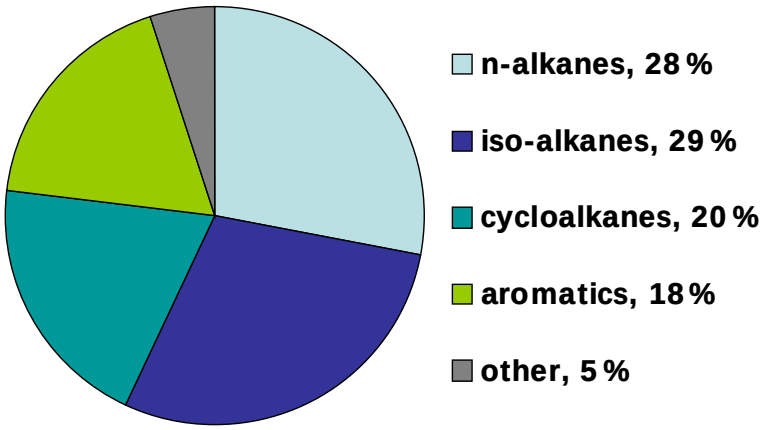

Figure 1.1 Typical Jet A or JP-8 compositional distribution by liquid volume [1-7].

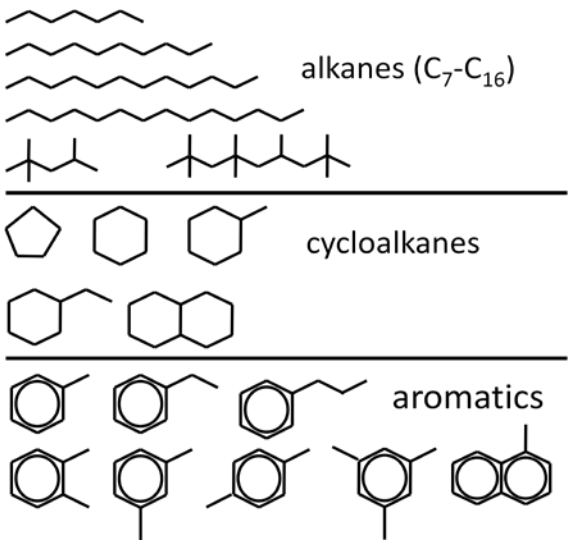

Figure 1.2 Hydrocarbon compounds studied as part of this project.

Table 1.1 Surrogate mixtures studied as part of this project with some relevant properties.

Princeton-MURI surrogate 1 [8] Molar: 42.7% n-decane, 33% iso-octane, 24.3% toluene Liquid volume: 50.8% n-decane, 33.3% iso-octane, 15.8% toluene	H/C = 2.01 MW =121 kg/kmol Aromatic content = 15.8% by liquid vol Derived cetane number (DNC) = 47.1 Threshold soot index (TSI) = 14.1 Liquid density (kg/m^3) = 750
RPI surrogate 1 Molar: 25.8% n-tetradecane, 16.8% iso-cetane, 30% methylcyclohexane, 27.4% n-propylbenzene Liquid volume: 35% n-tetradecane, 25% iso-cetane, 20% methylcyclohexane, 20% n-propylbenzene	H/C = 1.87 MW =151 kg/kmol Aromatic content = 20% by liquid vol Derived cetane number (DNC) = 42.8 Threshold soot index (TSI) = 16.7 Liquid density (kg/m^3) = 792

Table 1.2 Literature average JP-8 and the jet fuels studied as part of this project with some relevant properties.

Literature average JP-8 [1-7]	H/C = 1.84-2.07, avg = 1.9 MW =~153 kg/kmol Aromatic content = ~20% by liquid vol Derived cetane number (DNC) = 32-57, avg = 44 Threshold soot index (TSI) = 16-26, avg = 18 Liquid density (kg/m^3) = ~804
POSF 4658: average Jet A, blended from several Jet A samples by Dr. J.T. Edwards at AFRL [1-8]	H/C = 1.957 MW =142 kg/kmol Aromatic content = 18.4% by liquid vol Derived cetane number (DNC) = 47.1 Threshold soot index (TSI) = 21.4 Liquid density (kg/m^3) = 799
POSF 4658 with the JP-8 additive package, provided by Dr. J.T. Edwards at AFRL	Macroscopic properties are the same as above for POSF 4658

2. Experimental Method

Ignition delay times were measured in a heated high-pressure shock tube constructed at Rensselaer Polytechnic Institute (RPI) in 2007, the first year of this AFOSR project. The stainless steel shock tube has a 5.7 cm inner diameter with a 1.1 cm wall thickness and consists of a 4.11 m long driven section and 2.59 m driver section. Pressures up to 200 atm can be achieved safely behind the reflected shock wave. For the studies carried out here reflected shock pressures were varied between approximately 7 and 60 atm. See Figure 2.1 for a photograph of the shock tube facility.

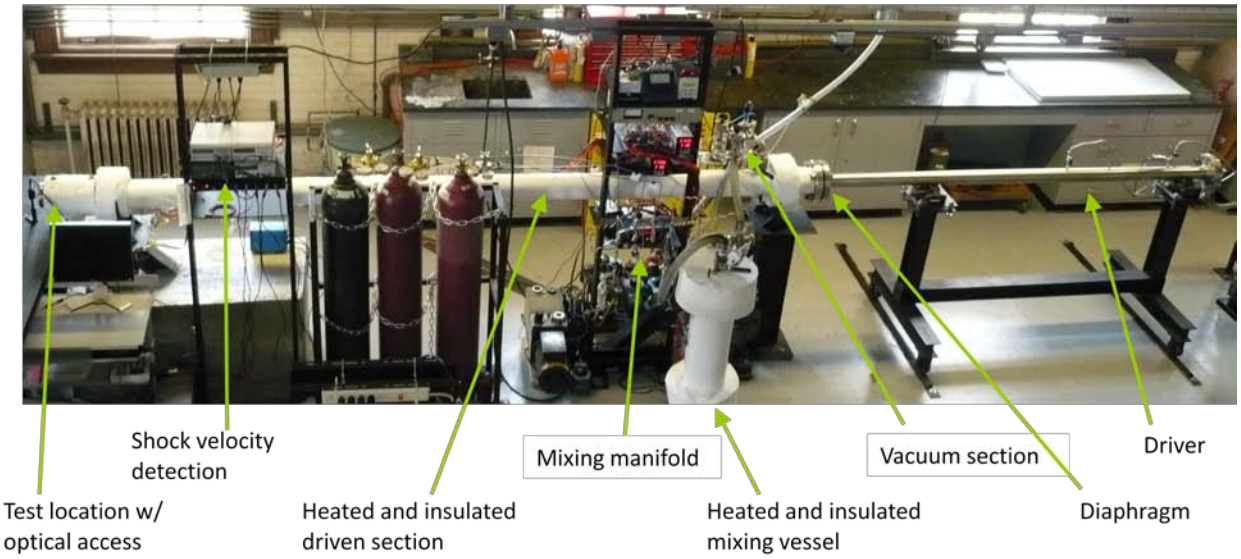

Figure 2.1 Photograph of the RPI heated high-pressure shock tube.

To perform elevated-pressure gas-phase shock tube experiments with low-vapor pressure compounds, such as jet fuels, the shock tube driven section can be heated externally. The shock tube driven section has been outfitted with an electronically controlled external heating system that allows for uniform heating to temperatures up to ~200 °C. The heating system consists of silicone heaters capable of providing uniform heat flux up to 0.775 W/cm^2, an Omega CN616TC1 zone heater controller that monitors the output from six type-K thermocouples spaced along the exterior walls of the driven section and controls the heat flux applied to six heated zones along the 4.11 m long driven section, and 2.5 cm thick mineral wool insulation that covers the entire heated driven section. The driven section temperature profiles are measured regularly by translating a thermocouple along the inner wall of the driven section to ensure uniformity prior to performing experiments. Example driven section temperature profiles are shown in Figure 2.2. The figure illustrates that the heating system provides uniformity within the thermocouple uncertainty (±2.2 °C) for all but the highest temperatures. Axial uniformity is important because a non-uniform driven section temperature profile will cause increased uncertainties in the shock conditions. Measurements for some compounds, e.g., ethylcyclohexane [9], have been made with the driven section both heated and unheated, yielding similar results and indicating that external heating does not influence ignition time measurements in any way other than increasing the available vapor pressure of the fuel of

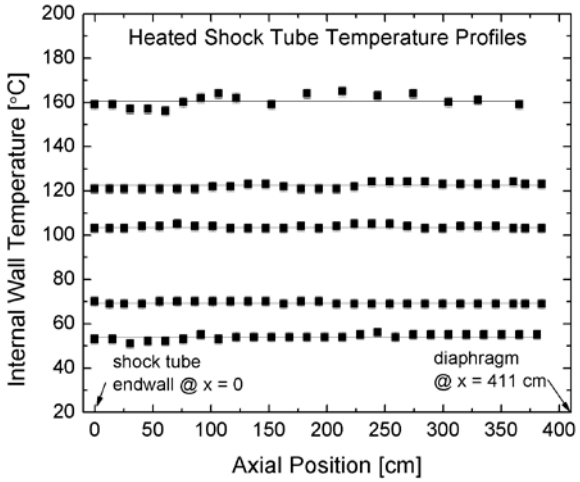

Figure 2.2 Typical heated shock tube inner wall temperature profiles (driven section).

interest. External heating, particularly for temperatures in excess of 120 °C, causes the ultimate vacuum pressure and leak rate to be degraded somewhat, although, when using large concentrations of liquid fuels, such as those used here, the impurities due to shock tube leaking and outgassing are small when compared to the impurities introduced by the liquid fuels (~99+% purity) themselves.

The shock tube driven section is evacuated prior to experiments using the combination of a Welch (model 1397) roughing pump and a Varian V70 turbomolecular pump, which provide an ultimate pressure of 2×10^{-6} Torr and leak rate of 5×10^{-6} Torr/minute in the driven section when the tube is unheated and evacuated overnight; however, most of the experiments presented here were preformed once a driven pressure of 1×10^{-5} Torr was obtained. Additionally, the shock tube was cleaned periodically, particularly often for experiments involving aromatics, using various solvents (ethanol, methanol, acetone, and toluene), sometimes followed by shock heating pure oxygen mixtures to oxidize any remaining impurities in the test section. The mixing tank also was cleaned periodically to avoid mixture contamination.

Shock waves were produced by bursting polycarbonate diaphragms (both scored and unscored) in a 5 cm-long square section at the diaphragm location by filling the driver section from high-pressure gas cylinders. The diaphragm rupture in the square section allows the diaphragm to open into four petals that do not fragment and produce significant particles that can interfere with optical measurements and cause localized hot-spot ignition at the test location. For experiments not requiring extended test times, helium was used as the driver gas; however, for experiments with observed ignition delay times approximately greater than 1.5 ms tailored helium/N_2 driver gas mixtures were used for extended test times (up to 10 ms for the experiments performed for this project). The tailored reflected shock pressure traces were monitored for non-ideal gasdynamic perturbations that result in an increase in temperature during the reflected shock test time. The variation in pressure over the test time varies with the reflected shock conditions but was found always to be in the range of dP/dt = 0 to +3 %/ms for properly tailored experiments performed in air. Assuming isentropic compression of the test gases following the reflected shock passage, shown to be valid [10-11], the resulting variation in temperature is approximately dT/dt = 0 to +0.75 %/ms. This variation in temperature during the induction period prior to ignition was taken into account in the estimation of ignition time uncertainty given below. Argon bath gases show greater pressure and temperature variation. See Figure 2.3 for example pressure traces for tailored reflected shocks. The pressure traces show relatively little variation (dP/dt = 0 to +2%/ms) over the induction period prior to ignition, indicating that the shock tube is well behaved.

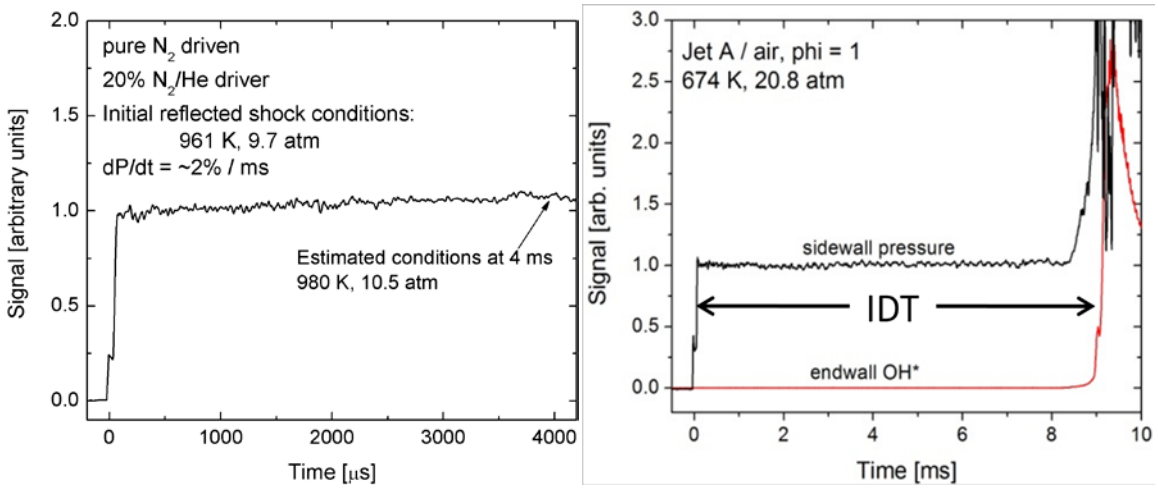

Figure 2.3 Example reflected shock pressure profiles: (left) the shock heating of a non-reactive N_2 driven gas and (right) an ignition delay time measurement for a Jet A/air mixture.

For the measurement of incident shock velocities, five PCB piezoelectric pressure transducers (model 111A22), with rise times of <1.0 μs, are mounted flush to the inner wall over the last meter of the driven section. The time intervals for shock passage between successive pressure transducers are determined by sending the five pressure signals to four 120 MHz Phillips 6666 counter-timers. The measured time intervals and distances between transducers allow the calculation of the incident shock velocity at four locations spaced over the last meter of the driven section. These shock velocities then are extrapolated linearly to the shock tube endwall to determine the incident shock velocity at the test location. See Figure 2.4 for an example incident shock velocity measurement.

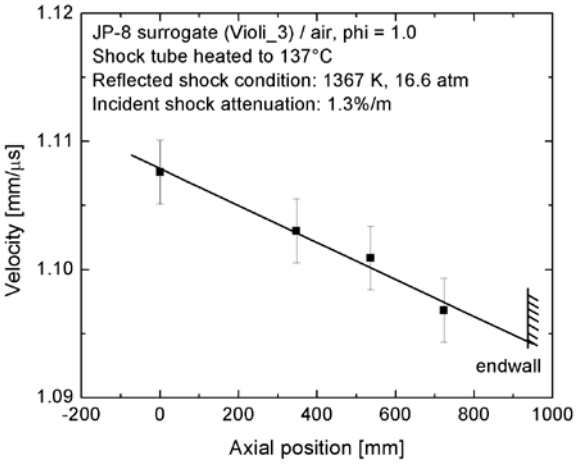

Figure 2.4 Example incident shock velocity measurement.

Calculation of the incident and reflected shock conditions (vibrationally equilibrated) was performed using the normal shock relations and thermochemical data for the species contained in the reactant mixture from the Burcat and Ruscic database [12]. Additionally, a Kistler pressure transducer (Model 603B1) located 2 cm from the endwall in the sidewall provided quantitative pressure measurements in good agreement (±2%) with calculated reflected shock pressures. Although there have been no previous studies, to our knowledge, pertaining to the vibrational relaxation of most of the large hydrocarbons studied as part of this project, we conservatively estimate that vibrational relaxation times are less than 2 μs behind the reflected shock for the mixtures and conditions studied here. This estimation is based on vibrational relaxation times measured by White [13] for O_2 with CH_4, C_2H_2, and C_2H_4. The vibrational relaxation times for the large hydrocarbons studied here are faster than those for the small hydrocarbons used for this estimation due to the significant large number of vibrational degrees of freedom.

Fuel-air mixtures, where air has been defined as pure O_2 and N_2 at a 0.21 to 0.79 molar ratio, were made in a stainless steel mixing tank with an internal magnetically-powered vane stirrer. The mixing vessel and associated manifold were evacuated using a Welch (model 1397) roughing pump and a Varian V70 turbomolecular pump. Mixtures were made with O_2 at 99.995% purity, N_2 at 99.995% purity, and for pure hydrocarbons and surrogate mixtures with purities from 97 to 99.9%. In the case of single component fuel/air mixtures, liquid chemicals were degassed to remove air and high volatility impurities prior to mixture preparation and introduced to the mixing vessel through a stainless steel manifold via vaporization. In the case of multi-component surrogates and distillate jet fuels, liquid fuels were injected directly into the heated mixing tank, where they evaporated. Gaseous O_2 and N_2 were introduced into the mixing vessel through the same stainless steel manifold from high-pressure cylinders. The influence of the two mixture methods, direct injection and vaporization (termed "traditional" in the figure), was

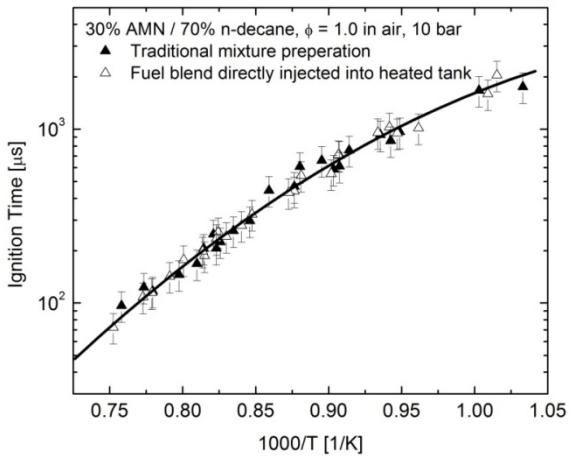

Figure 2.5 Comparison of ignition delay time measurements for two mixture preparation methods: "traditional" where the vapor pressure of the fuel components is used to load the mixing vessel and "direct injection" where the fuel blend is directly injected into the heated tank where it is then vaporized.

investigated for one specific α-methylnaphthalene/n-decane/air mixture with no discernible difference in ignition time measurements observed for the two mixture preparation methods, see Figure 2.5.

The entire mixing vessel and manifold can be heated by silicone electrical resistance heaters (up to 0.775 W/cm^2) to allow reactant mixtures of sufficient total pressure to be made using the available vapor pressure. To ensure uniform heating, the current supplied to the electrical resistance heaters was controlled by an Omega CN616TC1 zone heat controller that monitored the output of type-K thermocouples spaced along the exterior walls of the mixing vessel and manifold. The mixing manifold was insulated with 1.1 cm thick silicon foam rubber insulation, and the mixing vessel was insulated with 2.5 cm-thick mineral wool insulation. Experimental work for a number of compounds with variation in manifold and tank heating showed no observable difference in measured ignition time due to heating [14]. Mixture composition was determined manometrically with pressure measurements from a high-accuracy Baratron pressure manometer, two Setra diaphragm pressure gauges, and a high-temperature Omega pressure gauge. Mixtures were stirred vigorously for anywhere from 15 minutes to 24 hours before experiments, although no influence of mixing time on ignition time measurements was observed for mixing times in excess of 15 minutes. Additionally, Horning et al. [15] have shown previously, via *in situ* laser absorption and gas chromatograph measurements, that the loss of heavy hydrocarbon fuels to wall adsorption is negligible provided that mixtures are prepared with fuel partial pressures sufficiently lower than the fuel vapor pressure.

For the reflected shock experiments performed in the heated shock tube, we conservatively estimate the uncertainty in the initial reflected shock temperature and pressure at approximately 1.5% and 2% (95% probability), respectively. These uncertainties are somewhat greater than estimates for the shock tube unheated (1% and 1.5% in temperature and pressure) due to increased uncertainty in the reactant mixture temperature prior to shock heating; however, the uncertainty in measured incident shock velocity is still the largest contributor to uncertainty.

Measurements of ignition time were made using electronically excited OH (OH*) emission around 306 nm. OH* emission was observed through a UV fused silica optical window flush mounted to shock tube endwall and a UG-5 Schott glass filter, using a Thorlabs PDA36A silicon photodetector. A National Instruments 3 MHz 12-bit eight channel data acquisition card interfaced to a desktop computer with LabVIEW software recorded the voltage signals from the pressure transducer(s) and the photodetector. The ignition time is defined as the time between shock arrival at the endwall and the onset of ignition at the endwall. The time of shock arrival at the endwall was determined from the measured incident shock velocity and the time of passage at a pressure transducer location 2 cm from the endwall. The onset of ignition at the endwall was defined using the extrapolation of the maximum slope in observed OH* emission to the baseline (pre-ignition value), see Figure 2.6 for an example experiment and definition of ignition time.

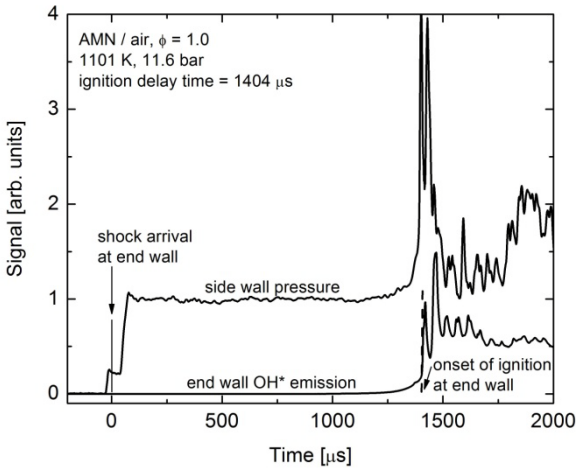

Figure 2.6 Example ignition delay time measurement made via side wall pressure and end wall OH* emission.

3. Results and Discussion

Shock tube ignition delay time studies were carried out for the neat hydrocarbon compounds, three jet fuel surrogate mixtures, and two specific jet fuels, as outlined in Figure 1.2 and Tables 1.1 and 1.2. The specific range of conditions examined for each compound is given in Table 3.1 below. A complete tabulation of experimental data is given in Appendix A.

Table 3.1 Fuels and conditions examined in ignition delay studies.

Mixture	Equivalence ratios, Φ	Pressure range	Temperature range
n-heptane/air	0.25, 0.5, 1.0	11-53 atm	786-1396 K
n-decane/air	0.25, 0.5, 1.0	9-51 atm	836-1378 K
n-dodecane/air	0.25, 0.5, 1.0	11-47 atm	877-1248 K
n-tetradecane/air	0.25, 0.5, 1.0	10-45 atm	884-1302 K
iso-octane/air	0.25, 0.5, 1.0	7-58 atm	886-1300 K
iso-octane/O_2/Ar	0.5, 1.0; ~20% O_2/~78% Ar	8-24 atm	950-1278 K
iso-cetane/air	0.5, 1.0, 1.5	8-47 atm	879-1394 K
cyclopentane/air	0.25, 0.5, 1.0	11-56 atm	900-1379 K
cyclohexane/air	0.25, 0.5, 1.0	11-59 atm	847-1270 K
methylcyclohexane/air	0.25, 0.5, 1.0	11-70 atm	818-1319 K
ethylcyclohexane/air	0.25, 0.5, 1.0	11-53 atm	896-1241 K
decalin/air	0.5, 1.0	9-48 atm	993-1305 K
toluene/air	0.25, 0.5, 1.0	10-62 atm	1021-1400 K
o-xylene/air	0.5, 1.0	11-44 atm	996-1403 K
m-xylene/air	0.5, 1.0	9-42 atm	1023-1408 K
p-xylene/air	0.5, 1.0	9-43 atm	1056-1400 K
ethylbenzene/air	0.5, 1.0	10-45 atm	941-1251 K
α-methylnaphthalene (AMN)/air	0.5, 1.0	8-45 atm	1061-1445 K
α-methylnaphthalene/n-decane/air	1.0; two AMN/n-decane blends: 30/70 by moles and 70/30 by moles	14-62 atm	848-1349 K
Jet-A (POSF 4658)/air	1.0	17-25 atm	674-1222 K
POSF 4658 with JP-8 additives/air	1.0	16-23 atm	906-1254 K
Princeton-MURI surrogate 1/air	1.0	18-23 atm	666-1207 K
RPI surrogate 1/air	1.0	17-23 atm	710-1210 K

3.1 Normal Alkanes

Normal alkanes are found in high concentrations in both traditional and alternative jet fuels and exhibit a high reactivity requiring a quantitative understanding of their oxidation and autoignition for the modeling of the combustion kinetics of jet fuels. Ignition delay results for select stoichiometric n-alkane/air mixtures at elevated pressures are displayed on Arrhenius axes in Figure 3.1, with comparison to previous shock tube and rapid compression machine studies performed at similar elevated pressures. The uncertainty in measured ignition time is estimated at ±20% based on contributions from: 1) the uncertainty in the determination of ignition time based on the ignition time definition and measured pressure and OH emission, 2) uncertainties in the initial reflected shock conditions (mixture composition, temperature, and pressure), and 3) estimated uncertainty due to changes in temperature and pressure caused by non-ideal gasdynamic effects.

In Figure 3.1 the ignition times exhibit clear negative temperature coefficient (NTC) behavior at the lower temperatures studied (T < 1000 K), as observed in the previous experiments and predicted by kinetic modeling studies. The NTC regime is the temperature region where the ignition delay times rollover and decrease or are unchanged with decreasing temperature. In the case of n-dodecane in Figure 3.1 (upper

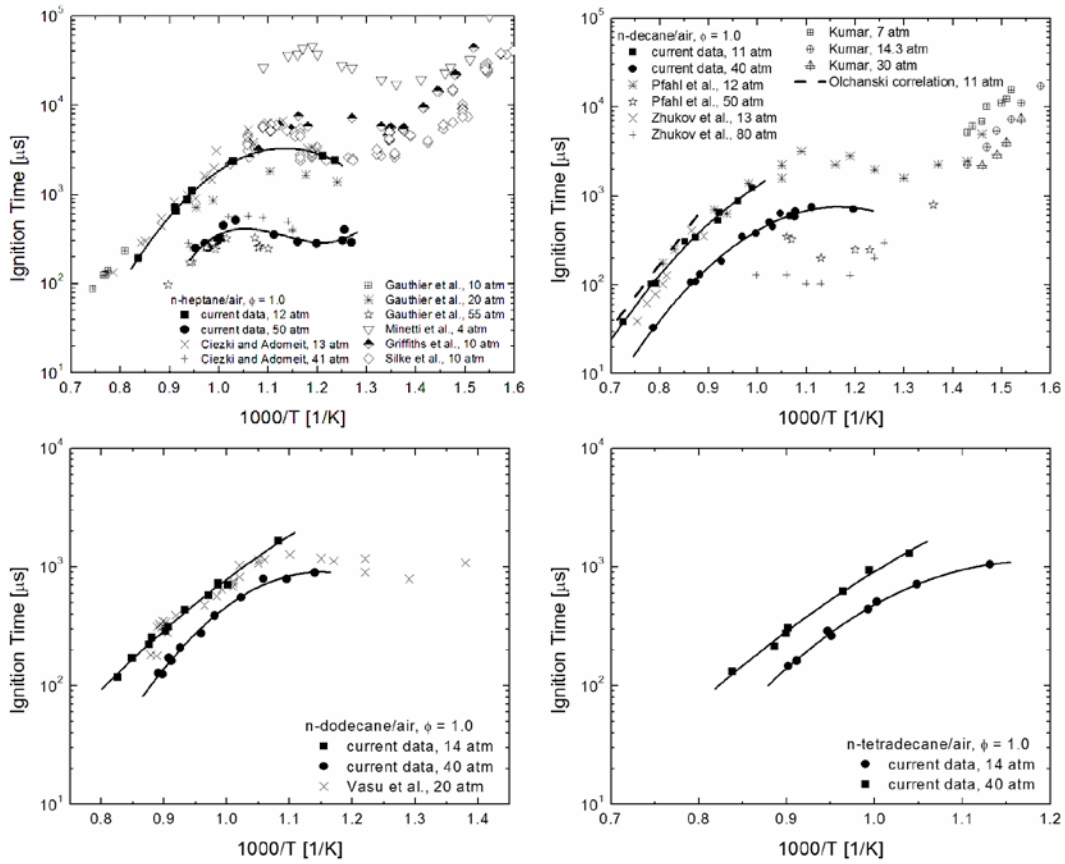

Figure 3.1 Ignition time measurements for n-heptane/air, n-decane/air, n-dodecane/air, and n-tetradecane/air mixtures with comparison to previous shock tube and rapid compression machine studies. All literature and current data scaled to the listed pressures using $\tau \propto P^{-1}$ to account for deviations in experimental pressure.

right) the NTC regime spans from approximately 900K (1000/*T* = 1.1) to 715 K (1000/*T* = 1.4). For all four n-alkanes studied and at temperatures greater than that where NTC behavior begins (T > 1000 K), the ignition time dependence on pressure follows the inverse relationship ($\tau \propto P^{-1}$) previously observed and employed for n-alkanes by other authors [16-18]. In the NTC regime (T < 1000 K) the ignition times exhibit dependence on pressure that is stronger than $\tau \propto P^{-1}$ (i.e., $\tau \propto P^{-a}$ where a > 1) due to the strong dependence of ignition times in the NTC regime on the low temperature peroxy oxidation pathway, which is strongly pressure dependent (see discussion in the next section). Ciezki and Adomeit [19] have observed strong ignition time dependence on pressure in the NTC for n-heptane. In Figure 3.1 all the data were scaled, due deviations in reflected shock pressure, to the common pressures given in the legend using $\tau \propto P^{-1}$. Although in the NTC the τ-P dependence is weaker than that observed experimentally, the deviations in reflected shock pressure for a given data set are not large enough for the pressure scaling to influence the comparisons made in Figure 3.1 significantly. Additionally, the current and previous data are not comprehensive enough to estimate the change in ignition time dependence on pressure with temperature in the NTC.

The agreement of the current ignition time measurements with previous studies performed at elevated pressures shown in Figure 3.1 is fairly good in the cases where the measurements are at similar pressures. The n-heptane data are in reasonably good agreement with the previous shock tube studies of Ciezki and Adomeit [19] and Gauthier et al. [20] and the recent rapid compression machine study of Silke et al. [21] at Φ = 1.0. The Φ = 1.0 n-decane data at 11 atm are in very good agreement with the previous measurements of Pfahl et al. [22] at 12 atm, and there is agreement between the current n-dodecane data and the 20 atm measurements of Vasu et al. [16]. The n-tetradecane measurements are the first, to the PI's knowledge, for any n-alkane larger than C_{12}.

The current ignition time measurements for n-heptane, n-decane, n-dodecane, and n-tetradecane also allow an assessment of the influence of n-alkane chain length on reactivity at the elevated pressure conditions studied. In Figure 3.2 all the ignition time measurements for Φ = 0.5 n-alkane/air mixtures are displayed on Arrhenius axes for pressures around 12 atm. Again, as in Figure 3.1 the data in Figure 3.2 are scaled to 12 atm using $\tau \propto P^{-1}$ to account for differences in experimental reflected shock pressure. The comparisons show that the ignition times for all four n-alkanes at these conditions fall within bands representing ±30% in measured ignition time. Additionally, the error bars for each ignition time (±20%) overlap with measurements for other n-alkanes. These results show that any differences in reactivity for the four n-alkanes are slight and not discernible within our experimental uncertainties. The indiscernible difference in reactivity for the n-alkanes illustrated in Figure 3.2 is common to all Φ and P conditions studied.

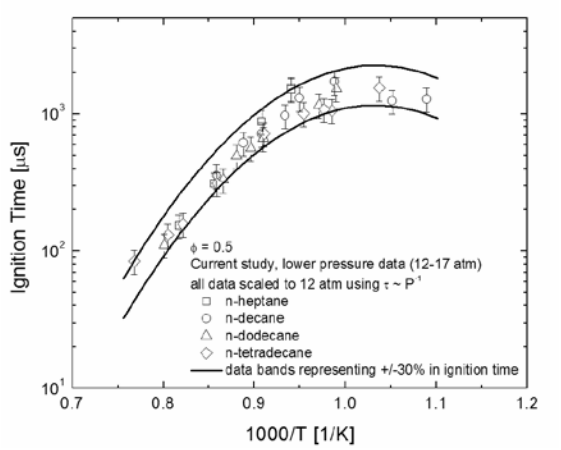

Figure 3.2 Comparison of ignition times for n-heptane/air, n-decane/air, n-dodecane/air, and n-tetradecane/air at Φ = 0.5.

In Figure 3.3 all the Φ = 1.0 n-alkane ignition time measurements performed near 12 atm are compared to previous shock tube and rapid compression machine measurements for n-heptane, n-decane, and n-dodecane made at similar pressures. Again, all the data is scaled to 12 atm using $\tau \propto P^{-1}$ to account for deviations in pressure. The compilation of the current data with those of the previous studies illustrates that all the data, except the n-heptane data of Ciezki and Adomeit [19], fall within a band representing ±40% in ignition time over the complete temperature range displayed (625-1430 K), indicating that any differences in reactivity are slight. There is, perhaps, a slight decrease in reactivity with increasing chain length in Figure 3.3; however, the decrease is small and this observation is influenced by the ignition time data for n-heptane reported by Ciezki and Adomeit [19], which are longer than both the current and Gauthier et al. [20] n-heptane data. Additionally, the coupled uncertainty resulting from the comparison of ignition time measurements made in different facilities using different techniques and the uncertainties resulting from applying $\tau \propto P^{-1}$ scaling at all temperatures, which, as discussed before, is over simplistic, certainly is near ±40% in ignition time.

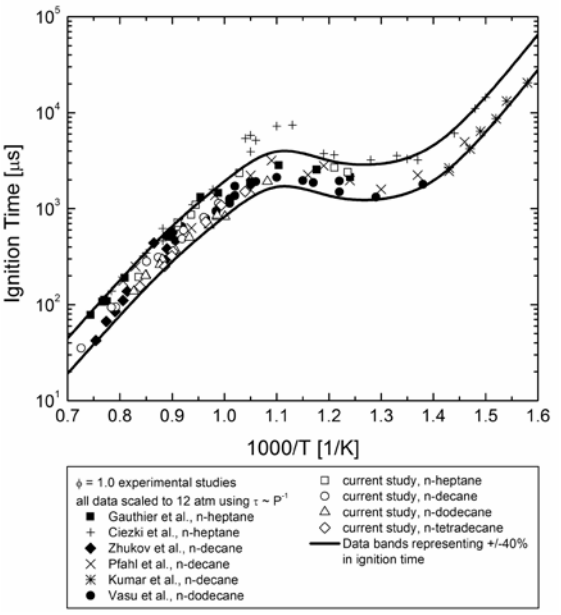

Figure 3.3 Comparison of current n-alkane/air ignition measurements at 12 atm with previous measurements made near 12 atm. The solid lines represent a ±40% band in ignition time, which most of the data falls within.

Comparison of the combined data for n-heptane, n-decane, n-dodecane, and n-tetradecane from these and previous studies with kinetic modeling predictions is made in Figure 3.4. The comparisons are made for Φ = 1.0 n-alkane/air mixtures at pressures near 12 atm with modeling predictions from the C_7-C_{16} n-alkane mechanisms of Curran et al. [23] and Westbrook et al. [24] (Lawrence Livermore National Laboratory, LLNL), the C_5-C_{16} n-alkane mechanism from Ranzi et al. [25] (Politecnico di Milano), who uses a lumped approach to reduce the number of intermediate species and reactions, and the C_7-C_{16} n-alkane mechanism of Biet et al. [26] developed using the EXGAS routine for automatic mechanism generation (Nancy Université).

The n-heptane and n-tetradecane predictions of Curran et al. and Westbrook et al. and the n-heptane and n-decane predictions of Ranzi et al. are in best accord with the measured ignition times. The predictions of the LLNL mechanisms (Curran et al. [23] and Westbrook et al. [24]) for n-heptane and n-tetradecane show no difference in reactivity at high and low temperatures and a slight decrease in ignition time in the NTC with increasing chain length. The maximum predicted difference in ignition time between n-heptane and n-tetradecane by the LLNL mechanisms is 30% in the NTC region. The Ranzi et al. [25] predictions for n-heptane and n-decane show negligible difference in reactivity for temperatures less than 750 K and deviation at lower temperatures with n-decane ignition times 50% shorter than those for n-heptane at 650 K. On the other hand, the Biet et al. [26] mechanism shows a large increase in reactivity with increasing n-alkane chain length, particularly in the NTC regime (750-1000 K) where the ignition times for n-tetradecane are as much as a factor of seven shorter than those for n-heptane, a prediction in disagreement with the combined data shown in Figures 3.3 and the other mechanisms shown in Figure 3.4.

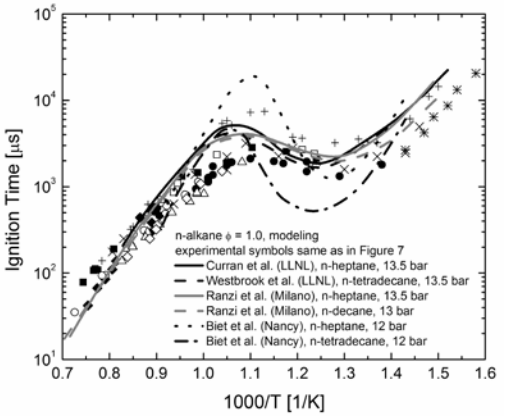

Figure 3.4 Comparison of the data shown above in Figure 3.3 with kinetic modeling predictions for n-alkane/air ignition from Curran et al. [23] and Westbrook et al. [24], Ranzi et al. [25], and Biet et al. [26].

The comparisons of experimental n-alkane ignition times displayed in Figures 3.2-3.4 indicate that the reactivity of n-alkane/air mixtures for C_7 and larger n-alkanes vary little with n-alkane chain length. These mixtures all have approximately common carbon content regardless of the length of the n-alkane chain. For example, a Φ =1.0 n-heptane/air mixture contains 1.874% molar n-heptane (nC7H16) and a Φ =1.0 n-tetradecane/air mixture contains 0.9677% molar n-tetradecane ($nC_{14}H_{30}$). While the n-heptane mixture contains approximately a factor of two more fuel molecules than the n-tetradecane mixture due to the different chain length of these two n-alkanes, the two mixtures differ in carbon atom content by only 3%.

The similarity in reactivity observed experimentally and predicted by the LLNL [23-24] and Ranzi et al. [25] mechanisms indicates that the oxidation kinetics of n-alkanes are influenced little by chain length. A schematic containing the major reaction pathways for alkanes is shown in Figure 3.5. This schematic and the description of the n-alkane oxidation pathways given below are consistent with and taken from the modeling approaches of the LLNL [23-24] and Nancy [26] groups. At temperatures below 1400 K the n-alkanes are consumed primarily via H-atom abstraction by small radicals (O, H, OH, HO_2, CH_3, and others) to produce alkyl radicals. At T > 1400 K n-alkane thermal decomposition competes. At higher temperatures (T > 900-1000 K) these alkyl radicals primarily decompose, which can be preceded by isomerization (H-atom transfer), to produce olefins, most of which are ethylene and propene for all n-alkanes regardless of chain length. At higher temperatures the intermediate olefin pool for all n-alkanes is similar, provided that the mixtures are of common carbon content, and therefore the measured and modeled ignition times are very similar.

At lower temperatures (T < 900-1000 K) the alkyl radicals add directly to O_2 to form alkylperoxy radicals (RO_2) that can dissociate back to alkyl and O_2 or isomerize to form hydroperoxy alkyl radicals (QOOH). The QOOH can add an additional O_2 to form hydroperoxy peroxy (OOQOOH) that can isomerize quickly to a ketohydroperoxide and an OH radical. The ketohydroperoxide can decompose to form a second OH radical and another radical. In total, this reaction sequence produces three radicals from the original alkyl radical and thus low-temperature radical chain branching. This reaction sequence occurs at temperatures lower than 800 K.

At moderate temperatures (700-1000 K) the low-temperature branching reaction pathway competes with the dissociation of QOOH to form different products: olefins and HO_2, cyclic ethers and OH, and β-scission products and alkyl radicals. These moderate temperature pathway results in no radical branching and lower reactivity is observed at moderate temperatures in the negative temperature coefficient (NTC) regime than at lower temperatures, where QOOH + O_2 is faster than QOOH decomposition. The competition between QOOH decomposition and QOOH + O_2 is strongly temperature-dependent and in the NTC regime the ignition times exhibit stronger pressure dependence than they do at higher temperatures. Near the transition from the NTC regime to the high-temperature regime decomposition of hydrogen peroxide, $H_2O_2 + M \rightarrow 2OH + M$, begins to become fast enough to enhance the radical pool and results in the end of the NTC regime (~900-1000 K) and a return to the traditional increase in reactivity with increasing temperature observed in the high-temperature regime (T > 1000 K). Hydrogen peroxide is formed via the sequence QOOH → olefin + HO_2 followed by n-alkane + HO_2 → alkyl + H_2O_2.

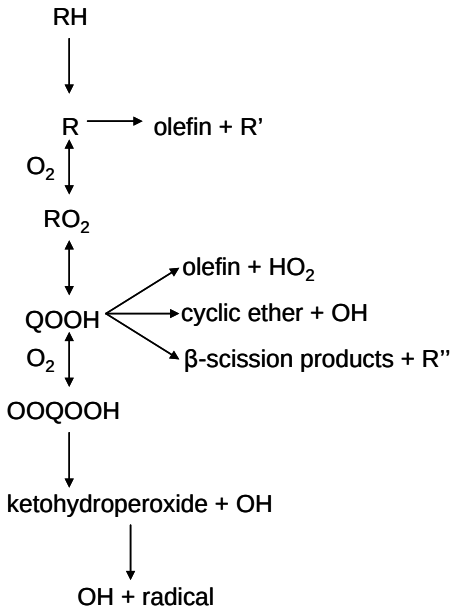

Figure 3.5 The primary reaction pathways for alkane oxidation.

The similarity of the measured ignition times in all the experimental studies shown in Figure 3.3 for temperatures less than 1000 K implies that the moderate- and low-temperature reaction pathways and rates are not influenced strongly by n-alkane chain length for C_7 and larger n-alkanes. In particular, reactions involving internal isomerization (RO_2 → QOOH and OOQOOH → OH + ketohydroperoxide), the rates of which are dependent on the length of R for smaller molecules, must not be strongly dependent on length for C_7 and larger alkyls. This conclusion is consistent with the premise that reactions proceeding through cyclic transition states typically proceed through 5-8 member rings and in the case of larger alkanes the addition of chain length does not add probable isomerization pathways.

3.2 Iso-Octane

Iso-octane (2,2,4 trimethylpentane), a primary reference fuel for octane rating in spark ignition engines, has drawn considerable interest as a model compound for branched alkane components found particularly in gasoline [27], but also those found in jet fuels [2,8]. Select iso-octane ignition delay data at stoichiometric conditions are shown in Figure 3.6 with comparison to the previous shock tube studies of Fieweger et al. [28] and Davidson et al. [29]. The results show little scatter and the uncertainty in measured ignition time is estimated at ±15%. The ignition time data exhibit reduction in overall activation energy (rollover) at lower temperatures, characteristic of negative temperature coefficient behavior common in alkane fuels where alkylperoxy chemistry contributes. The current data for iso-octane/air mixtures are in very good agreement with Fieweger et al. and Davidson et al. for almost all conditions. The agreement of the present study with the previous shock tube studies suggests that the ignition times for iso-octane/air mixtures at elevated pressures (8-50 atm) are well characterized.

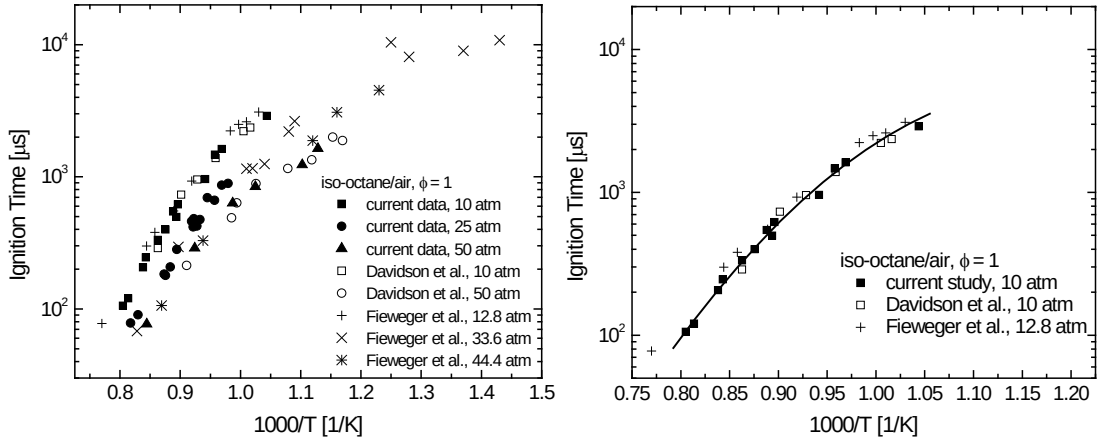

Figure 3.6 Comparison of iso-octane/air ignition time measurements with previously published data of Davidson et al. [29] and Fieweger et al. [28].

Due to the rollover in the ignition time at lower temperatures, regression of the data to a standard Arrhenius form is not possible; however, the data do exhibit power law dependence on pressure and equivalence ratio. The dependence of ignition time on pressure and equivalence ratio is represented by $\tau \propto P^{-0.75}$ and $\tau \propto \Phi^{-0.57}$ for the whole data set. The determined pressure dependence is in good agreement with that recommended by Davidson et al. for iso-octane at elevated pressures. All the iso-octane/air data have been scaled to a common condition of 10 atm and $\Phi = 1.0$ in Figure 3.7 and fit with a second-order polynomial. Note the excellent correlation provided by the power-law scaling factors.

Ignition time measurement for iso-octane/O_2/Ar mixtures with air-like O_2 concentrations (~20%) and $\Phi = 1.0$ and 0.5 are compared with the iso-octane/air results in Figure 3.8. These results are the first of their kind for iso-octane at elevated pressures, to our knowledge, and can be used to evaluate the influence of diluent gas on iso-octane ignition in a shock tube environment, as recently discussed by Wurmel et al. [30] and Davidson and Hanson [31]. The measured ignition times with argon as the diluent exhibit the same temperature dependence, pressure dependence (measured for $\Phi = 0.5$), and equivalence ratio dependence as those where N_2 is the diluent; however, the measured ignition times for argon mixtures are 20-40% shorter than those measured in nitrogen.

Ignition time measurements for iso-octane are compared to the predictions of three kinetic mechanisms in Figures 3.7 and 3.8. The data are compared with the detailed mechanisms of Curran et al. [33] (858 species and 3606 reactions), the detailed mechanism of Glaude et al. [32] (354 species and 1481 reactions) generated automatically with the EXGAS software of Battin-Leclerc and co-workers [50], and the skeletal mechanism of Golovitchev [36] (130 species and 690 reactions). The kinetic calculations were

performed using CHEMKIN and an adiabatic constant volume constraint. The simulated ignition times were defined using the extrapolation of the peak slope in the simulated OH concentration to zero in the same manner as the onset of ignition was defined in the experiments. Simulations also were performed with added chemistry for the creation and removal of electronically excited OH (OH*) from Hall and Petersen [35-36]. The difference in simulated ignition times using OH and OH* was negligible. All three mechanisms overpredict the ignition times for the temperature range studied. The Glaude et al. mechanism overpredicts by a factor of 2 to 8, and the Curran et al. and Golovitchev mechanisms overpredict by a factor of 1.5 to 3.5. Glaude et al. captures the temperature dependence somewhat better than the other two mechanisms for temperatures greater than 1000 K.

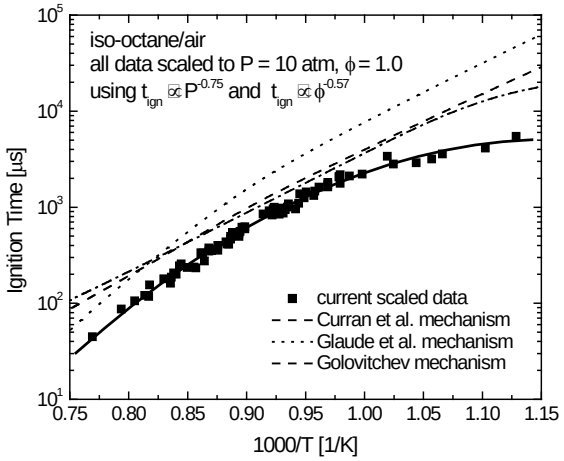

Figure 3.7 Ignition time measurements for all iso-octane/air experiments scaled to Φ = 1.0 and 10 atm with comparison to mechanism predictions of Curran et al. [32], Glaude et al. [33], and Golovitchev [34].

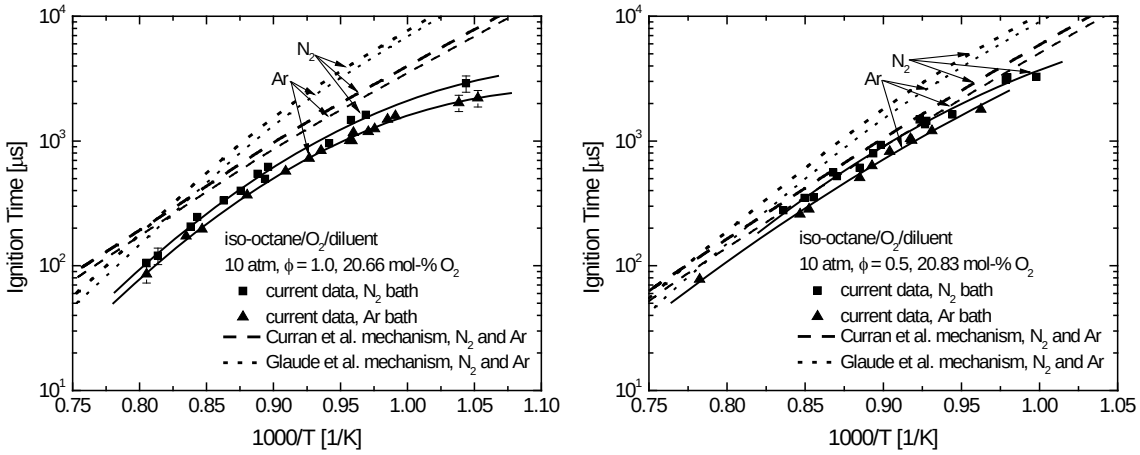

Figure 3.8 Ignition time measurements for iso-octane/air and iso-octane/O_2/Ar mixtures for 10 atm, Φ = 1.0 (left) and Φ = 0.5(right) with comparison to mechanism predictions of Curran et al. [32] and Glaude et al. [33].

Sensitivity analysis was performed using the Glaude et al. and the Golovitchev mechanisms to assess the reactions with the greatest influence over the ignition times at the conditions studied. The results of sensitivity for the two mechanisms were similar. In Figure 3.9 the sensitivity results of the Glaude et al. mechanism are shown. Sensitivity analysis for the Curran et al. mechanism was not performed due to its prohibitive size. The predicted ignition times show strong sensitivity to important reactions in the H_2/O_2 mechanism: $H_2O_2 + M \leftrightarrow OH + OH + M$, $HO_2 + HO_2 \leftrightarrow H_2O_2 + O_2$, and $H + O_2 \leftrightarrow OH + O$. Hydrogen peroxide decomposition, $H_2O_2 + M \leftrightarrow OH + OH + M$, and H-atom reaction with oxygen, $H + O_2 \leftrightarrow OH + O$, are two of the primary rate-controlling radical branching reactions for the condition studied. The association of hydroperoxyl radicals, $HO_2 + HO_2 \leftrightarrow H_2O_2 + O_2$, is an important radical removal reaction at moderate-temperature conditions and decelerates oxidation. Other small molecule reactions that are important are the association of methyl radicals, $CH_3 + CH_3 + M \leftrightarrow C_2H_6 + M$, which decelerates ignition by removing reactive methyl radicals, and the reaction of hydroperoxyl with methyl, $HO_2 + CH_3 \leftrightarrow CH_3O + OH$, which increases reactivity when followed by the fast decomposition of the methoxy radical, $CH_3O + M \leftrightarrow CH_2O + H$. Additionally, the two primary iso-octane consumption reactions exhibit strong sensitivity. H-atom abstraction from iso-octane by hydroperoxyl, $iC_8H_{18} + HO_2 \leftrightarrow H_2O_2 + C_8H_{17}$-3, exhibits strong sensitivity

at the lower temperatures studied and the thermal decomposition of iso-octane, $iC_8H_{18} \leftrightarrow C_4H_9 + C_4H_9$, shows strong sensitivity at the higher temperatures studied. The sensitivity analysis indicates the importance of small radical chemistry, and in particular the fate of the HO_2 radical for the prediction of iso-octane ignition times. This observation is typical of aliphatic fuels under moderate-temperature conditions. Two of the sensitive reactions with relatively large uncertainties that warrant further investigation are $HO_2 + HO_2 \leftrightarrow H_2O_2 + O_2$ and $HO_2 + CH_3 \leftrightarrow CH_3O + OH$; however, measurements of rate coefficients for these reactions are complicated by the difficulty in avoiding interfering chemistry and in generating and measuring HO_2. The $HO_2 + HO_2 \leftrightarrow H_2O_2 + O_2$ reaction has been shown to have extreme non-Arrhenius temperature dependence [37], complicating kinetic understanding, and the $HO_2 + CH_3 \leftrightarrow CH_3O + OH$ reaction has not been the subject of a direct experimental measurement, to our knowledge.

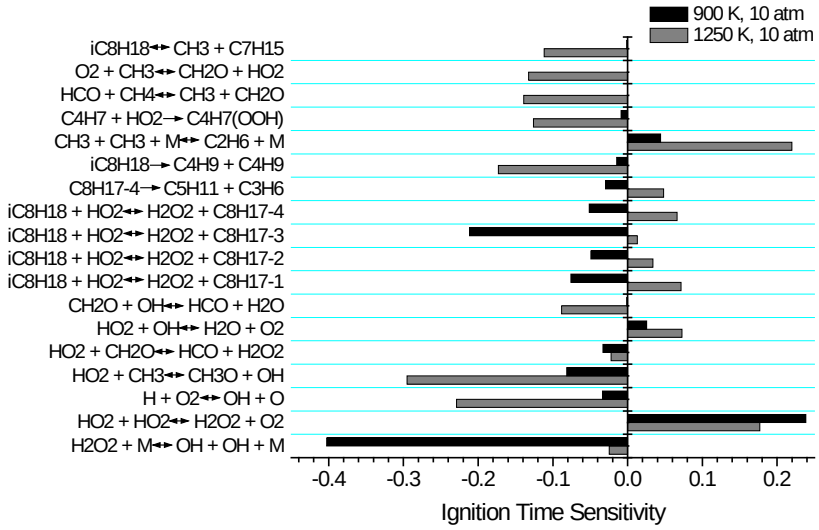

Figure 3.9 Ignition time sensitivity for iso-octane/air for 10 atm and Φ = 1.0 performed using the mechanism of Glaude et al. [33].

Diluent Gas Influence on iso-octane ignition

Figure 3.8 shows the variation in measured ignition time at 10 atm for Φ = 1.0 and Φ = 0.5 for N_2 and Ar diluent mixtures and the predictions of the Curran et al. [32] and Glaude et al. [33] mechanisms. The skeletal mechanism of Golovitchev [34] reproduces the predictions of the detailed Curran et al. mechanism for the conditions studied and is not shown. For Φ = 1.0 and 10 atm, the Ar ignition time measurements are approximately 20% shorter for the temperature range of 1000-1250 K and diverge to a 40% difference at the coldest temperatures studied, ~950 K. Both the Curran et al. and Glaude et al. mechanism predict Ar ignition times that are 15% shorter than those where N_2 is the diluent for the entire temperature range, in good agreement with the difference in the ignition measurements for all but the coldest temperatures. The 15% difference in the simulations for the two diluent gases is not a function of the constraint placed on the simulation and is nearly identical for both constant volume and constant pressure constraints. The uncertainty in the ignition time determinations given here is ±15%. It is likely that uncertainties would be systematic and, to first-order, affect both N_2 and Ar mixtures equally; however, those measurements made at the coldest temperatures are the most uncertain, due to non-ideal gasdynamic temperature fluctuations during the longer test times. It is possible that the divergence shown at 950 K in the difference between N_2 and Ar mixtures for Φ = 1.0 is simply a result of uncertainty in the ignition time measurements. It is also possible that the divergence is due to a greater level of induction period heat release occurring for the lowest temperatures studied than the mechanisms predict. A greater level of induction period heat release will cause a larger difference in ignition times for the two diluent gases due to the faster rise in temperature for argon relative to nitrogen prior to ignition. Even with the divergence near 950 K, the agreement between the measurement and predictions of the Curran et al. and Glaude et al. mechanisms for the influence of diluent gas on Φ = 1.0 iso-octane ignition times is very good. For Φ = 0.5 and 10 atm, the measured ignition times for argon are 20% shorter than those in nitrogen for the entire temperature range studied, also in good agreement with the predictions for the difference by the Curran et al. and Glaude et al. mechanisms, which both predict a difference of approximately 15%.

The difference in ignition time measurements in shock tubes for different diluent gases can be attributed to the specific heat of the diluent [30]. For the conditions studied here, where there is limited endothermic fuel thermal decomposition, the temperature and pressure remain constant at the reflected shock condition until the radical pool begins to build just prior to ignition. During the growth of the radical pool, exothermic chemistry causes the temperature and pressure to rise during the later part of the induction period. Due to the greater specific heat of diatomic nitrogen relative to monatomic argon, the induction period heat release causes the temperature and pressure to rise faster for argon mixtures than for nitrogen mixtures, accelerating radical pool growth and ignition. The influence of the induction period heat release on measured pressure and ignition time is exhibited in Figure 3.10 for experiments performed with nitrogen and argon as diluents. Comparison to predictions made using the Curran et al. mechanism also is shown. The magnitude of the pressure rise during the induction period predicted by the Curran et al. mechanism is in fair agreement with the measurement within our ability to discern the induction period pressure rise from the pressure measurement. The agreement between the simulated and measured difference in ignition time for N_2 and Ar mixtures indicates that the Curran et al. and Glaude et al. mechanisms predict an appropriate amount of induction period heat release, and modifications made to these mechanisms for improved kinetic predictability should not modify the amount of induction period heat release drastically.

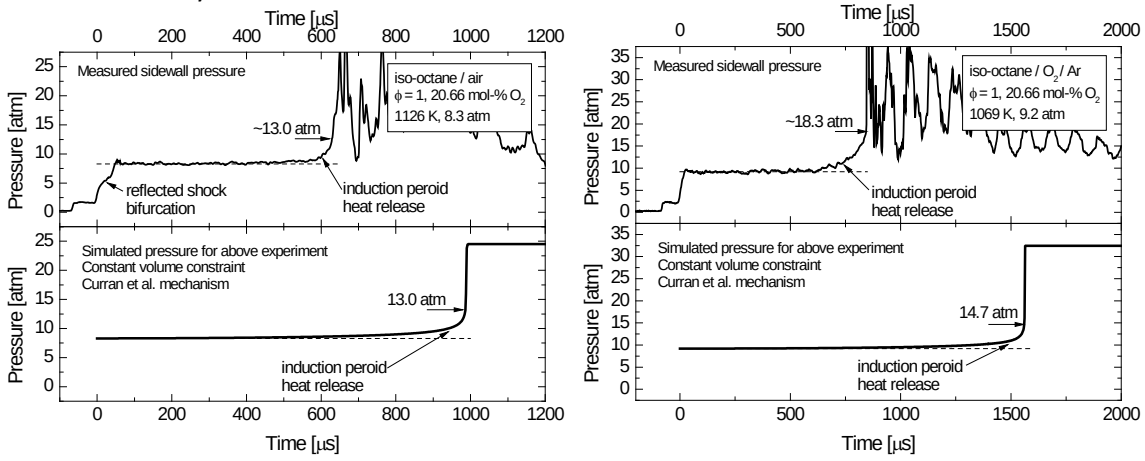

Figure 3.10 Example iso-octane/air (left) and iso-octane/O_2/air (right) measured pressure profiles compared to simulations performed using the Curran et al. mechanism [32].

The connection between induction period heat release and diluent gas influence on ignition time results in a varying influence of diluent gases for different fuels. Highly sensitive fuels (H_2, CH_4, C_2H_4, and C_2H_2) exhibit less induction period heat release relative to less sensitive fuels (iso-octane, n-heptane, larger alaphatics); therefore, the diluent gas will have less influence on the ignition times. For example, Petersen et al. [38] show negligible difference in ignition times for methane/O_2/diluent mixtures for N_2 and Ar diluents, and Gauthier et al. [20] show a significant difference in ignition times for synthetic gasoline mixtures in air versus those with added exhaust gas recirculation (H_2O and CO_2).

Simulations were performed to assess the influence of nitrogen chemistry by comparing predictions with the base Curran et al. mechanism and those performed with the inclusion of NO_x chemistry from GRIMech 3.0 [39]. As expected, at the moderate to low temperatures studied here, NO_x chemistry has no influence on the ignition times measured in nitrogen. Additionally, the influence of third body collision efficiencies for N_2 and Ar were investigated by performing simulations with collision efficiencies for N_2 of 1.0 and Ar of 0.7, as they are assigned in the Curran et al. mechanism, and simulations with collision efficiencies of 1.0 for both colliders. The difference in ignition time due to this change was approximately 1% for simulations at both 10 and 50 atm.

Finally, a point should be made regarding the influence of the commonly used adiabatic constant volume assumption for ignition phenomena behind reflected shock waves. Following reflection at the

endwall, the shock wave travels upstream into a non-uniform incident shock condition due to incident shock boundary layer attenuation. The non-uniform incident conditions cause the temperature and pressure to increase slightly during the reflected shock test time. In the experiments performed here this influence is minor for the ignition time determinations. At some point the mixture ignites, the heat release is rapid, and either a detonation or deflagration wave forms and processes the upstream gas. At ignition the constant volume constraint clearly breaks down due to the fluid motion caused by wave propagation, and the resulting pressure and temperature at the endwall are less than that predicted using the constant-volume constraint. See Davidson and Hanson [31] for experimental post-ignition pressure measurements versus constant-volume predictions and discussion. The constant volume constraint also has its shortcomings prior to ignition. When induction period heat release occurs, the temperature and pressure rise first at the endwall, and the gas near the endwall must expand upstream, causing a slightly lower pre-ignition temperature and pressure than predicted by the constant volume model. For the experiments performed here this influence is small (estimated at <5% in ignition time) due to the relatively small amount of induction period heat release and influences the results of measurements made in both diluent gases. Additionally, heat loss to the shock tube walls is small during the induction period. It is estimated that, for the longest shock tube test times (~3 ms), the heat loss due to conduction and convective losses to the walls during the induction period results in a reduction in reflected shock temperature of at most 5 K.

Ultimately to overcome the shortcomings of the constant volume constraint, 1-D computational fluid dynamics (CFD) coupled to reaction kinetics is required, which is a computationally intensive approach for the number of species and reactions in current detailed reaction mechanisms for practical fuels. To overcome some of the shortcomings of the constant volume constraint without resorting to 1-D CFD, Li et al. [40] have developed a simple, computationally cheaper, approach based on allowing the mixture, for an infinitesimal time step, to react at constant volume followed by isentropic compression or expansion to the measured pressure. This method does not differentiate between compression (or expansion) due to non-ideal gasdynamics or chemical reaction; hence, application of the method of Li et al. to experiments where induction period heat release is observed would result in the measured induction period pressure rise (due to heat release) causing a hastened pressure and temperature rise in the kinetic simulation (through gasdynamic compression) and an ignition process predicted by the simulation that is artificially accelerated by gasdynamics, providing better agreement between simulation and experiment; however, this agreement would not be indicative of the mechanisms kinetic predictability.

3.3 Iso-Cetane

Select ignition delay time measurements for iso-cetane, a reference fuel for cetane rating, are displayed on Arrhenius axes in Figure 3.11. The estimated uncertainty in measured ignition time is ±25% (95% confidence interval). In Figure 3.11 the data, when plotted on Arrhenius axes, show small scatter about linear least-squares fits; however, a single correlation for the data is not possible due to differences in the influence of equivalence ratio on ignition time across the range of lean to rich conditions studied. Additionally, as can be observed from the kinetic modeling, at the lowest temperatures there is a mild reduction in the overall activation energy due to low-temperature chemistry (mild negative-temperature-coefficient behavior), and thus a linear Arrhenius fit is not suitable. All data sets (Φ = 0.5, 1.0, and 1.5) do show a very similar ignition time dependence on pressure ($\tau \propto P^{-0.8}$) analysis, where τ is the ignition time. The data in Figure 3.11 are scaled to common pressures (10 and 40 atm) using $\tau \propto P^{-0.8}$ to account for the cted shock pressure that result primarily from inconsistent diaphragm rupture, which is exacerbated when the shock tube is heated. The $\tau \propto P^{-0.8}$ pressure dependence should not be ext he range of conditions studied, as is the case with all ignition time correlations, because different ignition time dependencies on pressure will result at different conditions due to inherent differences in the governing chemistry with variation in pressure, temperature, O_2, and fuel concentrations (e.g., T-P-[O_2] dependence in the high-temperature regime versus the NTC regime).

Through collaboration with C.K. Westbrook and W.J. Pitz at Lawrence Livermore National Laboratory a kinetic model was generated for iso-cetane in the same modular fashion as in their previous studies of large straight-chain and branched alkane fuels [23,24,32]. The reaction rate rules were updated for iso-octane [32], and further reaction pathways and reaction rate rules have been proposed [24], but the present mechanism for iso-cetane is nearly identical to those already tested extensively for other fuel molecules. Reaction pathways for both the high-temperature and low-temperature regimes were included. For the present application to high-temperature shock tube ignition, none of the low-temperature, alkylperoxy radical isomerization pathways were found to be significant. For detailed discussion regarding the reaction mechanism see reference 41.

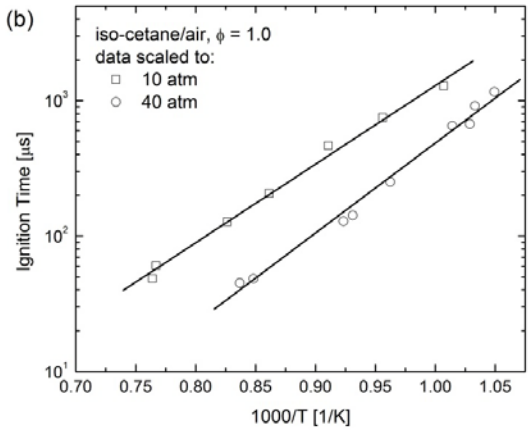

Figure 3.11 Ignition time measurements for Φ = 1.0 iso-cetane/air mixtures. Data scaled to 10 and 40 atm using pressure scaling based on regression analysis, $\tau \propto P^{-0.8}$.

Kinetic simulations were performed using the iso-cetane mechanism and are compared with the stoichiometric shock tube ignition delay time measurements in Figure 3.12. For computational purposes, the ignition time was defined as the time at which the temperature had increased by 400 K from the initial reflected shock temperature, which for the very exothermic mixtures studied closely coincides with the maximum slope in OH extrapolated to zero, as used in the experiment. The maximum deviation between experiment and simulation is a factor of two in ignition time; however, much of the data agrees with the kinetic simulations within the experimental uncertainties, ±25% in ignition time. We consider the agreement to be very good considering the size and complexity of the kinetic mechanism and because the mechanism was developed *a priori* using rate coefficient rules previously developed for aliphatic compounds with no adjustments made to rate parameters for better agreement with the present measurements. The agreement between experiment and mechanism for such a large alkane illustrates that the rate coefficient rules developed for alkanes [23,24,32] can be extended with some confidence to the prediction of ignition at high to moderate temperatures for other fuels where data and mechanisms currently do not exist.

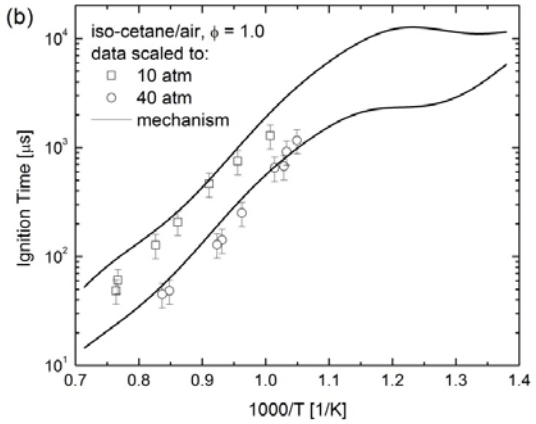

Figure 3.12 Measured Φ = 1.0 iso-cetane/air ignition delay times compared to predictions of detailed mechanism.

The kinetic model also was used to extend the simulations to temperatures considerably lower than those of the present experiments. A low temperature reaction regime, including negative temperature coefficient behavior, can be seen in Figure 3.12 beginning at temperatures below about 900 K. Evidently, ignition data are needed at lower temperatures for more comprehensive mechanism validation, which could be obtained using rapid compression machines or tailored driver gas shock tube methods.

While there are no previous iso-cetane ignition data for comparison to the current measurements, the current data can be compared to the ignition measurements for iso-octane. A comparison of selected results (40 atm, Φ = 1.0 in air) for iso-cetane and iso-octane is shown in Figure 3.13 along with kinetic simulation for the two branched alkanes. Although there is a high degree of similarity in the oxidation kinetics of iso-octane and iso-cetane at high to moderate temperatures, in Figure 3.13 both the experiments and simulations show that the ignition delay times for iso-octane are somewhat (i.e., 50-100%) longer than those for iso-cetane in the temperature range of the measurements (950-1250 K for conditions displayed). At lower temperatures in the NTC regime, the computationally predicted difference is larger, with iso-octane ignition times up to a factor of three longer than those for iso-cetane.

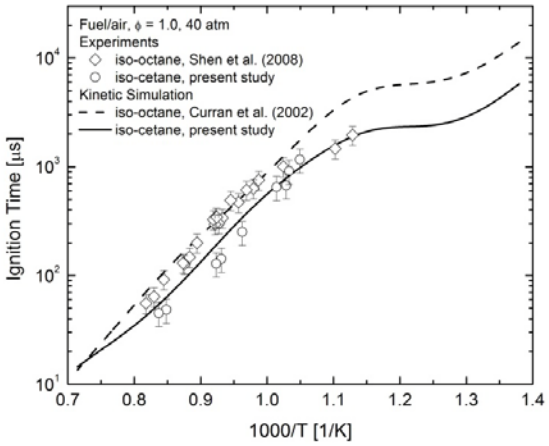

Figure 3.13 Measured iso-octane and iso-cetane (current study) ignition delay times Φ = 1.0 fuel/air mixtures at 40 atm compared to kinetic predictions based on references [32] and [41].

At the high to moderate temperatures for which experimental data are displayed in Figure 3.13, the difference in reactivity between iso-cetane and iso-octane can be attributed to two factors that are related to the structure of the iso-cetane molecule. First, 15 of the 18 H bonds in iso-octane are bonded at primary sites in the molecule, while a smaller fraction, 27 out of 34, of the H atoms in iso-cetane are bonded at primary sites. A correspondingly larger fraction of the H atoms in iso-cetane are bonded at secondary and tertiary sites. Since primary C-H bonds are stronger than secondary or tertiary bonds, it is easier and faster to abstract H atoms from iso-cetane. Second, following H-atom abstraction iso-cetane produces a greater fraction of reactive H atoms during the subsequent fragmentation of its alkyl radicals than does iso-octane. H atoms generated from alkyl radical decomposition provide chain branching through reaction with O_2 ($H + O_2 \rightarrow OH + O$), generating additional radicals that can consume more fuel and intermediates. In contrast, CH_3 radicals generated by alkyl radical decomposition recombine ($CH_3 + CH_3 \rightarrow C_2H_6$), a chain termination step that leads to a smaller and less reactive intermediate radical pool. The production of H atoms is proportionally greater and the production of methyl radicals is proportionally smaller in iso-cetane than in iso-octane, producing a slightly more rapid ignition for iso-cetane in the temperature range of these experiments. These distinctions, faster H atom abstraction and a slightly more reactive intermediate pool for iso-cetane relative to iso-octane, are quite small, producing differences in ignition delay of not more than a factor of two over the range of temperatures studied.

Although outside the range of conditions examined here, at temperatures below 900 K another reaction pathway increases the differences between the modeled iso-cetane and iso-octane ignition times. The increased differences are due to the rates of alkylperoxy radical isomerization ($RO_2 \leftrightarrow QOOH$), which control radical production in the low-temperature oxidation sequence ($R + O_2 \leftrightarrow RO_2 \leftrightarrow QOOH (+O_2) \leftrightarrow OOQOOH \rightarrow 2OH$ + products). These reaction pathways are inhibited in the case of iso-octane [32], but for iso-cetane [41], which has three CH_2 groups appropriately spaced for six-membered transition states for RO_2 isomerization between CH_2 groups, these reaction pathways more readily produce radicals than in the case of iso-octane, which has only one CH_2 group. These differences between the mechanisms of iso-cetane and iso-octane ignition at low temperatures are distinct from those differences at higher temperatures that lead to the differences observed in the present experimental results.

3.4 Cyclopentane and Cyclohexane

Cyclopentane and cyclohexane are the smallest and simplest cycloalkanes, a class of compounds found in significant concentrations in jet fuels (~20%) and in even greater concentrations in synthetic fuels derived from oil sands and coal-to-liquid processes. In Figure 3.14 select data for cyclopentane at stoichiometric conditions are illustrated. The data are characterized by little scatter and Arrhenius temperature dependence, with no observation of NTC behavior under the conditions studied. The measured ignition times can be correlated, for the three equivalence ratios studied, using Arrhenius temperature dependence and power-law pressure dependence: $\tau = AP^{-n}\exp(E_A/T)$. The results of regression analysis are as follows:

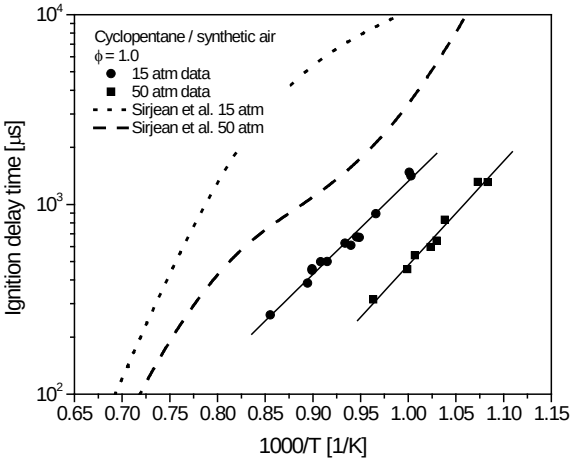

Figure 3.14 Ignition time measurements for cyclopentane/air mixtures at 15 and 50 atm and Φ = 1.0 with comparison to predictions of the Sirjean et al. [42] kinetic mechanism. Ignition times were scaled to 15 and 50 atm, to account for deviations in reflected shock pressure, using power-law pressure scaling as determined by regression analysis.

Cyclopentane

$\Phi = 1.0$: $\tau = 9.89\times10^{-8} P^{-0.90} \exp(12010/T\ [K])$ sec

$\Phi = 0.5$: $\tau = 1.26\times10^{-7} P^{-0.90} \exp(12090/T\ [K])$ sec

$\Phi = 0.25$: $\tau = 9.60\times10^{-8} P^{-0.60} \exp(11780/T\ [K])$ sec

Cyclohexane

$\Phi = 1.0$: $\tau = 1.55\times10^{-8} P^{-1.1} \exp(13890/T\ [K])$ sec

$\Phi = 0.5$: $\tau = 1.48\times10^{-9} P^{-0.67} \exp(14760/T\ [K])$ sec

$\Phi = 0.25$: $\tau = 3.09\times10^{-9} P^{-0.49} \exp(14210/T\ [K])$ sec

where τ is the ignition time in seconds, T the temperature in Kelvins, and P the pressure in atmospheres. In Figure 3.15 the data for Φ = 1.0, 0.5, and 0.25, for cyclopentane and cyclohexane respectively, are shown and compared at a common scaled pressure of 50 atm. The experimental results indicate that the overall activation energies for ignition, E_A, for both cycloalkanes remain constant, within the ability to discern them, over the conditions studied. The results also show that there is a decrease in ignition time with increasing pressure and increasing equivalence ratio for lean to stoichiometric mixtures.

The current ignition time measurements for cyclohexane/air mixtures at Φ = 1.0 are compared with the rapid compression machine (RCM) results of Lemaire et al. [43] in Figure 3.16. Lemaire et al. measured ignition times for stoichiometric cyclohexane/O_2/inert mixtures containing approximately 20% O_2 at

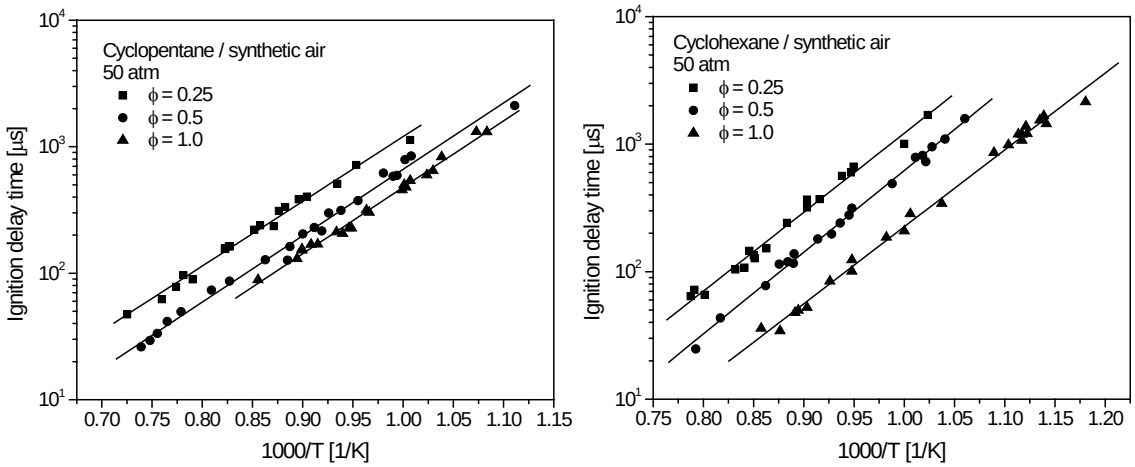

Figure 3.15 Ignition time measurements for cyclopentane/air (left) and cyclohexane/air (right) scaled to 50 atm using power-law pressure scaling factors provided in the text.

pressures ranging from 11 atm to 14 atm. In Figure 3.16, the current data are scaled to 12.5 atm using the pressure scaling derived in this study for stoichiometric cyclohexane mixtures ($\tau \propto P^{-1.1}$) to allow for comparison to Lemaire et al. There is good agreement at the intersection of the two data sets near 900 K, prior to where Lemaire et al. observe the beginning of NTC behavior at colder temperatures. This agreement is important because it suggests that the combination of the two data sets provide kinetic validation targets for stoichiometric cyclohexane/air mixtures for a large temperature range important in practical combustion engines, 600-1200 K.

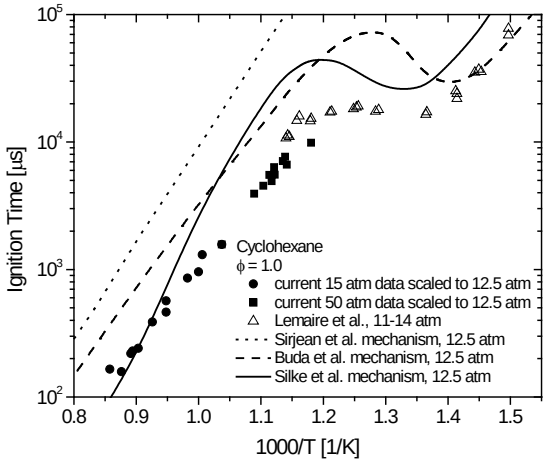

Figure 3.16 Comparison of ignition time measurements for cyclohexane/synthetic air at Φ = 1.0 scaled to 12.5 atm with the rapid compression machine study of Lemaire et al. [43] and predictions of the kinetic mechanisms of Sirjean et al. [42], Buda et al. [44], and Silke et al. [45].

A comparison of the measured ignition times for cyclopentane and cyclohexane for Φ = 1.0 is shown in Figure 3.17. The activation energy for cyclopentane ignition is a bit lower over the temperature range studied, and the cyclohexane ignition times are approximately a factor of two shorter than those for cyclopentane in this temperature range. The lower reactivity (longer ignition times) for cyclopentane in comparison to cyclohexane also was observed by Sirjean et al. [42], who, in their kinetic analysis, concluded that the dissimilarity in reactivity is due to the difference in stability of primary C_5 and C_6 cycloalkyl radicals. Cyclohexyl radicals are more likely to yield H atoms, which lead to branching via $H + O_2 \rightarrow OH + O$, than cyclopentyl radicals.

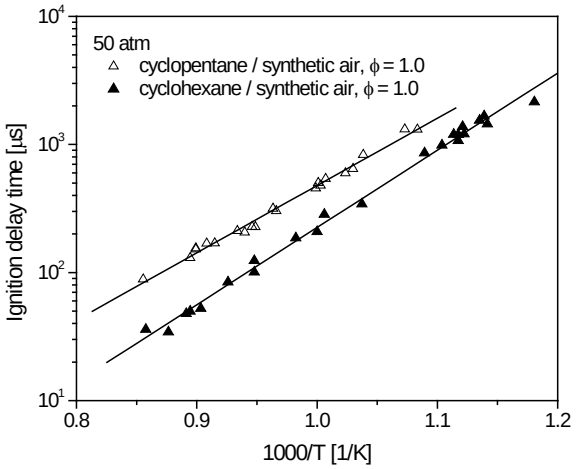

Figure 3.17 Comparison of ignition times for cyclopentane/air and cyclohexane/air at Φ = 1.0 scaled to 50 atm using power-law pressure scaling factors given in text.

The predictions of four recently published detailed cyclopentane and cyclohexane kinetic mechanisms are compared with the current ignition time measurements in Figures 3.14 and 3.16. The mechanisms examined are the cyclopentane (233 species and 1204 reactions) and cyclohexane (372 species and 1633 reactions) mechanisms of Sirjean et al. [42], and the cyclohexane mechanisms of Buda et al. [44] (499 species and 2323 reactions) and Silke et al. [45] (1081 species and 4269 reactions). The Sirjean et al. and Buda et al. mechanisms are based on an improved version of the EXGAS automatic mechanism generation software developed by Battin-Leclerc and co-workers [33]. The Sirjean et al. EXGAS mechanisms for both cyclopentane and cyclohexane were developed for high temperatures (T > 1000 K) and contain no peroxy chemistry. The Sirjean et al. mechanisms have been shown to predict the highly argon-dilute Sirjean et al. shock tube measurements effectively. The Buda et al. EXGAS mechanism for cyclohexane contains the same base chemistry in the Sirjean et al. mechanism, with the addition of the necessary peroxy chemistry for lower temperature oxidation (T < 1000 K). The mechanism of Silke et al. was developed by adding low- and high-temperature cyclohexane chemistry to the previously-developed mechanism of Curran et al. [23], which contains hydrocarbons up to C_6. The comparisons show that the Sirjean et al. EXGAS mechanisms, developed for high-temperature cyclopentane and cyclohexane oxidation (no peroxy chemistry), significantly overpredict the ignition times for all conditions studied. As shown in Figure 3.16, the Buda et al. and Silke et al. mechanisms, when compared

jointly to the current Φ = 1.0 data scaled to 12.5 atm, and the Lemaire et al. Φ = 1.0 data measured at 11-14 atm, do a fair job at capturing the general trend in ignition time. Both mechanisms overpredict the ignition times, and the Silke et al. mechanism, for temperatures greater than 1000 K, predicts an overall activation energy greater than measured.

3.5 Methylcyclohexame and Ethylcyclohexane

Substituted cyclohexanes, in particular methylcyclohexane (MCH), have received interest as cycloalkane representatives in jet fuel surrogate mixtures. Methylcyclohexane also is of importance because it makes up a very large fraction of the high-energy-density missile fuel JP-9, which is a blend of three high heating value hydrocarbons: methylcyclohexane, exo-tetrahydrodicyclopentadiene (JP-10), and perhydronorbornadiene dimer. Example ignition time results for methylcyclohexane and ethylcyclohexane are shown in Figure 3.18. The measured ignition times have estimated uncertainties of ±15%. The ignition time measurements show Arrhenius exponential dependence on inverse temperature at high-temperatures and rollover at lower temperatures. The onset of NTC (rollover) is shown clearly in the MCH 50 atm data for Φ = 1.0. The rollover at low temperatures is the beginning of the negative temperature coefficient (NTC) regime that also has been observed for MCH by Vasu et al. [46] in shock tube measurements and Pitz et al. [47] in RCM measurements. The ignition time data also show an expected inverse dependence on pressure and equivalence ratio for stoichiometric-to-lean mixtures (i.e., ignition time decreases with increasing pressure and equivalence ratio).

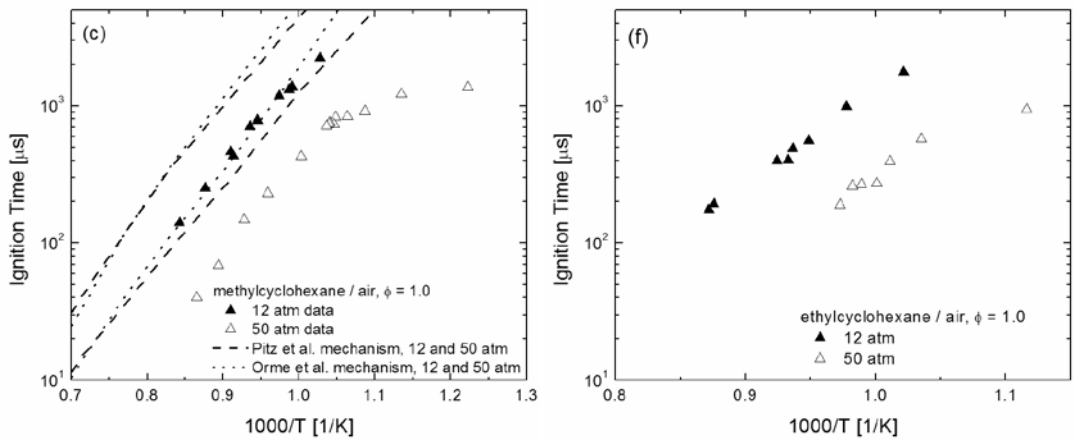

Figure 3.18 Ignition time measurements for methylcyclohexane/air (left) and ethylcyclohexane/air (right) mixtures with comparison to the predictions of the Pitz et al. [47] and Orme et al. [48] mechanisms for methylcyclohexane. Data scaled to 12 and 50 using power-law pressure scaling parameters given in Table 3.2 to account for deviations in reflected shock pressure.

Here, due to the low-temperature rollover in ignition time observed at the beginning of NTC, the data cannot be correlated using an exponential dependence on inverse temperature; however, at temperatures greater than that where NTC behavior begins the measurements for MCH and ECH have a common slope. The high-temperature activation energy is in the range of 31-33 kcal/mol for MCH and 28-30 kcal/mol for ECH, very similar to that observed for other hydrocarbons in the high-temperature regime under the conditions studied.

Despite the observed low-temperature rollover in ignition times, power-law scaling parameters for ignition time dependence on pressure, $\tau \propto P^n$, were determined by finding the values of n that provide a best fit second-order polynomial to the measurements for a given mixture. The pressure scaling parameters are given in Table 3.2. It was found that there is a decrease in pressure dependence with decreasing equivalence ratio for both MCH and ECH, as also was observed for cyclopentane/air and cyclohexane/air ignition. No dependence on temperature was observed for the power-law pressure scaling factor, n. The correlated data scaled to a common pressure (50 atm) using the power-law pressure scaling parameters

given in Table 3.2, as shown in Figure 3.19. The data in Figure 3.18 are scaled to common pressures (12 and 50 atm) using the above pressure scaling parameters to account for variations in the reflected shock pressure within a given data set.

Table 3.2 MCH and ECH power-law pressure scaling factors, $\tau \propto P^n$.

Compound	Φ	n
methylcyclohexane	0.25	-0.66
methylcyclohexane	0.5	-0.66
methylcyclohexane	1.0	-0.99
ethylcyclohexane	0.25	-0.55
ethylcyclohexane	0.5	-0.65
ethylcyclohexane	1.0	-0.98

The data for MCH and ECH at Φ = 1.0 and 50 atm are compared in Figure 3.20. The ignition times show similar temperature dependence. The ignition times for ECH are 20-40% shorter than those for MCH, indicating that for alkylcyclohexanes the reactivity increases for larger alkyl side chains. Roubaud et al. [49] found similar results for alkylbenzenes in RCM experiments. They found that ignition times decreased as the size of the alkyl side chain increased for toluene, ethylbenzene, and n-butylbenzene, which also has been observed as part of this work in shock tube measurements for toluene and ethylbenzene. The reduction in ignition time for increasing alkyl group size presumably is due to the greater number of H atoms available for abstraction and, importantly, the addition of secondary C-H bonds that allow H-atom abstraction more readily than primary bonded H atoms.

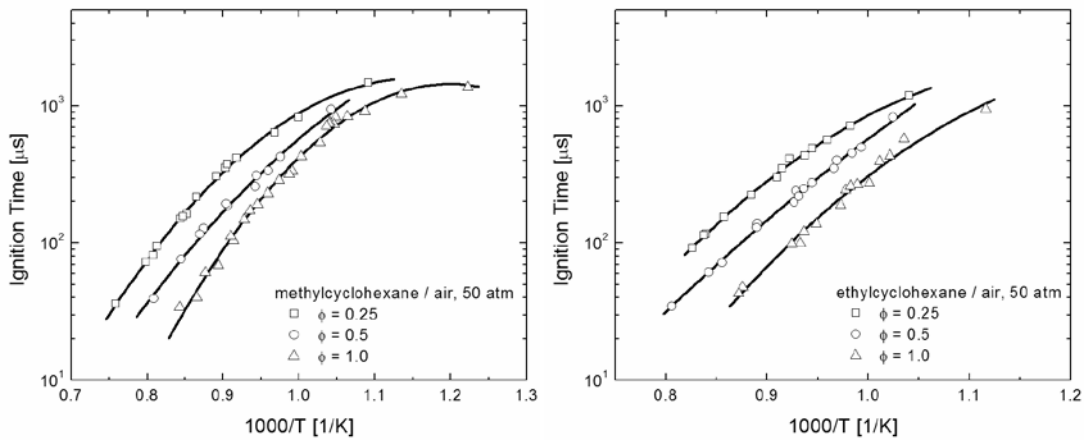

Figure 3.19 Ignition times for methylcyclohexane/air (left) and ethylcyclohexane/air (right) mixtures scaled to 50 atm using power-law pressure scaling parameters given in Table 3.2.

Comparisons of the current Φ = 1.0 MCH data with the previous shock tube studies of Orme et al. [48] and Vasu et al. [46] and the RCM study of Pitz et al. are made in Figure 3.21. The graph on the left in Figure 3.21 shows the raw data from these previous studies and the current study. The Φ = 1.0 Orme et al. measurements were performed for 1% MCH / 10.5% O_2 / Ar mixtures at 1, 2, and 4 atm and cover the temperature range 1220-1650 K. The Φ = 1.0 Vasu et al. measurements were performed for MCH/air mixtures (1.962% MCH / 20.60% O_2 / N_2) near 45 atm and cover the temperature range of 790-1120 K. The current study is in excellent agreement with the Vasu et al. measurements. Vasu et al. also made measurements for 1% MCH / 10.5% O_2 / Ar mixtures at 1.3-2.9 atm and 1225-1560 K, which agree fairly well with the Orme et al. measurements made for the same mixture at similar conditions.

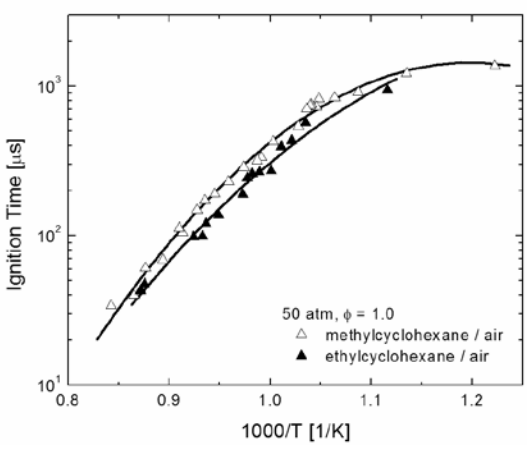

Figure 3.20 Comparison of ignition times for methylcyclohexane/air and ethylcyclohexane/air mixtures at Φ = 1.0 and 50 atm; data scaled to 50 atm using power-law pressure scaling parameters given in Table 3.2.

Direct comparison of the Orme et al. and Pitz et al. data with the current data and Vasu et al. data is not particularly useful due to the wide range of

experimental conditions investigated; however, the data can be scaled to a common condition to provide a useful comparison. Figure 3.21 (graph on the right) shows a comparison of the Φ = 1.0 data scaled to a common condition of 1.962% MCH (MCH concentration for stoichiometric MCH/air mixtures) and 50 atm. The data were scaled using $\tau \propto P^{-0.99}$, found in this study and in agreement with the Vasu et al. recommendation of $\tau \propto P^{-0.98}$ at lower pressures, and $\tau \propto X_{MCH}^{-0.82}$ (X_{MCH} is the MCH mole fraction), recommended by Vasu et al. These scaling parameters may vary at temperatures lower than those studied here where the chemistry shifts away from high- and moderate-temperature oxidation controlled by small molecule radical branching to low-temperature oxidation through peroxy compounds. With that caveat in mind, scaling the data using the above power law parameters provides excellent agreement between the current data, the Orme et al. data, the Vasu et al. data, and the 15 and 20 atm Pitz data at the intersections and overlap in the data sets. The 10 atm data of Pitz et al. does not agree with the current study or Vasu et al. when scaled. This difference presumably represents a failure of the simple power-law pressure dependence in the NTC regime. In combination these data sets provide kinetic targets for MCH over a large temperature range, 680 to 1650 K.

In addition to the comparison with previous experimental results, comparison is made with the two recently published kinetic mechanisms for MCH of Orme et al. [48] (190 species and 904 reactions) and Pitz et al. [47] (1001 species and 4436 reactions) in Figures 3.18 and 3.21. The Orme et al. mechanism was developed to describe the high-temperature oxidation of MCH and reproduces their shock tube results well. The Pitz et al. mechanism was developed to describe both the low- and high-temperature oxidation of MCH and was developed by starting with a base set of reactions for C_1-C_6 chemistry from previous mechanisms of Pitz, Westbrook, and co-workers [23,32], adding the high-temperature MCH reactions from the Orme et al. mechanism and the low-temperature chemistry of MCH. The mechanism subsequently was compared to the Pitz et al. RCM data, and modifications were made to the low-temperature MCH peroxy chemistry based on the static reactor work on peroxy reactions of Walker and co-workers [50-51] to predict the NTC behavior observed in the RCM experiments better. The Orme et al. and Pitz et al. mechanisms provide the same results for temperatures greater than 1200 K. The Orme et al. mechanism does not contain low-temperature peroxy chemistry. For all conditions, both mechanisms overpredict the measured ignition times. The Pitz et al. mechanism does a good job of predicting the temperature dependence throughout the large temperature range of the combined data sets in Figure 3.21 (graph on the right), capturing both the high-temperature activation energy and NTC behavior; however, the Pitz et al. predictions are a factor of three to five in excess of the measured ignition times.

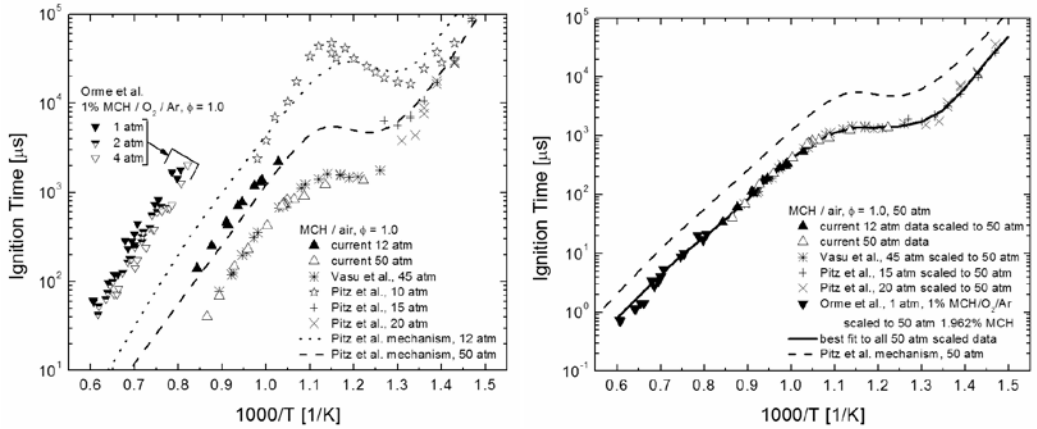

Figure 3.21 Current Φ = 1.0 methylcyclohexane ignition time measurements with comparison to previous shock tube measurements of Vasu et al. [46] and Orme et al. [48] and rapid compression machine (RCM) measurements and mechanism predictions of Pitz et al. [47].

Unfortunately, due to its large size we were unable to perform sensitivity analysis using the Pitz et al. mechanism. We did, however, perform sensitivity analysis using the Orme et al. mechanism for temperatures greater than 1000 K. The OH concentration, a marker of ignition and related to the ignition

time sensitivity, showed sensitivity to many of the reactions to which Orme et al. found ignition time sensitivity in their analysis at 1250 K and 1 atm. The sensitive reactions include many small molecule radical consumption and generation reactions, including hydrogen peroxide decomposition, $H_2O_2 + M \leftrightarrow 2OH + M$, and reaction with molecular oxygen, $H_2O_2 + O_2 \leftrightarrow 2HO_2$, H-atom reactions with molecular oxygen, $H + O_2 \leftrightarrow OH + O$ and $H + O_2 + M \leftrightarrow HO_2 + M$, methyl recombination, $CH_3 + CH_3 + M \leftrightarrow C_2H_6 + M$, and others. Other reactions that show sensitivity are the H-atom abstraction reactions from MCH, with $MCH + HO_2 \leftrightarrow C_7H_{13} + H_2O_2$ having the largest sensitivity. The accurate temperature-dependence prediction but over prediction of ignition time by the Pitz et al. mechanism for all temperatures, perhaps, suggests that the MCH consumption reactions in the mechanism are too slow. Over most of the temperature range displayed in Figure 3.21, H-atom abstraction is the primary means of MCH consumption, with thermal decomposition playing a role at the highest temperatures. There have been no measurements of H-atom abstraction rates from MCH, and the rate coefficients used in the Pitz et al. mechanism are based on rate coefficient estimation rules [23,32]. We arbitrarily increased the rate coefficients for H-atom abstraction from MCH in the Pitz et al. mechanism by a factor of five and found that the mechanism gave somewhat better agreement. The overprediction in ignition time was reduced from a factor of approximately three to five to a factor of approximately 1.5 to 2.5. The factor of five adjustment to MCH H-atom abstraction reactions is made without basis, and may be unreasonably large, but it does point out that the rates for H-atom abstraction are of importance and accurate measurement or quantum chemical calculation of these rates may provide improved predictions.

3.6 Decalin

Decalin has received previous interest as a jet fuel surrogate component [52] as well as an endothermic propulsion fuel or additive, potentially enabling cooling systems for hypersonic flight that use both chemical and sensible energy absorption. Example ignition time data for decalin are displayed on Arrhenius axes in Figure 3.22. In the temperature range investigated the ignition time measurements show exponential dependence on inverse temperature with no indication of NTC behavior. The ignition time results are characterized by little scatter about the linear least-squares fits shown in Figure 3.22 (±10%), and the uncertainty is estimated at ±20% in ignition time. The measured ignition times can be correlated using Arrhenius temperature dependence and power-law dependence on pressure and equivalence ratio resulting in $\tau = 4.05\times10^{-9}\ P^{-0.78}\ \Phi^{-0.81}\ \exp(14930/T\ [K])$ sec, where τ is the ignition time in seconds, T the temperature in Kelvins, and P the pressure in atmospheres. The data as presented in Figure 3.22, have been scaled to 12 and 40 atm to account for deviations in reflected shock pressure using the power-law pressure scaling given above. To the PI's knowledge, there have been no previous decalin ignition delay time measurements at conditions similar to those investigated here for comparison to the current study.

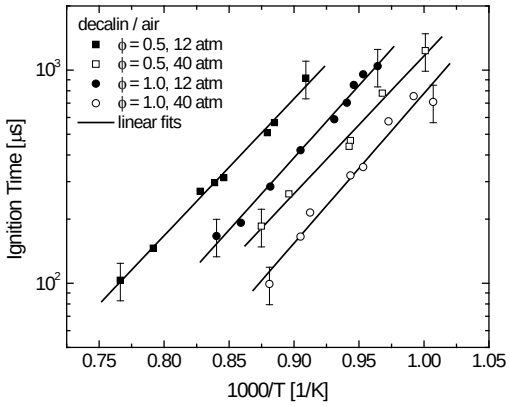

Figure 3.22 Ignition time results for decalin/air mixtures at Φ = 0.5 and 1.0.

A semi-detailed kinetic mechanism for the description of the high-temperature oxidation and pyrolysis of decalin has been developed by collaborators with our group at Politecnico di Milano (Eliseo Ranzi, Alessio Frassoldati, and Sauro Pierucci). The mechanism is based on simplified lumped reactions and species for description of the formation of decalin decomposition products. The further decomposition and/or oxidation of these smaller radicals and molecules then is described in a semi-detailed oxidation mechanism. The complete mechanism contains more than 300 species and more than 7000 reactions and is given in a joint paper by our group at RPI and the group at Politecnico di Milano [53].

Figure 3.23 shows the comparisons of measured ignition times with predictions from the Milano decalin mechanism. The kinetic predictions are in good agreement at Φ = 0.5, while ignition times are overpredicted systematically by 20-40% at Φ = 1.0. We consider the deviations of at most 40% to be good agreement in light of the kinetic complexity of decalin oxidation (7000 reactions in this lumped mechanism) and because the mechanism was developed *a priori* with no adjustments to rate parameters to fit data. A detailed mechanism would contain more than 75,000 reactions.

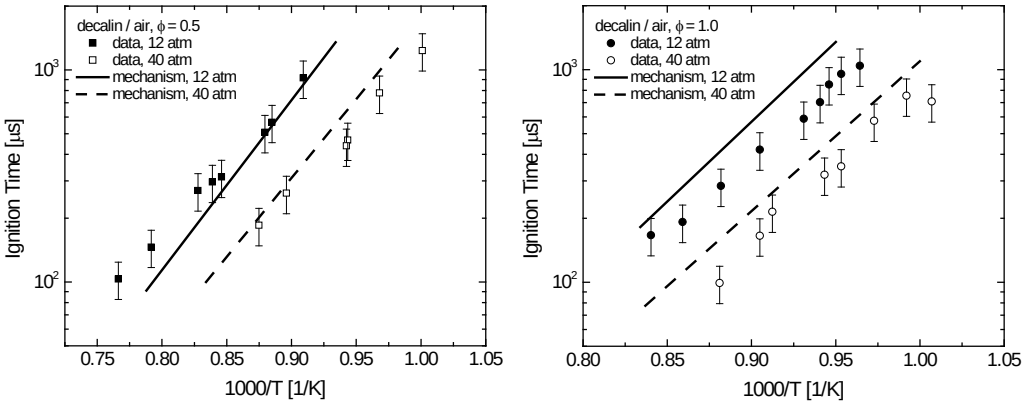

Figure 3.23 Comparison of measured ignition time with mechanism predictions.

Sensitivity analysis has been performed at a variety of stoichiometries, temperatures, and pressures. The results are summarized briefly in Figure 3.24. At 1000 K the analysis shows that, together with the H_2O_2 decomposition, the H-abstraction reactions for decalin are the most important reactions and increasing the rate coefficients for these reactions has a promoting influence on the overall reactivity. The sensitivity analysis also indicates that the decomposition of the decalin radical ($C_{10}H_{17}$) to form ethyl radicals and C_8 aromatics (ethylbenzene and xylenes) has an inhibiting effect on reactivity, while the decomposition path to form cyclohexane and C_4H_7 radicals has a promoting effect.

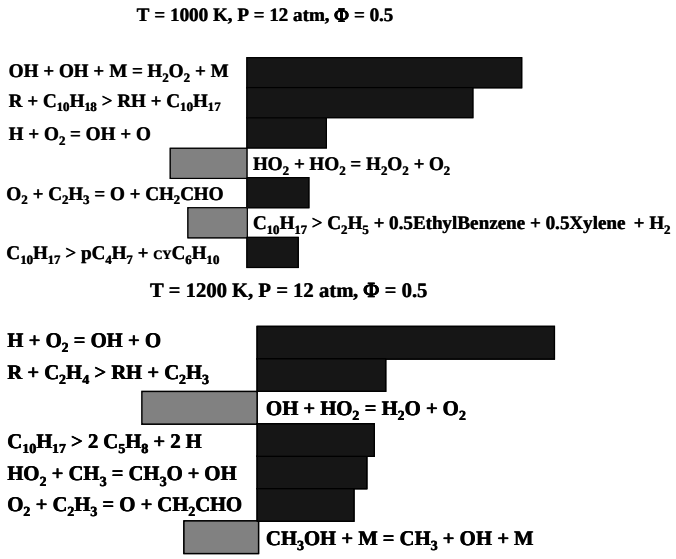

Figure 3.24 Sensitivity analysis for OH formation at 1000 K (top) and 1200 K (bottom).

As typical for hydrocarbon fuels, at 1200 K the reactivity is controlled by the H + O_2 → OH + O radical branching reaction. Also showing positive sensitivity (promoting reactions) are the H-abstraction reactions from ethylene (C_2H_4) to form the vinyl radical (C_2H_3), which, due to the successive branching reaction O_2 + C_2H_3 → CH_2CHO + OH, has a promoting influenced on overall reactivity. Abstraction reactions from decalin show negligible sensitivity, while the decomposition of the decalin radical ($C_{10}H_{17}$) to pentadiene (C_5H_8) and H atoms has a positive sensitivity. Although there are a large number of alternative reaction paths for the decalin radical, the sensitivity of the reaction flux fractions is small, while the sensitivity of the overall rate is significant. Improvement of this decalin kinetic mechanism will require more detailed analysis of the decomposition of decalin and additional experiments to probe this process adequately; however, the decalin kinetic mechanism developed by the Milano group is the first comprehensive oxidation mechanism for decalin and pushes the boundaries in terms of size (from a combustion kinetic modeling perspective, decalin is a very large molecule). The comparisons made here between experiment and kinetic simulations are quite good in light of the kinetic modeling challenges.

3.7 Toluene

Example ignition delay results for toluene, an important representative aromatic compound, are shown in Figure 3.25. The results show little scatter, with rms scatter about the linear fits of ±8%, and the uncertainty in measured ignition time is estimated at ±15%. The ignition times show no variation in overall activation energy in the studied temperature range and no indication of negative temperature coefficient behavior. The ignition times show power-law pressure dependence, $\tau \propto P^{-n}$; however, the power-law exponent, n, was observed to vary as a function of equivalence ratio, Φ. A single correlation for ignition time cannot be formulated, but correlations for the three studied equivalence ratios in terms of pressure and temperature can be formulated. The following correlations result from regression analysis for the ignition times at Φ = 1.0, 0.5, and 0.25:

$$\Phi = 1.0: \tau = 2.37 \times 10^{-8}\, P^{-1.09} \exp(15640 / T\,[\mathrm{K}])\ \mathrm{sec},$$

$$\Phi = 0.5: \tau = 5.14 \times 10^{-9}\, P^{-0.50} \exp(15330 / T\,[\mathrm{K}])\ \mathrm{sec},$$

$$\Phi = 0.25: \tau = 1.24 \times 10^{-8}\, P^{-0.23} \exp(13540 / T\,[\mathrm{K}])\ \mathrm{sec},$$

where τ is the ignition time in seconds, T the temperature in Kelvins, and P the pressure in atmospheres. Figure 3.26 shows the ignition data scaled to 50 atm using the above power-law pressure scaling. The differing ignition time dependence on pressure for different equivalence ratios results in different dependence of ignition time on equivalence ratio at the two studied pressures (nominally 12 and 50 atm).

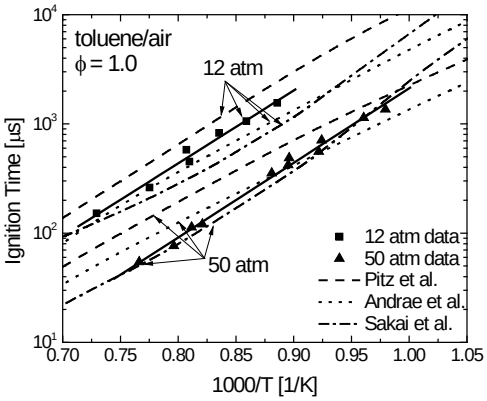

Figure 3.25 Ignition time measurements for toluene/air mixtures at 12 and 50 atm and Φ = 1.0 with comparison to predictions of three kinetic mechanisms. Ignition times were scaled to 12 and 50 atm, to account for slight deviations in reflected shock pressure, using power-law pressure scaling as determined by regression analysis.

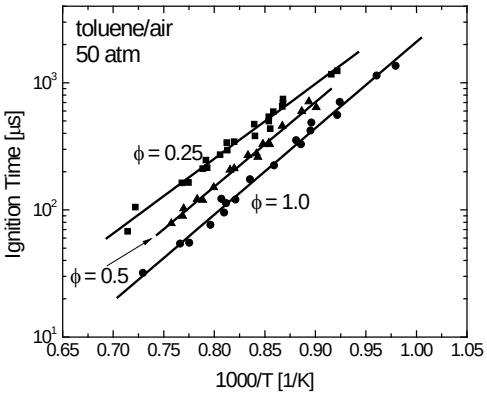

Figure 3.26 Ignition time measurements for toluene/air scaled to 50 atm using power-law pressure scaling.

The measured ignition times for Φ = 1.0 and 0.5 are compared to the data of Davidson et al. [29] and Mittal and Sung [54] in Figure 3.27 using scaling factors given by those authors to scale the data to common conditions. The data of Davidson et al. are in agreement for Φ = 0.5 and for temperatures in excess of 1100 K for Φ = 1.0. For Φ = 1.0 and temperatures less than 1100 K, Davidson et al. report shorter ignition times than measured here. The RCM experiments of Mittal and Sung were performed in argon/N_2 baths at temperatures of 920-1100 K, pressures of 25-45 atm, Φ = 0.5-1.0, and O_2 concentrations of 5.4-17.3%. Their data display an overall activation energy (61.1 kcal/mol) a factor of two greater than that observed in these experiments (31.1 kcal/mol at Φ = 1.0). The difference between these two results likely is due to the heat loss that occurs following compression in the Mittal and Sung RCM versus the near adiabatic shock tube environment utilized here. See Würmel et al. [30] for a detailed discussion of the influence of heat loss on ignition experiments.

The predictions of three recently published toluene kinetic mechanisms are compared to the current ignition measurements in Figure 3.25. The mechanisms examined are those of Pitz et al. (379 species and 1621 reactions) [55], Sakai et al. (758 species and 2883 reactions) [56], and Andrae et al. (1083 species and 4635 reactions) [57]. These mechanisms all are related to the mechanisms developed by Pitz, Westbrook, and coworkers at Lawrence Livermore National Laboratory (LLNL) [23,32]. Both the Sakai et al. and Andrae et al. mechanisms were developed to model n-heptane/iso-octane/toluene mixtures and were

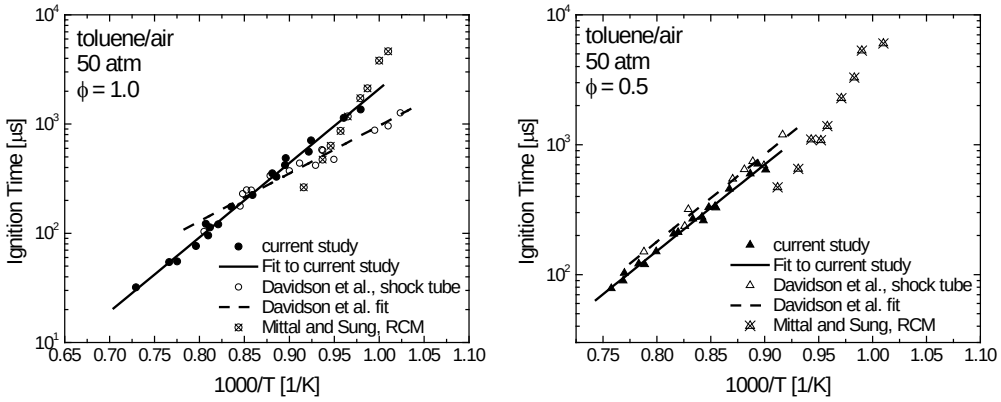

Figure 3.27 Comparison of current ignition time measurements for toluene/air at 50 atm and Φ = 1.0 (left) and Φ = 0.5 (right) with previous studies.

formed using the LLNL primary reference fuel (PRF) mechanism for n-heptane and iso-octane [23,32] as a starting point. In the Sakai et al. mechanism much of the toluene chemistry comes from the original Pitz et al. toluene mechanism. Sakai et al. modified the Pitz et al. mechanism by updating rate coefficients for several toluene and benzyl reactions using values from recent experimental and theoretical studies. The Andrae et al. mechanism was formed by adding the toluene submechanism of Sivaramakrishnan et al. [58] to the LLNL PRF mechanism. Sakai et al. also made rate coefficient changes and additions for several reactions involving the benzyl radical ($C_6H_5CH_2$), the alkoxy benzyl radical ($C_6H_5CH_2O$), and toluene ($C_6H_5CH_3$).

The comparisons (Figure 3.25) indicate that all of the mechanisms do a reasonable job at predicting the measured ignition times. The Pitz et al. mechanism predicts ignition times that are generally longer than that measured with a maximum difference of a factor of two. The Andrae et al. mechanism predicts ignition times that are in fair agreement with the current data but with overall activation energies that are generally lower. The predictions of the Sakai et al. mechanism are in good overall agreement, with differences of at most 20% with the 50 atm data and differences of at most 50% when compared to the 12 atm data.

Sensitivity analysis was performed using all three mechanisms to examine how the differences in the toluene submechanisms influenced ignition time predictions. The results of the Pitz et al. mechanism displayed strong sensitivity for $H+O_2+M \rightarrow HO_2+M$, $H+O_2 \rightarrow O+OH$, $C_6H_5CH_3+H \rightarrow C_6H_6+CH_3$, $CH_2O+OH \rightarrow HCO+H_2O$, and others but did not exhibit sensitivity to $C_6H_5CH_3+O_2$ or $C_6H_5CH_2+O_2$. The Andrae et al. mechanism displays extremely strong sensitivity for the lumped reaction $C_6H_5CH_2+O_2 \rightarrow C_6H_5+CH_2O+O$, for which they tuned the rate coefficient to fit the ignition times at 50 atm of Davidson et al. [29], and much weaker sensitivity for all other reactions. The products suggested by Andrae et al. are not predicted to be likely by quantum chemical calculations of the $C_6H_5CH_2+O_2$ potential energy surface by Murakami et al. [59] and are not likely from the perspective of the reverse reaction.

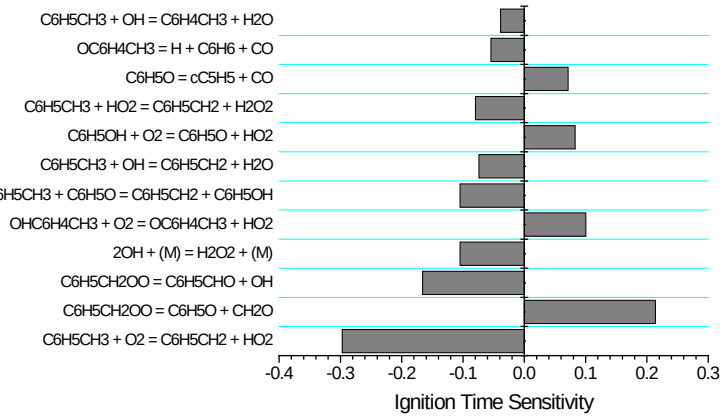

Figure 3.28 Ignition time sensitivity, $\partial(\tau/\partial k_i)(k_i/\tau)$, calculated with Sakai et al. mechanism [56] for toluene/air at 1100 K, 50 atm, and Φ = 1.0.

The mechanism of Sakai et al., which is in good agreement with the current data, shows the strongest sensitivity to the oxygen reaction with toluene, $C_6H_5CH_3+O_2 \rightarrow C_6H_5CH_2+HO_2$, and the two product channels for benzylperoxy unimolecular decomposition, $C_6H_5CH_2OO \rightarrow C_6H_5CHO+OH$ and $C_6H_5CH_2OO \rightarrow C_6H_5O+CH_2O$. Benzylperoxy is formed via the chemical activation reaction $C_6H_5CH_2+O_2$. See Figure 3.28 for ignition time sensitivity using the Sakai et al. mechanism at 1100 K and 50 atm. Sakai et al. use a rate coefficient for $C_6H_5CH_3+O_2$ taken from the direct experimental determination of Oehlschlaeger et al. [60], which has small uncertainty (±20%). The rate parameters for the formation and decomposition of benzylperoxy have far greater uncertainty. Sakai et al. use product channels ($C_6H_5CHO+OH$ and $C_6H_5O+CH_2O$) and estimated pressure-dependent rate coefficients for $C_6H_5CH_2+O_2 \leftrightarrow C_6H_5CH_2OO$, $C_6H_5CH_2OO \rightarrow C_6H_5CHO+OH$, and $C_6H_5CH_2OO \rightarrow C_6H_5O+CH_2O$ based on a quantum chemical calculation performed by Murakami et al. [59]. This reaction is pressure dependent, has multiple product channels, and is slow relative to other radical + O_2 reactions due to the low well depth for the benzylperoxy radical (approximately -22 kcal) that favors dissociation back to $C_6H_5CH_2+O_2$. The strong sensitivity that the ignition times exhibit for $C_6H_5CH_2+O_2$, the complexity of this reaction (multiple channels and pressure dependence), and the lack of previous direct experimental and theoretical investigations indicate that this reaction should be investigated further and improvements to the toluene mechanisms might result from improved knowledge of the rate parameters for $C_6H_5CH_2+O_2$. As is shown in Figure 3.28, the ignition delay exhibits opposite sensitivity for the two product channels of benzylperoxy decomposition, and changes to the pressure dependence of the product fractions will modify the predicted ignition time dependence on pressure and equivalence ratio.

3.8 C_8H_{10} Aromatics

See Figure 3.29 for examples of autoignition results for the C_8H_{10} aromatics, compounds that are representative of the lighter aromatics found in jet fuels. The uncertainty in measured ignition time is estimated at ±20% (95% probability). The overlap in data points and the small scatter in Figure 3.29 illustrates the high level of repeatability for these measurements. The ignition data exhibit Arrhenius temperature dependence with no NTC behavior at the conditions studied and power-law pressure dependence. Thus, ignition time correlations of the form $\tau = A\ P^{n} \exp(B / T)$ can be formulated for each mixture studied. See Table 3.3 for correlation parameters. The data displayed in Figure 3.29 have been scaled to 10 and 40 atm using the correlations given in Table 3.3 to account for deviations in the reflected shock pressure. The correlations should not be extrapolated far from the conditions of the current experiments, as the governing chemistry and mixture exothermicity will vary with differences in condition and mixture, resulting in variation in ignition time dependence on temperature and pressure.

Table 3.3 Ignition time correlation parameters based on least-squares regression. Correlations are of the form $\tau = A\ P^{n} \exp(B / T)$ where the ignition time, τ, is in seconds, temperature, *T*, is in Kelvins, and pressure, *P*, is in atmospheres.

Compound	Φ	A [sec]	n	B [K]	rms scatter [%]
o-xylene	0.5	$2.24(\pm0.48) \times 10^{-8}$	-0.90 (± 0.03)	14870 (±290)	5.7
o-xylene	1.0	$4.32(\pm1.57) \times 10^{-8}$	-1.06 (± 0.05)	14300 (±450)	7.9
m-xylene	0.5	$1.05(\pm0.36) \times 10^{-8}$	-0.70 (± 0.04)	15150 (±440)	7.1
m-xylene	1.0	$1.66(\pm0.80) \times 10^{-8}$	-0.98 (± 0.08)	15400 (±680)	9.1
p-xylene	0.5	$1.75(\pm0.45) \times 10^{-8}$	-0.68 (± 0.04)	14590 (±320)	6.4
p-xylene	1.0	$1.74(\pm0.74) \times 10^{-8}$	-0.97 (± 0.05)	15580 (±520)	8.1
ethylbenzene	0.5	$5.59(\pm3.24) \times 10^{-10}$	-0.45 (± 0.05)	16390 (±530)	8.8
ethylbenzene	1.0	$3.19(\pm2.16) \times 10^{-9}$	-1.00 (± 0.07)	15880 (±690)	8.4

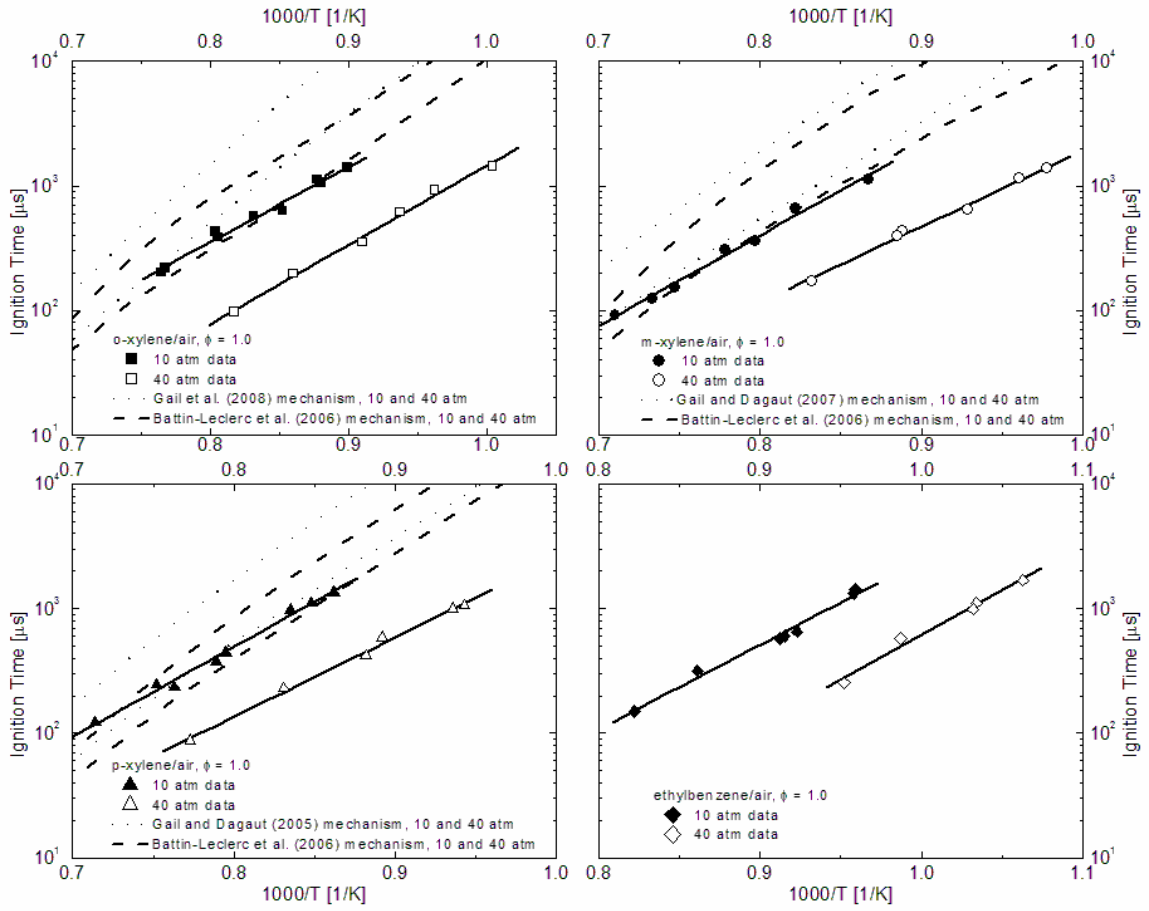

Figure 3.29 Ignition time measurements for Φ = 1.0 C_8H_{10}/air mixtures with comparison to mechanisms for the three xylene isomers [61-64]. Data scaled to 10 and 40 atm using power-law pressure scaling factors given in Table 3.3, to account for deviations in reflected shock pressure.

Ignition times for m-xylene, o-xylene, p-xylene, and ethylbenzene, all scaled to 40 atm using the pressure scaling parameters given in Table 3.3 are compared in Figure 3.30 along with a comparison the toluene results at 40 atm. The ignition times for all the C_8H_{10} aromatics and toluene (C_7H_8) exhibit approximately the same overall activation energy; however, there are differences in the ignition times of the aromatic compounds. The ignition times for the C_8H_{10} compounds vary from longest (least reactive) to shortest (most reactive) in the order p-xylene, m-xylene, o-xylene, and ethylbenzene. The ignition times for p-xylene are essentially identical to those for toluene, and the difference in the p-xylene and m-xylene ignition times is small (10-20%, within the uncertainties). The o-xylene ignition times are approximately 20-30% shorter than those for m-xylene, while the ethylbenzene ignition times are a factor of two to three shorter than those for o-xylene. In previous RCM studies Roubaud et al. [65] observed that o-xylene and ethylbenzene display significantly greater reactivity than p-xylene, m-xylene, and toluene at temperatures below 900 K at 16 bar. At the conditions encountered in the Roubaud et al. RCM, ignition times were shorter for o-xylene than for ethylbenzene. The opposite was found in this study at higher temperatures. In contrast to both this study and Roubaud et al. [65], Battin-Leclerc et al. [64] observed essentially no difference in ignition delay time for the three xylene isomers at higher temperatures (1330-1800 K) for dilute mixtures.

The differences in reactivity observed for the C_8H_{10} aromatics in the three experimental studies (this study, Roubaud et al. [65], and Battin-Leclerc et al. [64]) are due to different chemical pathways of importance at low and high temperatures. At the high-temperature dilute conditions studied by Battin-Leclerc et al. [64], unimolecular decomposition consumes most of the fuel, and the reactivity is controlled

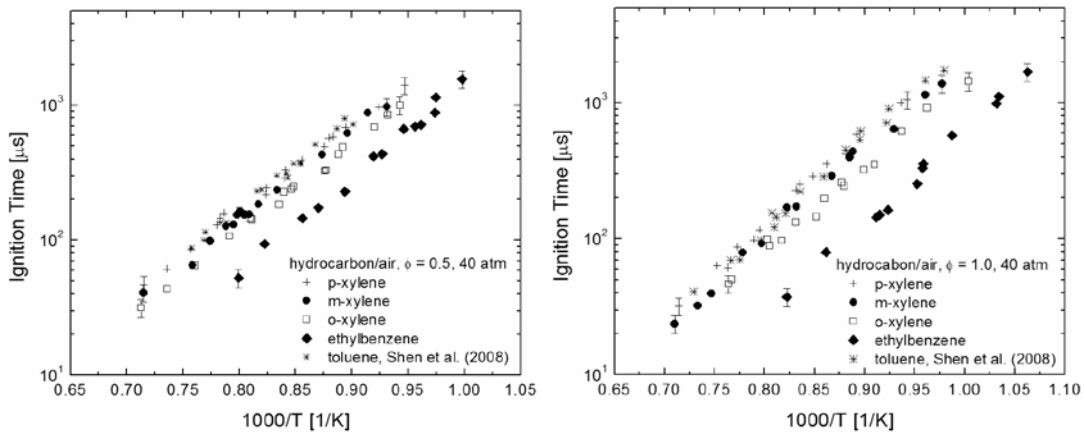

Figure 3.30 Ignition times for C_8H_{10}/air mixtures and toluene/air scaled to 40 atm using power-law pressure scaling factors given in Table 3.3: Φ = 0.5 (left) and Φ = 1.0 (right).

simply by the number of H atoms in the fuel and the C-C and C-H bond strengths, which are independent of xylene isomeric structure; thus, approximately the same ignition time was observed for the three xylene isomers under their high-temperature, low-pressure dilute shock tube conditions. At the lower temperatures encountered in the Roubaud et al. studies, the aromatics are consumed primarily via H-atom abstraction, creating primary aromatic radicals, with the radical site on the side chain, which associates with molecular oxygen to form a peroxy radical and reacts via a low-temperature oxidation reaction pathway [65]. The relative reactivity of alkylbenzenes at low temperatures is controlled by the rate of isomerization (H-atom transfer) following O_2 addition to the primary radical, which is controlled by the number, length, and position of the side chains.

For the moderate-temperature conditions studied here (941-1408 K) there is presumably primary influence from high-temperature oxidation chemistry; however, at these temperatures the fuel consumption takes place via both H-atom abstraction by radicals (H, O, OH, HO_2, CH_3, etc.) and O_2 and unimolecular decomposition. Here the fuel consumption for ethylbenzene is faster than that for the xylenes because of the weak C-C bond (77.6 kcal/mol bond energy) in the ethylbenzene ethyl group, which allows relatively fast unimolecular decomposition, $C_6H_5C_2H_5 \rightarrow C_6H_5CH_2 + CH_3$. Additionally, the two secondarily bonded H atoms in the ethylbenzene ethyl group (85.4 kcal/mol bond energy) are abstracted more easily than the primarily bonded H atoms in the xylene methyl groups (87.3-88.8 kcal/mol bond energy). The primary channel for the unimolecular decomposition of the xylene isomers, $CH_3C_6H_4CH_3 \rightarrow CH_3C_6H_4CH_2 + H$, is relatively slow at the conditions studied due to the relatively high bond energies. The xylene isomers are consumed primarily via H-atom abstraction by radicals to produce methylbenzyl and phenyl$(CH_3)_2$ radicals. C-C bond fission for the xylenes is a minor secondary channel of negligible importance at these conditions. The faster fuel consumption during ethylbenzene oxidation provides a more rapid build up in the radical pool and shorter ignition times relative to the xylenes.

The subtle differences observed in the xylene isomer ignition measurements at temperatures below 1200 K likely are due to the secondary influence of $CH_3C_6H_4CH_2$ (methylbenzyl) + $O_2 \rightarrow CH_2C_6H_4CH_2$ (xylylene) + HO_2. This reaction proceeds via the addition of O_2 to methylbenzyl, the isomerization of the methylbenzyl peroxy radical (H-atom transfer), and the scission of the hydroperoxyl radical. This reaction proceeds more quickly for o-xylene because of the unstrained transition state that occurs when the H atom is transferred from a methyl group in the ortho-position. In the case of m-xylene and p-xylene the H-atom transfer from a methyl group located in the meta- or para-position results in a strained transition state and slow reaction to HO_2 and xylylene. This reaction is of minor importance relative to the consumption of methylbenzyl by radicals at the conditions studied; hence, the differences in measured ignition times for the xylene isomers are small.

The xylene ignition time measurements are compared to predictions of the comprehensive kinetic mechanisms of Battin-Leclerc et al. [64] and Gaïl et al. [61-63] for the three isomers of xylene in Figure 3.29.

The Battin-Leclerc et al. and Gaïl et al. mechanisms were developed to describe low-pressure xylene oxidation and validated using low-pressure shock tube, jet-stirred reactor, and flow reactor data and greatly over predict the ignition times at the elevated-pressure conditions studied here. Sensitivity analysis was performed using the Battin-Leclerc et al. mechanisms to determine reactions that could be considered for improvement to the mechanism predictions. Results of the sensitivity analysis are shown in Figure 3.31 for 1100 K and 40 atm for the three xylene isomers. The two most sensitive reactions are the abstraction of H atoms from the xylenes by OH to form methylbenzyl ($CH_3C_6H_4CH_2$) and H_2O, which is the primary xylene consumption reaction at the conditions studied, and the association of HO_2 with methylbenzyl, which leads to more reactive OH radicals and H atoms through the following sequence:

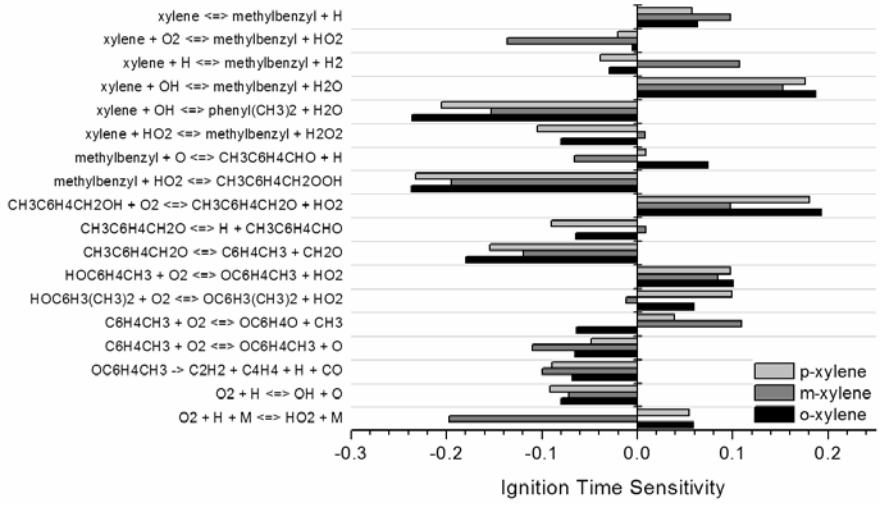

Figure 3.31 Ignition time sensitivity calculated with the Battin-Leclerc et al. [64] mechanism for the ignition of a Φ = 1.0 xylene/air mixture at 1100 K and 40 atm. Ignition time sensitivity defined as fractional change in ignition time for an increase in the rate coefficient for a given reaction of a factor of two.

$$\text{methylbenzyl} + HO_2 \rightarrow CH_3C_6H_4CH_2OOH \quad \text{(R1)}$$
$$CH_3C_6H_4CH_2OOH \rightarrow CH_3C_6H_4CH_2O + OH \quad \text{(R2)}$$
$$CH_3C_6H_4CH_2O \rightarrow CH_3C_6H_4CHO + H \quad \text{(R3)}$$
$$CH_3C_6H_4CH_2O \rightarrow C_6H_4CH_3 + CH_2O \quad \text{(R4)}$$

The rate coefficients for xylene + OH → methylbenzyl + H_2O used in the Battin-Leclerc et al. [64] mechanism are taken from the IUPAC review (Baulch et al. [66]) and are in good accord with low uncertainty (±25%) measurements of the similar toluene + OH → benzyl + H_2O reaction [67-68]; therefore, large changes to these rate coefficients, which would be needed for better agreement with the ignition time measurements, are not justified.

On the other hand, the rate coefficient for the association of HO_2 with methylbenzyl has large uncertainty, and adjustment of this rate may be justified. To our knowledge, there have been no measurements or theoretical calculations of the methylbenzyl + HO_2 reactions; however, there has been some work on the similar reaction of benzyl with HO_2. The Battin-Leclerc et al. mechanism uses a rate coefficient of 5×10^{12} $cm^3mol^{-1}s^{-1}$ for R1, methylbenzyl + HO_2, which was recommended by Hippler et al. [69] for benzyl + HO_2 based on fitting benzyl oxidation experiments. Recently, da Silva and Bozzelli [70] also have recommended a rate coefficient of 5×10^{12} $cm^3mol^{-1}s^{-1}$ for R1 based on quantum chemical calculations. On the other hand, Sivaramakrishnan et al. [58] recommend a much higher rate coefficient for benzyl + HO_2 based on collision theory, fitting their high-pressure toluene oxidation measurements at similar conditions to those studied here, and recommend rate coefficients of 3.67×10^{14} $cm^3mol^{-1}s^{-1}$ and 1.17×10^{14} $cm^3mol^{-1}s^{-1}$ for the overall reactions benzyl + HO_2 → C_6H_5CHO + OH + H and benzyl + HO_2 → C_6H_5 + CH_2O + OH, respectively. Other mechanistic studies of toluene oxidation also have employed rate coefficients greater than 5×10^{12} $cm^3mol^{-1}s^{-1}$ for R1. For example Pitz et al. [55] in their mechanism, use a three-parameter Arrhenius expression for R1 ($k_1 = 2.46\times10^{55}$ $T^{-11.97}$ exp(-14555[K]/T) $cm^3mol^{-1}s^{-1}$) that yields a rate coefficient near 1.4×10^{13} $cm^3mol^{-1}s^{-1}$ for 1000-1500 K.

In Figure 3.32 simulations performed using two sets of modifications (labeled “Modification 1” and “Modification 2”) to the Battin-Leclerc et al. base mechanism are presented for m-xylene. In the simulations

labeled "Modification 1" the rate coefficients for methylbenzyl + HO_2 are taken from the Sivaramakrishnan et al. toluene study (i.e., $k = 3.67\times10^{14}$ $cm^3mol^{-1}s^{-1}$ and $k = 1.17\times10^{14}$ $cm^3mol^{-1}s^{-1}$ for methylbenzyl + $HO_2 \rightarrow CH_3C_6H_4CHO + OH + H$ and methylbenzyl + $HO_2 \rightarrow C_6H_4CH_3 + CH_2O + OH$, respectively). In the simulations labeled "Modification 2" the rate coefficient for methylbenzyl + $HO_2 \rightarrow CH_3C_6H_4CH_2OOH$, within the reaction scheme contained in the original Battin-Leclerc et al. [64] mechanism (R1-R4), was adjusted to best fit the ignition time data for the three xylene isomers presented here, resulting in $k_1 = 3.0\times10^{13}$ $cm^3mol^{-1}s^{-1}$ (a factor of six greater than the base mechanism). In addition to changes made to the methylbenzyl + HO_2 reaction, in both "Modification 1" and "Modification 2" the rate coefficients for xylene + $O_2 \rightarrow$ methylbenzyl + HO_2 were changed to twice the value measured by Oehlschlaeger et al. [60] for toluene + $O_2 \rightarrow$ benzyl + HO_2. The factor of two adjustment was included to account for the two methyl side chains in the xylenes versus the single methyl side chain in toluene. The changes made to the rate coefficients for the xylene + O_2 reactions result in an approximately 25% reduction in the predicted ignition time in Modifications 1 and 2 versus the base Battin-Leclerc et al. mechanism. The remainder of the large reduction in ignition time predictions for the two modified mechanisms relative to the base Battin-Leclerc et al. mechanism (factor of 3-8 shown in Figure 3.32) is due to the changes made to the methylbenzyl + HO_2 reactions. Finally, simulations using the modified mechanisms were preformed for all three xylene isomers and yielded very similar results. The best fit for R1 in "Modification 2", $k_1 = 3.0\times10^{13}$ $cm^3mol^{-1}s^{-1}$, is the result of fitting all the data for the three isomers. Based on this analysis, we suggest that further experimental and theoretical study of methylbenzyl + HO_2 and benzyl + HO_2 is warranted.

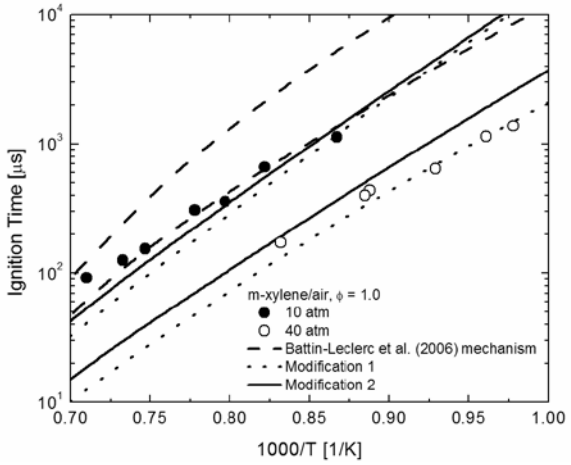

Figure 3.32 Comparison of m-xylene/air ignition measurements at 10 and 40 atm with the base Battin-Leclerc et al. [64] mechanism (dashed lines) and simulations in which the Battin-Leclerc et al. mechanism was modified (dotted and solid lines). See the text for a description of the modifications.

3.9 α-Methylnaphthalene and α-Methylnaphthalene/n-Decane Blends

Example ignition delay times for α-methylnaphthalene (AMN)/air mixtures are displayed in Figure 3.33. The ignition times for neat AMN exhibit strictly Arrhenius temperature dependence with no change in activation energy throughout the studied temperature range. The lack of non-Arrhenius NTC behavior in the ignition delay plots is consistent with results for monocyclic aromatics hydrocarbons (toluene, p-, m-, and o-xylene, and ethylbenzene) at similar conditions. The AMN/air ignition delay results can be fit to a correlation of the form $\tau = A\ P^n\ \Phi^m \exp(B/T)$. The resulting correlation for the 60 AMN/air experiments reported is $\tau = 1.27 \times 10^{-2}\ P^{-0.85}\ \Phi^{-0.43} \exp[15200 / T]$ (μs), where the pressure P is in bars, the temperature T is in Kelvins, and the ignition delay time τ is in microseconds. In Figure 3.33 and in all figures to follow the ignition delay times have been scaled to pressures of 10 and 40 bar for comparison using $\tau \propto P^n$, where n is determined by experiment, to account

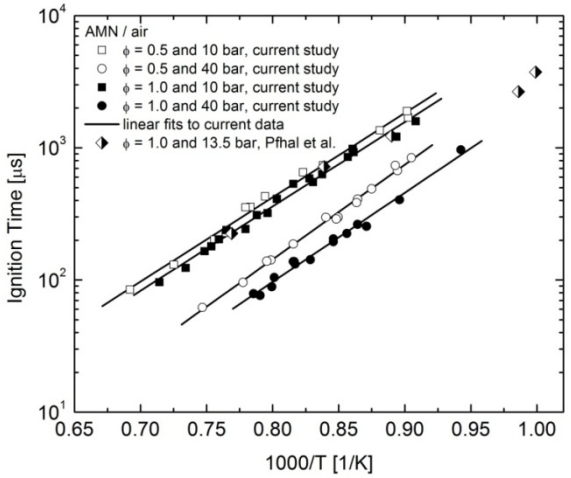

Figure 3.33 Ignition delay times for AMN/air mixtures. To account for deviations in pressure, current data are scaled to 10 and 40 bar using $\tau \propto P^{-0.85}$.

for deviations in reflected shock pressure. When scaled for pressure deviations, the experimental data exhibit a low level of scatter. The data in Figure 3.33 have scatter about the linear least-squares fits of ±7% (1σ standard deviation). The small scatter relative to the estimated uncertainties is indicative of the high level of reproducibility of these experiments, characteristic of this facility, and illustrates that most of the estimated uncertainty in ignition delay time stems from potential sources of systematic uncertainty (most importantly, initial reflected shock temperature), whose uncertainties have been estimated conservatively (95% probability).

Figure 3.33 also shows a comparison of the current ignition delay measurements for AMN/air with the results of Pfhal et al. [22] for Φ = 1.0 AMN/air mixtures at reflected shock pressures near 13.5 bar. In this plot, we only display experiments for which Pfhal et al. report strong ignition (five experiments of seven). Pfhal et al. report the observation of a mild ignition process (i.e., energy release indicated by a rise in pressure) that occurs prior to strong ignition (indicated by a rapid spike in pressure) for their five experiments from 1000 to 1300 K. In the Pfhal et al. experiments the mild ignition process results in a significant amount of energy release prior to strong ignition, an increase in measured pressure from ~13 bar to 20-30 bar over a time period that is approximately 20-30% of the total delay time to detonation. See Figure 2.6 for a neat AMN/air example. We did not observe a large pressure rise prior to strong ignition in this high- to moderate-temperature regime. Instead we observed a flat pressure profile, followed by a very rapid release in energy that leads directly to strong ignition. Despite the differences in pressure profiles, the ignition times reported by Pfahl et al. and are in good agreement with those reported here. The kinetic models available in the literature for AMN do not show the pressure behavior observed by Pfahl et al., and a simple understanding of the low-temperature peroxy reaction sequence, which is responsible for low-temperature mild ignition processes in alkanes, indicates that it should be very slow for AMN (i.e., H-atom transfer from the aromatic ring, $RO_2 \rightarrow QOOH$ that is an initial and rate-limiting step in the low-temperature radical branching sequence R ($+O_2$) → RO_2 → QOOH ($+O_2$) → OOQOOH → 2OH + products is very slow for AMN due to the high strength of the ring-H bonds).

The ignition delay times for 30%-molar/70%-molar and 70%-molar/30%-molar AMN/n-decane blends (CN = 58 and 28) at Φ = 1.0 in air are shown in Figure 3.34 with comparison to the Φ = 1.0 neat AMN/air (CN = 0) and Φ = 1.0 neat n-decane/air (CN = 76) data obtained as part of this project. The difference in ignition time between neat AMN and n-decane is around a factor of four for temperatures of approximately 1150 to 1350 K, and, at lower temperatures, the differences become larger due to NTC rollover in the ignition delay times for neat n-decane. The ignition delay times for AMN/n-decane blends fall between the measurements for neat AMN and n-decane with decreasing ignition time and increasing NTC behavior for increasing n-decane fraction. Additionally, as expected, the ignition delay times for AMN/n-decane blends decrease and exhibit increased NTC behavior with increasing pressure. The ignition time dependence on AMN fraction and cetane number is non-linear and non-power-law as is illustrated best by the small differences in the ignition delay times for stoichiometric neat n-decane/air and 30%-molar AMN / 70% n-decane / air mixtures, indicating that the addition of a significant fraction of the low-reactivity radical-scavenging AMN does not alter the ignition time significantly from that of neat n-decane. The ignition times for Φ = 1.0 30%-molar AMN / 70% n-decane / air mixtures are 15-30% longer than those for Φ = 1.0 neat n-decane/air based on the differences in second-order polynomial least-squares fits to the data sets not shown in the figures for readability.

Because of the NTC rollover with decreasing temperature exhibited by the ignition times for AMN/n-decane blends on Arrhenius axes, the data cannot be correlated using an Arrhenius expression; however, the ignition data do follow the same pressure dependence as observed for neat AMN, $\tau \propto P^{-0.85}$. The suitability of the $\tau \propto P^{-0.85}$ scaling is illustrated in Figure 3.35, where the ignition times are scaled to a common pressure of 40 bar and fit to common second-order polynomials. The neat n-decane data were scaled to common pressures using $\tau \propto P^{-1.0}$, as previously applied.

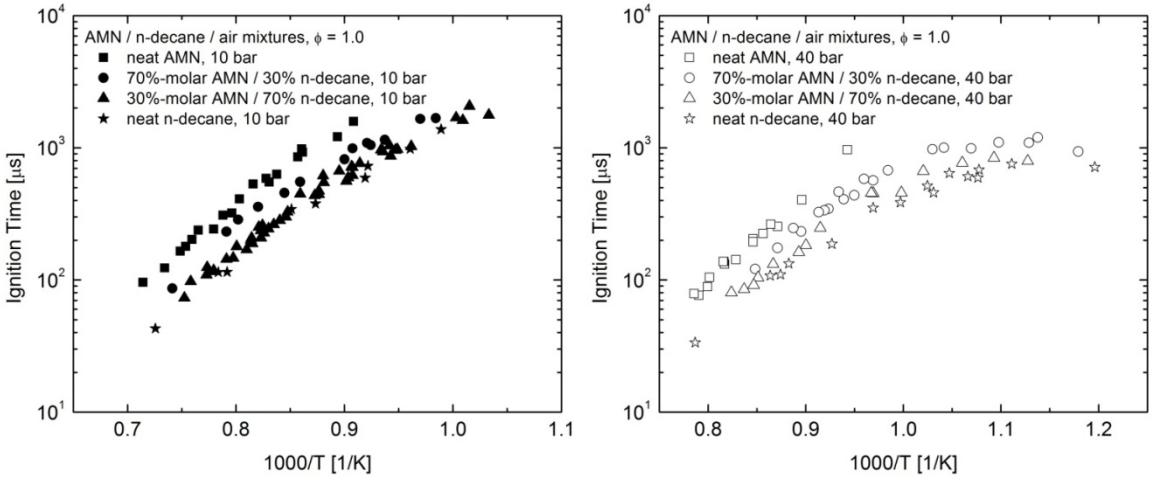

Figure 3.34 Ignition delay times at 10 bar (left) and 40 bar (right) for Φ = 1.0 AMN/air, n-decane/air, and 70%-molar/30%-molar and 30%-molar/70%-molar mixtures of AMN and n-decane in air. To account for deviations in pressure, data are scaled to 10 bar using $\tau \propto P^n$, where n = -0.85 for neat AMN and AMN/n-decane mixtures and n = -1.0 for neat n-decane mixtures.

To describe the oxidation of AMN/n-decane blends, the mechanism previously proposed by Bounaceur et al. [71] has been updated and modified through collaboration with the EXGAS group at Nancy led by F. Battin-Lerclerc. The mechanism developed includes oxidation kinetics for n-decane, automatically generated using the EXGAS software routine, a mechanism for the oxidation of AMN, and the cross reactions necessary to describe the interactions between the two fuels. The complete mechanism includes 3884 reactions involving 662 species, see [72]. Comparisons of ignition delay time measurements with simulations made using the detailed mechanism are shown in Figure 3.36. The predictions of ignition delay times for Φ = 1.0 and 0.5 AMN/air mixtures are in excellent agreement with experiment, and the simulations for AMN/n-decane blends are in very good agreement with the experimental data in all cases for T > 1100 K. At 10 bar and for both fuel blends there is a slight reduction in overall activation energy (slope) that occurs from approximately 1000 to 1100 K, the high-temperature entrance to the NTC regime, in the experimental data that is not predicted by the simulation. On the other hand, the NTC behavior predicted for the 40 bar 30% AMN/70% n-decane blend is stronger than observed experimentally. These discrepancies result in differences between the experiments and the simulation of at most a factor of three. The differences in the NTC regime are indicative of the uncertainty in the rate parameters for the low-temperature peroxy chemistry for alkyl radicals, in this case decyl, that causes the NTC behavior observed for AMN/n-decane blends. Considering the complexity of the kinetics required to describe these binary fuel blends (nearly 700 species and 4000 reactions) and the general lack of kinetic information available in the literature for AMN oxidation and pyrolysis, we consider the comparisons between experiments and the kinetic simulation to be quite good, particularly in the high-temperature regime.

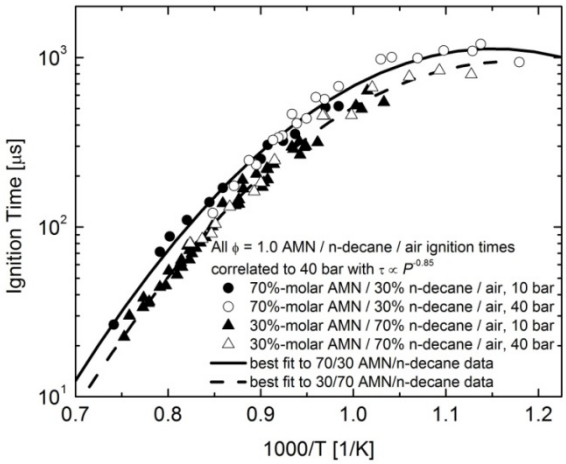

Figure 3.35 Ignition delay times for AMN/n-decane/air mixtures correlated to 40 bar using $\tau \propto P^{-0.85}$.

Sensitivity analysis was performed and shows the important inhibiting effect of reactions leading to resonance-stabilized radicals, especially the H-atom abstraction from AMN by OH radicals to give phenylbenzyl radicals. The competing H-atom abstractions leading to methylnaphthyl radicals have a

promoting effect due to the avoidance of formation of the relatively unreactive phenylbenzyl radical and are also important.

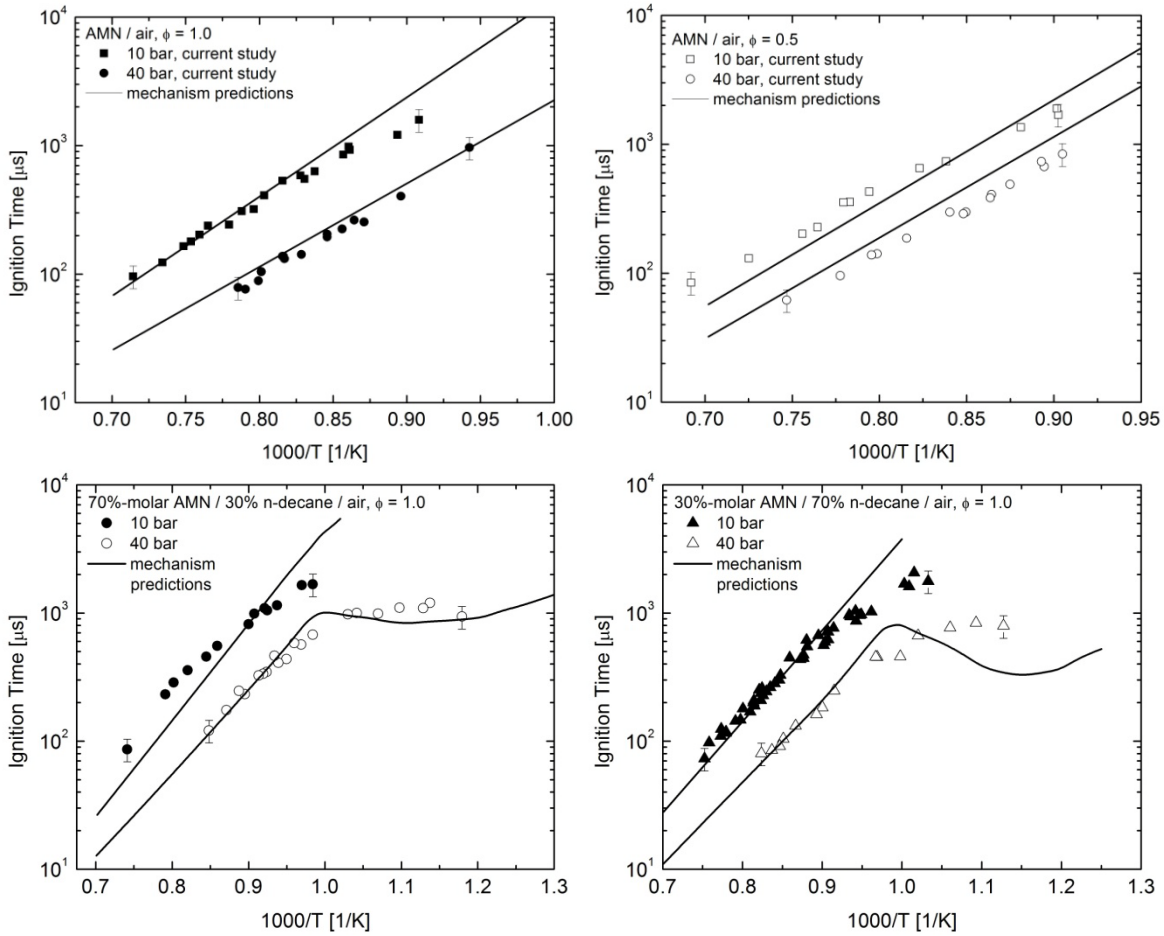

Figure 3.36 Comparison of kinetic simulations with measured ignition delay times for Φ = 1.0 and 0.5 neat AMN/air mixtures and Φ = 1.0 70%-molar AMN / 30% n-decane / air mixtures and Φ = 1.0 30%-molar AMN / 70% n-decane / air mixtures.

3.10 Jet Fuels and Surrogates

Ignition delay time measurements were carried out for stoichiometric jet fuel/air, at pressures near 20 atm, and at a large range of temperatures (670-1230 K). Two jet fuel samples provided by J.T. Edwards at AFRL were tested. The first, which is referred to as Jet A here, is a blend of many different jet fuels obtained by the Air Force and is intended to represent an average Jet A. This fuel is labeled as the POSF 4658 sample and has been used by many researchers in the combustion and fuels properties research communities. The second, referred to as JP-8 here, is that same blended Jet A with the addition of the JP-8 additive package. See Table 1.2 for properties of these fuels.

The temperature range (670-1230 K at 20 atm) that we have examined in shock tube experiments is extremely wide for a single experimental device and ranges from the high-temperature regime, where shock tube measurements are traditionally reported, through the negative-temperature-coefficient (NTC) regime, and well into the low-temperature regime, where rapid compression machines (RCMs) traditionally operate. The large range of temperatures was enabled through the use of tailored driver gas N_2/He mixtures for extended test times at low temperatures. Because long shock tube test times can result in experimental observables that are compromised by non-ideal gasdynamics in the reflected shock region, care must be taken to quantify the influence through careful monitoring of the reflected shock pressure histories. See Figure 3.37 for example ignition time measurements for stoichiometric Jet-A/air autoignition near 20 atm and at a relatively low temperature and long ignition delay time. The figure illustrates a very flat pressure profile, where any rise in pressure dP/dt is small (<1%/ms) for the nearly 9 ms ignition delay time. The pressure profile, as the most direct indicator of the temporal behavior of the conditions at the test location, illustrates that non-ideal gasdynamics effects have a small influence at these conditions on the reflected shock temperature time history and the observed ignition delay time.

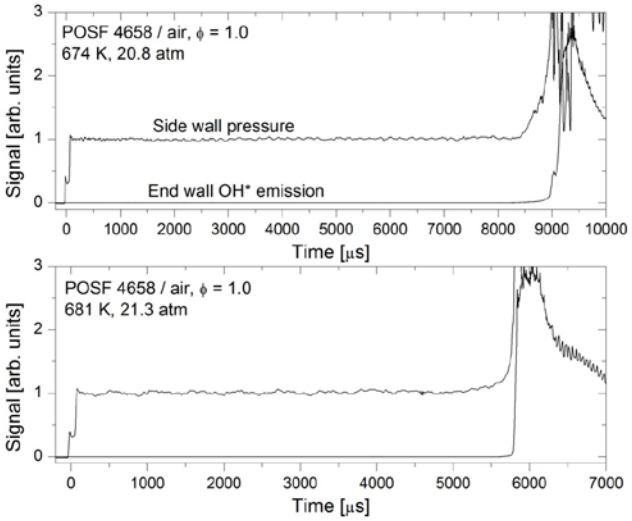

Figure 3.37 Example ignition delay time measurements for Jet A (POSF 4658)/air mixtures.

The entire ignition delay data set for both Jet-A and JP-8 near 20 atm is illustrated in Figure 3.38 (left). The scatter in the data is small (<10%), and the additive package included in the JP-8 sample has no discernible influence on the results. The data illustrate quite clearly the NTC turnover at the transition from the high- to intermediate-temperature regime around 900 K (1000/T = 1.1) and then the turn up in ignition time at the transition to the low-temperature regime around 750 K (1000/T = 1.35). A comparison with recent RCM measurements made by Kumar and Sung at the University of Connecticut [8] and several previous studies found in the literature, including the Dean et al. [73] and Vasu et al. [18] shock tube measurements and the Spadaccini and Tevelde [74] flow reactor measurements, also is illustrated in Figure 3.38 (right). Where overlap exists, there is reasonable agreement among all data sets. It is particularly satisfying that, at the coldest temperatures, there is good agreement between the shock tube and RCM measurements, which is not always the case due to the non-ideal behavior of these two facilities (non-ideal gasdynamics in shock tubes and heat loss and compression-stroke reaction in RCMs).

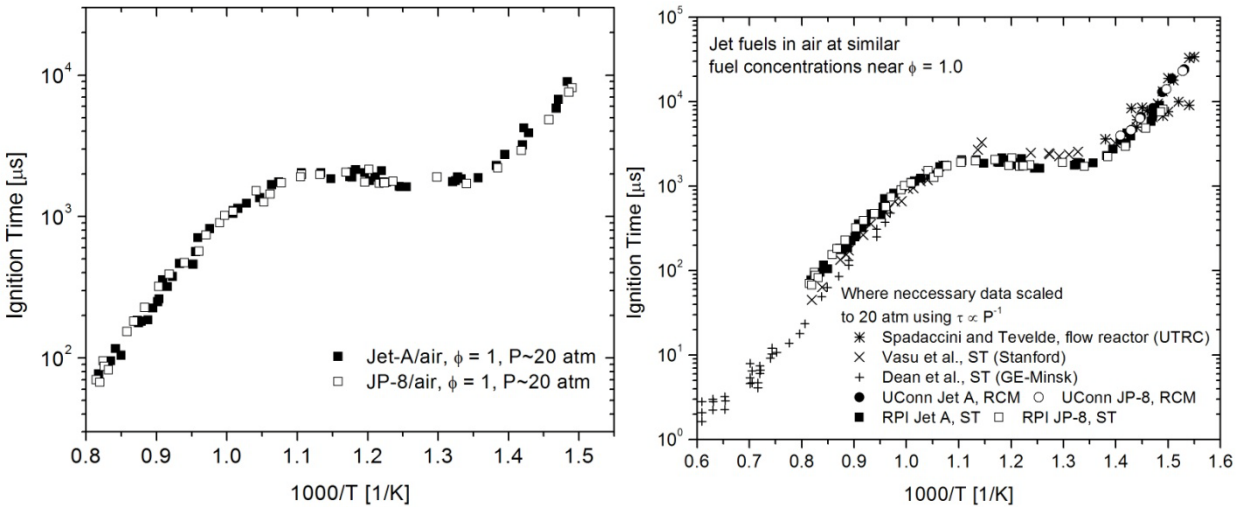

Figure 3.38 RPI Jet-A and JP-8 ignition delay measurements (right) and comparison with previous jet fuel autoignition studies (left).

The autoignition of two surrogate mixtures, designed to mimic jet fuels, also has been investigated. The surrogates studied include a mixture developed by the AFOSR MURI program led by F.L. Dryer at Princeton University (42.67% n-decane, 33.02% iso-octane, and 24.31% toluene by moles [8]) and a four-component surrogate developed by our group at RPI (25.8% n-tetradecane, 16.8% iso-cetane, 30% methylcyclohexane, and 27.4% n-propylbenzene). Both of these surrogates were designed to mimic the jet fuel H/C, derived cetane number (DCN), and aromatic content. See reference [8] for details regarding surrogate formulation and Table 1.1 and 1.2 for surrogate and real fuel properties. Additionally, the RPI surrogate also was designed to match the jet fuel threshold soot index (TSI), average molecular weight, and liquid density.

As in the jet fuel experiments, the autoignition of the surrogates was studied for a wide range of temperatures around 20 atm, again using N_2/He tailored driver gases to extend the test times up to 10 ms. The shock tube displayed fairly good gasdyanamic characteristics at long test times, as shown in the example pressure traces illustrated in Figure 3.39 for ignition delay measurements for the MURI surrogate.

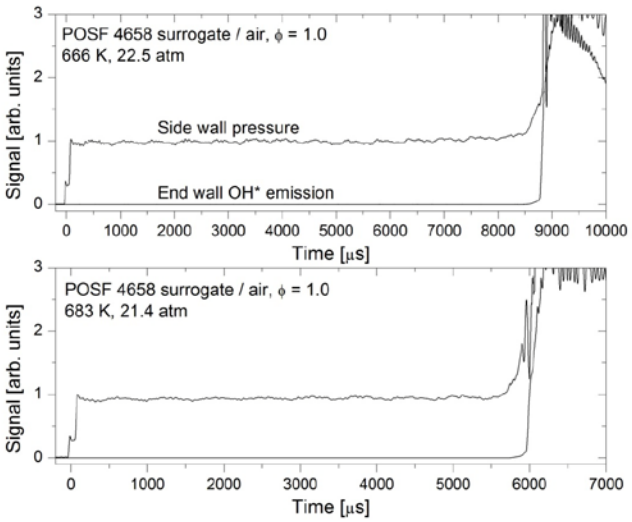

Figure 3.39 Example ignition delay time measurements for MURI surrogate/air mixtures.

In Figure 3.40 ignition delay measurements for jet fuel surrogates made by both by both our group (RPI) and by Kumar and Sung (UConn, RCM) [8] are compared to Jet A measurements at the same conditions (stoichiometric fuel/air mixtures at pressures near 20 atm). Both the MURI surrogate, for which there are both shock tube and RCM data, and the RPI surrogate, for which there are only shock tube data, do a fairly good job at capturing the Jet A ignition delay. The MURI surrogate matches more closely the Jet A ignition delay because it more closely matches the Jet A DCN. For both the Jet A sample (POSF 4658) and the MURI surrogate the DCN is 47.1, while for the RPI surrogate, the DCN is 42.8. These differences are due to the fact that we originally targeted a DCN of 44 when formulating the RPI surrogate *a priori* based on literature cetane numbers [75] (CN, different from DCN). Later, the Princeton-led (F.L. Dryer) MURI group measured the DCN for the RPI surrogate and found it to be 42.8. The MURI team, on the other hand, first measured the DCN for the POSF 4658 Jet A sample and

then empirically formulated, using a matrix of DCN measurements, their surrogate to match the measured DCN of the Jet A sample exactly. These differences in DCN and the differences in ignition delay times at moderate to low temperatures illustrated in Figure 3.40 (right side) illustrate that our shock tube technique is sensitive to relatively small changes in DCN and hence will be sensitive to slight fuel differences that may be introduced in the future (e.g., through alternative fuel blends).

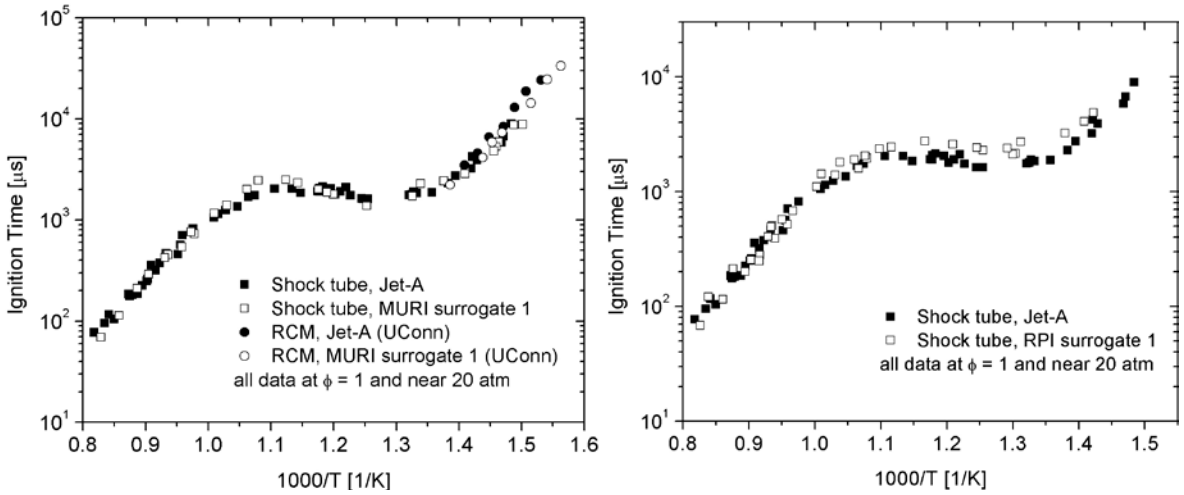

Figure 3.40. Ignition delay times for Jet A (POSF 4658), Princeton-MURI surrogate 1, and RPI surrogate 1. All measurements are for Φ = 1.0 and near 20 atm.

The RPI surrogate has been formulated in an attempt to mimic jet fuel reactivity (ignition delay and DNC), H/C, threshold soot index, molecular weight, liquid density, and aromatic content. To mimic all these jet fuel properties required the selection of large compounds for which kinetic models are still limited and under development. On the other hand, the MURI surrogate, which only mimics reactivity (DNC and ignition delay as illustrated in Figure 3.40), H/C ratio, and aromatic content, is made up of smaller compounds (n-decane, iso-octane, and toluene), typically thought to be representative of petroleum-based gasoline, for which there has been a wealth of kinetic model development. At present, there is a clear tradeoff among surrogate mixture complexity (in terms of both the size and number of components), kinetic modeling capabilities, and the number of jet fuel properties that can be represented.

4. Conclusions

In this AFOSR-supported work four major accomplishments were achieved: 1) a heated high-pressure shock tube facility designed for the kinetic study of low-boiling point liquid fuels, such as jet fuels, was constructed; 2) the autoignition of many jet fuel representative hydrocarbon components was characterized at elevated engine-relevant conditions (650-1400 K, 7-60 atm, Φ = 0.25-1.5); 3) the ignition delay of Jet A fuel at elevated pressures (~20 atm) was characterized for a very large range of temperatures spanning from the high-temperature ignition regime through the negative-temperature coefficient regime and into the low-temperature regime; and 4) the autoignition of two surrogate mixtures designed to mimic the overall reactivity of jet fuels was quantified.

The components chosen for study include n-heptane, n-decane, n-dodecane, n-tetradecane, iso-octane, iso-cetane, cyclopentane, cyclohexane, methylcyclohexane, ethylcyclohexane, decalin, toluene, o-, m-, and p-xylene, ethylbenzene, and α-methylnaphthalene. The chosen hydrocarbons include compounds found in large quantities in jet fuels (e.g., n-dodecane), model compounds within organic classifications (e.g., toluene and methylcyclohexane), and compounds considered as potential surrogate candidates that have been the subject of significant kinetic modeling efforts. Additionally, many of these compounds are the starting points for the development of kinetic understanding and modeling for larger compounds found in jet fuels.

The studies presented here for neat hydrocarbon components not only serve as targets for the development, assessment, and validation of kinetic models but also provide an understanding of the reactivity-structure dependencies that are crucial for formulating surrogates to mimic real fuels and for understanding how perturbations to the fuel supply, perhaps through the addition/blending of alternative fuels in the future, will influence the reactivity of jet fuels. For example, these studies illustrate the influence or lack of influence of chain length on large n-alkane reactivity, the differences in reactivity for C_5 and C_6 cycloalkane rings, and the influence of side chain length and proximity for substituted cyclohexanes and aromatics.

The autoignition of Jet A, as characterized here, provides a quantitative temperature-dependent reactivity target for future surrogate formulations, as well as a quantitative target for the tuning of empirical reduced-order kinetic schemes for implementation in computational fluid dynamic simulations. Finally, two simple surrogates (three and four components) formulated by the Princeton-led MURI team [8] and by our group at RPI adequately match the reactivity of Jet A to show that there is promise in using the derived cetane number (DCN) as a global indicator of reactivity for the formulation of surrogates, although further investigation is needed to be conclusive.

5. Participating Personnel

Principle Investigator
Prof. Matthew Oehlschlaeger

Graduate Students
Hsi-Ping Shawn Shen (AFOSR funded), PhD received December 2008 under this grant, currently at Raytheon, Tucson, AZ
Haowei Wang (AFOSR funded), MS received August 2009, PhD in progress with M. Oehlschlaeger
Jeremy Vanderover (RPI funded), PhD received May 2009, currently at General Electric Global Research, Niskayuna, NY
Shane Daley (RPI funded), MS received December 2007, currently at Northrop Grumman, El Segundo, CA
Andrew Berkowitz (RPI funded), MS received December 2009, currently at SpaceX, McGregor, TX
Steven Warner (RPI funded), MS received December 2009, currently at Simulia, Warwick, RI

Undergraduate Students
Justin Steinberg, BS 2010, currently at Knolls Atomic Power Laboratory, Niskayuna, NY

Collaborators
Dr. Charles Westbrook, Lawrence Livermore National Laboratory
Dr. William Pitz, Lawrence Livermore National Laboratory
Prof. Frederick Dryer, Princeton University
Dr. Frederique Battin-Leclerc, Nancy Université, Nancy, France
Prof. Eliseo Ranzi, Politecnico di Milano, Milan, Italy

6. Journal Publications

1. S. Dooley, S.H. Won, M. Chaos, J. Heyne, Y. Ju, F.L. Dryer, K. Kumar, C.J. Sung, H. Wang, M.A. Oehlschlaeger, R.J. Santoro, T.A. Litzinger, "A Jet Fuel Surrogate Formulated by Real Fuel Properties," *Combustion and Flame*, doi:10.1016/j.combustflame.2010.07.001.

2. H. Wang, S.J. Warner, M.A. Oehlschlaeger, R. Bounaceur, P.A. Glaude, F. Battin-Leclerc, "An Experimental and Kinetic Modeling Study of the Autoignition of α-Methylnaphthalene/Air and α-Methylnaphthalene/n-Decane/Air Mixtures at Elevated Pressures," *Combustion and Flame,* 157, 1976-1988 (2010).

3. M.A. Oehlschlaeger, J. Steinberg, C.K. Westbrook, and W.J. Pitz, "The Autoignition of Iso-Cetane at High to Moderate Temperatures and Elevated Pressures: Shock Tube Experiments and Kinetic Modeling," *Combustion and Flame*, 156, 2165-2172 (2009).

4. H.-P.S. Shen, J. Steinberg, J. Vanderover, and M.A. Oehlschlaeger, "A Shock Tube Study of the Ignition of n-Heptane, n-Decane, n-Dodecane, and n-Tetradecane at Elevated Pressures," *Energy and Fuels*, 23, 2482-2489 (2009).

5. M.A. Oehlschlaeger, H.-P.S. Shen, A. Frassoldati, S. Pierucci, and E. Ranzi, "An Experimental and Kinetic Modeling Study of the Pyrolysis and Oxidation of Decalin," *Energy and Fuels*, 23, 1464-1472 (2009).

6. H.-P. S. Shen and M.A. Oehlschlaeger, "The Ignition of C_8H_{10} Aromatics at Elevated Pressures," *Combustion and Flame*, 156, 1053-1062 (2009).

7. H.-P.S. Shen, J. Vanderover, and M.A. Oehlschlaeger, "A Shock Tube Study of the Auto-Ignition of Toluene/Air Mixtures at High Pressures," *Proceedings of the Combustion Institute* 32, 165-172 (2009).

8. J. Vanderover and M.A. Oehlschlaeger, "Ignition Time Measurements for Methylcyclohexane- and Ethylcyclohexane-Air Mixtures at Elevated Pressures," *International Journal of Chemical Kinetics*, 41, 82-91 (2009).

9. H.-P.S. Shen, J. Vanderover, and M.A. Oehlschlaeger, "A Shock Tube Study of Iso-Octane Ignition at Elevated Pressures: the Influence of Diluent Gases," *Combustion and Flame*, 155, 739-755 (2008).

10. S.M. Daley, A.M. Berkowitz, and M. A. Oehlschlaeger, "A Shock Tube Study of Cyclopentane and Cyclohexane Ignition at Elevated Pressures," *International Journal of Chemical Kinetics*, 40, 624-634 (2008).

7. Interactions

During this project, the PI had interactions with Dr. J. Tim Edwards at AFRL regarding the sourcing of fuels and the composition of traditional and alternative jet fuels. The PI also had interactions with Dr. Peter Schihl (Army Ground Vehicle Propulsion and Mobility Laboratory) regarding operating conditions for JP-8 fueled diesel engines and Dr. Med Colket (United Technologies) regarding operating conditions of gas turbine main combustors and thrust augmentors.

8. References

1. T. Edwards, L.Q. Maurice, J. Power and Prop. 17 (2001) 461-466.
2. M. Colket, J.T. Edwards, S. Williams, N.P. Cernansky, D.L. Miller, F.N. Egolfopoulos, P. Lindstedt, K. Seshadri, F.L. Dryer, C.K. Law, D.G. Friend, D.B. Lenhert, H. Pitsch, A. Sarofim, M. Smooke, W. Tsang, AIAA Paper AIAA-2007-0770 (2007).
3. L. Shafer, R. Striebich, J. Gomach, T. Edwards, AIAA Paper AIAA-2006-7972, 2006.
4. Northrop Grumman, Northrop Grumman Petroleum Product Survey Reports, updated annually, http://pps.ms.northropgrumman.com/.
5. B.L. Smith, T.J. Bruno, Energy and Fuels 21 (2007) 2853-2862.
6. B.L. Smith, T.J. Bruno, J. Power and Prop. 24 (2008) 618-623.
7. S. Outcalt, A. Laesecke, M.B. Freund, Energy and Fuels 23 (2009) 1626-1633.
8. S. Dooley, S.H. Won, M. Chaos, J. Heyne, Y. Ju, F.L. Dryer, K. Kumar, C.J. Sung, H. Wang, M.A. Oehlschlaeger, R.J. Santoro, T.A. Litzinger, Combust. Flame, doi:10.1016/j.combustflame.2010.07.001.
9. J. Vanderover, M.A. Oehlschlaeger, Int. J. Chem. Kinet. 41 (2009) 82-91.
10. M.A. Oehlschlaeger, D.F. Davidson, J.B. Jeffries, Appl. Optics 44 (2005) 6599-6605.
11. H. Li, Z.C. Owens, D.F. Davidson, R.K. Hanson, Int. J. Chem. Kinet. 40 (2008) 189-198.
12. A. Burcat, B. Ruscic, Ideal gas thermochemical database with updates from active thermochemical tables; available at http://garfield.chem.elte.hu/burcat/burcat.html.
13. D.R. White, J. Chem. Phys. 42 (1965) 2028-2032.
14. H.-P. S. Shen, J. Vanderover, M.A. Oehlschlaeger, Proc. Combust. Inst. 32 (2009) 165-172.
15. D. Horning, A Study of the High-Temperature Autoignition and Thermal Decomposition of Hydrocarbons, Ph.D. Thesis, Stanford University (2001).
16. S.S Vasu, D.F. Davidson, Z. Hong, V. Vasudevan, R.K. Hanson, Proc. Combust. Inst. 32 (2009) 173-180.
17. D.F. Davidson, D.R. Haylett, R.K. Hanson, Combust. Flame 155 (2008) 108-117.
18. S.S. Vasu, D.F. Davidson, R.K. Hanson, Combust. Flame 152 (2008) 125-143.
19. H.K. Ciezki, G. Adomeit, Combust. Flame 93 (1993) 421-433.
20. B.M. Gauthier, D.F. Davidson, R.K. Hanson, Combust. Flame 139 (2004) 300-311.
21. E.J. Silke, H.J. Curran, J.M. Simmie, Proc. Combust. Inst. 30 (2005) 2639-2647.
22. U. Pfahl, K. Fieweger, G. Adomeit, Proc. Combust. Inst. 26 (1996) 781-789.
23. Curran, H.J.; Gaffuri, P.; Pitz, W.J.; Westbrook, C.K. Combust. Flame 114 (1998) 149-177.
24. C.K. Westbrook, W.J. Pitz, O. Herbinet, H.J. Curran, E.J. Silke, Combust. Flame 156 (2009) 181-199.
25. E. Ranzi, A. Frassoldati, S. Granata, T. Faravelli, Ind. Eng. Chem. Res. 44 (2005) 5170-5183.
26. J. Biet, M.H. Hakka, V. Warth, P.-A. Glaude, F. Battin-Leclerc, Energy Fuels 22 (2008) 2258-2269.
27. W.J. Pitz, N.P. Cernansky, F.L. Dryer, F.N. Egolfopoulos, J.T. Farrell, D.G. Friend, H. Pitsch, SAE Paper 2007-01-0175 (2007).
28. K. Fieweger, R. Blumenthal, G. Adomeit, Combust. Flame 109 (1997) 599-619.
29. D.F. Davidson, B.M. Gauthier, R.K. Hanson, Proc. Combust. Inst. 30 (2005) 1175-1182.
30. J. Würmel, E.J. Silke, H.J. Curran, M.S. Ó Conaire, J.M. Simmie, Combust. Flame 151 (2007) 289-302.
31. D.F. Davidson, R.K. Hanson, Int. J. Chem. Kinet. 36 (2004) 510-523.
32. H.J. Curran, P. Gaffuri, W.J. Pitz, C.K. Westbrook, Combust. Flame 129 (2002) 253-280.
33. P.A. Glaude, R. Fournet, V. Warth, F. Battin-Leclerc, G.M. Côme, G. Sacchi http://www.ensic.u-nancy.fr/DCPR/Anglais/GCR/generatedmecanisms/isooctane (2002).
34. V. Golovitchev, http://www.tfd.chalmers.se/~valeri/ (2008).
35. J.M. Hall, E.L. Petersen, Int. J. Chem. Kinet. 38 (2006) 714-724.
36. J.M. Hall, M.J.A. Rickard, E.L. Petersen, Comb. Sci. Tech. 177 (2005) 455-483.
37. Ch. Kappel, K. Luther, J. Troe, Phys. Chem. Chem. Phys. 4 (2002) 4392-4398.
38. E.L. Petersen, D.F. Davidson, R.K. Hanson, Combust. Flame 117 (1999) 272-290.
39. G.P. Smith, D.M. Golden, M. Frenklach, N.W. Moriaty, B. Eiteneer, M. Goldenberg, C.T. Bowman, R.K. Hanson, S. Song, W.C. Gardiner Jr., V.V. Lissiansky, Z. Qin, GRI-Mech 3.0, http://www.me.berkeley.edu/gri_mech/.

40. H. Li, Z.C. Owens, D.F. Davidson, R.K. Hanson, Int J Chem Kinet 40 (2008) 189-198.
41. M.A. Oehlschlaeger, J. Steinberg, C.K. Westbrook, W.J. Pitz, Combust. Flame 156 (2009) 2165-2172.
42. B. Sirjean, F. Buda, H. Hakka, P.-A. Glaude, R. Fournet, V. Warth, F, Battin-Leclerc, M. Ruiz-Lopez, Proc Combust Inst 31 (2007) 277-284.
43. O. Lemaire, M. Ribaucour, M. Carlier, R. Minetti, Combust Flame 127 (2001) 1971-1980.
44. F. Buda, B. Heyberger, R. Fournet, P.-A. Glaude, V. Warth, F. Battin-Leclerc, Energy Fuels 20 (2006) 1450-1459.
45. E.J. Silke, W.J. Pitz, C.K. Westbrook, M. Ribaucour, J Phys Chem A 111 (2007) 3761-3775.
46. S. Vasu, N.N. Parikh, D.F. Davidson, R.K. Hanson, Methylcyclohexane oxidation: Shock tube experiments and modeling over a wide range of pressures and temperatures; Proceedings of the 5th Joint Meeting of the U.S. Sections of the Combustion Institute, San Diego, CA, 2007.
47. W.J. Pitz, C.V. Naik, T. Ní Mhaoldúin, C.K. Westbrook, H.J. Curran, J.P. Orme, J.M. Simmie, Proc Combust Inst 31 (2007) 267-275.
48. J.P. Orme, H.J. Curran, J.M. Simmie, J Phys Chem A 110 (2006) 114-131.
49. A. Roubaud, R. Minetti, L.R. Sochet, Combust Flame 121 (2000) 535-541.
50. S.K. Gulati, R.W Walker, J Chem Soc Faraday Trans 2 (1989) 1799-1812.
51. S.M. Handford-Styring, R.W. Walker, Phys Chem Chem Phys 3 (2001) 2043-2052.
52. E.G. Eddings, S. Yan, W. Ciro, A.F. Sarofim, Combust. Sci. Technol. 177 (2005) 715–739.
53. M.A. Oehlschlaeger, H.-P.S. Shen, A. Frassoldati, S. Pierucci, E. Ranzi, Energy and Fuels 23 (2009) 1464-1472.
54. G. Mittal, C.-J. Sung, Combust. Flame 150 (2007) 355-368.
55. W. J. Pitz, R. Seiser, J. W. Bozzelli, I. Da Costa, R. Fournet, F. Billaud, F. Battin-Leclerc, K. Seshadri, C.K. Westbrook, Chemical Kinetic Characterization of the Combustion of Toluene, Proc. of the 2nd Joint Meeting of the U.S. Sections of the Combustion Institute (2001).
56. Y. Sakai, T. Inamura, T. Ogura, M. Koshi, W.J. Pitz, Detailed Kinetic Modeling of Toluene Combustion over a Wide Range of Temperature and Pressure, SAE 2007-01-1885 (2007).
57. J.C.G. Andrae, P. Björnbom, R.F. Cracknell, G.T. Kalghatgi, Combust. Flame 149 (2007) 2-24.
58. R. Sivaramakrishnan, R.S. Tranter, K. Brezinsky, Proc. Combust. Inst. 30 (2005) 1165-1173.
59. Y. Murakami, T. Oguchi, K. Hashimoto, Y. Nosaka, J. Phys. Chem. A. 111 (2007) 13200-13208.
60. M.A. Oehlschlaeger, D.F. Davidson, R.K. Hanson, Combust. Flame 147 (2006) 195-208.
61. S. Gaïl, P. Dagaut, Combust. Flame 141 (2005) 281-297.
62. S. Gaïl, P. Dagaut, Combust. Sci. Technol. 179 (2007) 813-844.
63. S. Gaïl, P. Dagaut, G. Black, J.M. Simmie, Combust. Sci. Technol. 180 (2008) 1748-1771.
64. F. Battin-Leclerc, R. Bounaceur, N. Belmekki, and P.A. Glaude, Int. J. Chem. Kinet. 38 (2006) 284-302.
65. A. Roubaud, R. Minetti, L.R. Sochet, Combust. Flame 121 (2000) 535-541.
66. D.L. Baulch, C.J. Cobos, R.A. Cox, P. Franck, G.D. Hayman, Th. Just, J.A. Kerr, T.P. Murrells, M.J. Pilling, J. Troe, R.W. Walker, J. Warnatz, Combust. Flame 98 (1994) 59-79.
67. V. Vasudevan, D.F. Davidson, R.K. Hanson, J. Phys. Chem. A 109 (2005) 3352-3359.
68. F.P. Tully, A.R. Ravishankara, R.L. Thompson, J.M. Nicovich, R.C. Shah, N.M. Kreutter, P.H. Wine, J. Phys. Chem. 85 (1981) 2262-2269.
69. H. Hippler, C. Reihs, J. Troe, Proc. Combust. Inst. 23 (1990) 37-43.
70. G. da Silva, J.W. Bozzelli, Proc. Combust. Inst. 32 (2009) 287-294.
71. R. Bounaceur, P.A. Glaude, R. Fournet, F. Battin-Leclerc, Int. J. Vehicle Des. 44 (2007) 124–142.
72. H. Wang, S.J. Warner, M.A. Oehlschlaeger, R. Bounaceur, J. Biet, P.A. Glaude, F. Battin-Leclerc, Combust. Flame 157 (2010) 1976-1988.
73. A.J. Dean, O.G. Penyazkov, K.L. Sevruk, B. Varatharajan, Proc. Combust. Inst. 31 (2007) 2481-2488.
74. L.J. Spadaccini, J.A. Tevelde, Combust. Flame 46 (1982) 283-300.
75. M.J. Murphy, J.D. Taylor, R.L. McCormick, Compendium of experimental cetane number data, NREL report NREL/SR-540-36805 (2004).

9. Appendix: Experimental Data

Table A.1. Measured ignition times for n-heptane/air mixtures.

n-heptane/air, Φ = 0.25; 0.4752% n-C_7H_{16}, 20.91% O_2, 78.62% N_2			n-heptane/air, Φ = 0.5; 0.9459% n-C_7H_{16}, 20.81% O_2, 78.24% N_2			n-heptane/air, Φ = 1.0; 1.874% n-C_7H_{16}, 20.62% O_2, 77.51% N_2		
T_5 [K]	P_5 [atm]	τ [μs]	T_5 [K]	P_5 [atm]	τ [μs]	T_5 [K]	P_5 [atm]	τ [μs]
1064	13.5	1687	1063	14.9	1028	809	10.8	2672
1078	12.6	1111	1063	14.7	1027	826	10.6	3048
1092	13.0	1378	1101	12.7	692	972	11.8	2384
1116	12.2	868	1168	12.8	243	1058	11.9	1101
1133	13.0	719	1224	11.8	130	1068	11.4	911
1204	10.5	373	829	38.7	669	1096	11.9	653
1206	12.7	339	873	40.7	758	1098	12.6	678
1248	11.9	228	944	44.3	824	1196	12.3	189
1309	12.7	108	1014	47.3	611	788	49.2	295
1317	12.1	96	1082	43.5	258	797	53.6	379
1336	12.8	88	1110	51.6	210	799	47.7	319
1396	11.8	42	1161	46.2	90	834	49.4	284
786	49.9	1500				862	49.7	295
791	38.0	1443				899	46.4	381
830	39.7	1344				967	52.5	491
831	48.3	1402				991	50.3	447
836	52.0	1289				996	48.1	336
856	39.7	1503				1003	43.5	344
872	50.9	1374				1022	45.0	282
920	43.1	1498				1029	47.5	297
948	42.3	1566				1050	48.4	259
987	42.0	1518						
1055	43.9	626						
1099	43.4	386						
1147	47.4	229						
1178	42.5	193						
1230	39.6	93						

Table A.2. Measured ignition times for n-decane/air mixtures.

n-decane/air, Φ = 0.25; 0.3377% n-$C_{10}H_{22}$, 20.94% O_2, 78.73% N_2			n-decane/air, Φ = 0.5; 0.6731% n-$C_{10}H_{22}$, 20.87% O_2, 78.46% N_2			n-decane/air, Φ = 1.0; 1.337% n-$C_{10}H_{22}$, 20.73% O_2, 77.94% N_2		
T_5 [K]	P_5 [atm]	τ [μs]	T_5 [K]	P_5 [atm]	τ [μs]	T_5 [K]	P_5 [atm]	τ [μs]
1098	11.5	977	918	11.7	1094	1011	12.0	1135
1139	11.2	648	951	12.0	1035	1041	11.0	881
1169	11.0	460	1012	13.5	1267	1085	11.7	615
1189	9.5	391	1053	13.7	953	1088	11.4	513
1194	11.2	335	1071	13.0	747	1145	10.4	359
1252	10.3	198	1126	9.4	652	1175	10.9	311
1255	10.1	198	1101	12.6	567	1263	10.5	108
1280	10.3	157	1165	12.8	279	1276	9.9	114
1321	10.2	99	1004	51.0	472	1378	10.6	40
992	41.5	946	1014	50.1	413	836	37.2	757
1014	40.2	815	1082	49.1	199	900	43.1	692
1017	37.1	912	1213	57.7	61	928	43.1	625
1056	33.1	752				929	42.5	551
1111	32.8	423				938	42.4	565
1173	31.0	222				955	42.5	597
1241	31.5	87				970	45.6	397
						976	43.3	471
						1003	41.9	364
						1032	39.5	351
						1079	39.8	186
						1133	38.9	135
						1144	33.9	128
						1158	37.7	113
						1271	35.8	37

Table A.3. Measured ignition times for n-dodecane/air mixtures.

n-dodecane/air, Φ = 0.5; 0.5646% n-$C_{12}H_{26}$, 20.89% O_2, 78.55% N_2			n-dodecane/air, Φ = 1.0; 1.123% n-$C_{12}H_{26}$, 20.77% O_2, 78.10% N_2		
T_5 [K]	P_5 [atm]	τ [μs]	T_5 [K]	P_5 [atm]	τ [μs]
1010	15.6	976	924	17.8	1299
1030	15.4	753	999	12.1	822
1099	14.4	463	1014	13.9	713
1116	16.6	339	1014	13.8	740
1136	15.4	320	1030	12.3	656
1155	12.1	275	1072	11.7	517
1248	11.9	93	1103	12.8	343
931	42.6	1188	1109	10.8	374
947	42.7	1101	1135	13.9	257
989	45.2	664	1141	11.8	265
1037	46.9	433	1177	14.9	162
1039	41.3	443	1178	12.4	194
1054	46.0	398	1210	13.4	123
1113	41.2	207	877	45.0	801
1118	37.4	220	913	41.8	757
1164	38.8	146	945	43.2	737
			978	43.8	506
			1020	45.2	342
			1043	41.0	270
			1080	40.6	206
			1097	41.3	157
			1102	44.2	155
			1114	38.6	129
			1122	42.6	120

Table A.4. Measured ignition times for n-tetradecane/air mixtures.

n-tetradecane/air, Φ = 0.5; 0.4862% n-$C_{14}H_{30}$, 20.91% O_2, 78.61% N_2			n-tetradecane/air, Φ = 1.0; 0.9677% n-$C_{14}H_{30}$, 20.81% O_2, 78.23% N_2		
T_5 [K]	P_5 [atm]	τ [μs]	T_5 [K]	P_5 [atm]	τ [μs]
964	14.3	1082	962	15.4	1180
1015	13.4	789	1006	17.4	751
1024	12.1	890	1037	16.5	532
1048	12.8	783	1109	15.5	277
1098	13.9	516	1112	12.8	301
1164	11.9	261	1129	11.1	272
1217	12.2	129	1193	10.3	180
1242	12.7	103	884	41.8	1008
1302	11.7	72	954	42.5	673
983	38.5	808	997	44.7	455
996	41.2	708	1007	43.1	406
1000	35.6	675	1052	39.6	265
1024	36.9	569	1056	39.3	295
1084	41.7	306	1097	34.5	188
1096	38.4	280	1109	35.9	163

Table A.5. Measured ignition times for iso-octane/air mixtures.

Mixture: 1.653% iso-octane, 20.66% O_2, and 77.69% N_2; Φ = 1.0			Mixture: 0.833% iso-octane, 20.83% O_2, and 78.33% N_2; Φ = 0.50			Mixture: 0.418% iso-octane, 20.92% O_2, and 78.66% N_2; Φ = 0.25		
T_5 [K]	P_5 [atm]	τ [μs]	T_5 [K]	P_5 [atm]	τ [μs]	T_5 [K]	P_5 [atm]	τ [μs]
958	10.2	2851	1002	11.7	2907	1074	12.4	1621
1032	9.4	1699	1021	12.0	2817	1133	12.5	812
1044	8.7	1633	1022	11.9	2710	1167	12.7	430
1062	8.1	1123	1059	12.5	1376	1197	12.3	305
1116	9.6	638	1078	13.4	1165	1224	13.4	208
1119	6.9	656	1079	12.8	1128	1260	12.4	163
1126	8.3	627	1083	13.4	1191	1300	11.3	90
1142	9.2	425	1113	14.3	711	981	38.4	2720
1159	8.7	370	1119	11.3	725	1022	47.9	1400
1186	9.3	259	1130	13.0	502	1040	48.9	1082
1193	8.8	227	1149	12.8	434	1054	47.9	850
1229	8.5	136	1152	12.4	475	1069	46.8	750
1242	7.9	126	1169	11.9	310	1094	46.6	589
1021	19.8	1059	1177	11.4	317	1113	40.7	457
1032	25.5	850	1196	12.1	241	1128	40.9	379
1045	26.0	645	938	37.3	1984	1161	37.5	274
1058	24.5	704	946	39.1	1697	1190	36.9	166
1072	22.8	509	1032	47.4	836			
1078	23.9	439	1070	42.6	503			
1084	24.2	494	1128	48.2	212			
1085	24.1	429	1152	40.9	180			
1088	25.9	449	1157	38.8	148			
1118	23.5	295						
1132	23.2	220						
1142	19.0	220						
1145	21.3	207						
1205	20.7	104						
1223	20.4	91						
886	37.6	2027						
907	58.1	1099						
976	54.2	792						
1013	54.6	591						
1082	50.0	288						
1184	47.4	80						

Table A.6. Measured ignition times for iso-octane/O_2/Ar mixtures.

Mixture: 1.653% iso-octane, 20.66% O_2, and 77.69% Ar; Φ = 1.0			Mixture: 0.833% iso-octane, 20.83% O_2, and 78.33% Ar; Φ = 0.50		
T_5 [K]	P_5 [atm]	τ [μs]	T_5 [K]	P_5 [atm]	τ [μs]
950	10.6	2113	1039	9.6	1847
963	10.4	1966	1074	9.6	1243
1009	10.2	1567	1089	9.4	1058
1015	8.6	1671	1090	9.5	1086
1025	10.2	1229	1106	9.1	885
1030	8.4	1352	1120	9.3	668
1042	8.6	1306	1130	9.4	532
1043	9.5	1041	1173	10.1	282
1045	9.5	1045	1181	10.0	259
1069	9.2	890	1278	11.5	70
1079	9.4	758	1002	18.8	1430
1100	9.4	599	1040	19.4	1178
1136	9.5	383	1057	19.3	936
1181	9.9	198	1111	20.3	434
1198	11.0	161	1117	17.9	457
1242	10.4	83	1123	18.9	447
			1146	18.8	295
			1150	18.1	293
			1239	23.9	62

Table A.7. Measured ignition times for iso-cetane/air mixtures.

iso-cetane/air, Φ = 0.5: 0.4269% iso-cetane, 20.92% O_2, 78.65% N_2			iso-cetane/air, Φ = 1.0: 0.8502% iso-cetane, 20.83% O_2, 78.32% N_2			iso-cetane, Φ = 1.5: 1.270% iso-cetane, 20.74% O_2, 77.99% N_2		
P_5 [atm]	T_5 [K]	τ [μs]	P_5 [atm]	T_5 [K]	τ [μs]	P_5 [atm]	T_5 [K]	τ [μs]
14.1	1033	1064	14.0	993	984	15.3	957	1402
8.1	1043	1160	11.7	1046	662	16.7	1025	516
13.4	1053	853	9.8	1098	472	8.7	1055	739
10.9	1085	550	12.5	1161	173	11.0	1060	490
12.5	1086	610	10.9	1210	119	8.4	1095	490
11.5	1120	372	10.4	1304	59	9.9	1121	362
11.8	1129	418	9.9	1309	49	14.4	1132	197
9.0	1169	323	46.9	953	1014	12.5	1153	198
10.4	1279	127	37.1	968	963	10.2	1159	251
10.3	1350	69	31.2	972	813	13.3	1169	158
9.2	1374	71	43.8	986	600	12.5	1206	138
10.7	1394	53	31.8	1039	299	15.4	1300	70
33.1	1007	847	27.0	1074	193	29.4	879	1289
25.9	1014	895	25.4	1083	183	40.7	966	467
33.1	1021	567	28.5	1179	63	47.1	1031	246
26.9	1070	375	26.5	1195	62	33.4	1065	180
40.7	1143	140				42.6	1073	136
37.9	1160	142				45.3	1102	98
40.4	1189	96				42.6	1121	99
35.3	1238	51				43.4	1122	92
40.8	1266	49				44.3	1125	94

Table A.8. Measured ignition times for cyclopentane/air mixtures.

Mixture: 2.725% cyclopentane, 20.44% O_2, and 76.84% N_2; Φ = 1.0			Mixture: 1.381% cyclopentane, 20.72% O_2, and 77.90% N_2; Φ = 0.50			Mixture: 0.6954% cyclopentane, 20.86% O_2, and 78.44% N_2; Φ = 0.25		
T_5 [K]	P_5 [atm]	τ [μs]	T_5 [K]	P_5 [atm]	τ [μs]	T_5 [K]	P_5 [atm]	τ [μs]
997	14.7	1438	1047	15.7	1065	1070	13.9	1094
999	14.0	1576	1066	13.6	1012	1116	13.9	826
1035	14.5	923	1080	16.3	820	1133	12.9	752
1054	13.7	728	1097	16.2	630	1141	12.6	710
1057	14.4	700	1111	16.1	567	1174	12.9	499
1064	13.7	658	1127	15.3	472	1209	13.1	362
1071	13.6	683	1159	14.2	396	1210	12.3	379
1093	12.8	577	1209	15.8	243	1216	11.7	370
1101	13.6	544	1236	14.5	224	1265	11.3	218
1112	12.8	520	1284	13.6	160	1316	11.4	151
1112	13.4	508	1307	13.5	135	1379	11.6	113
1118	13.6	420	1324	12.4	117	993	46.2	1183
1169	11.2	341	1337	12.6	101	1049	47.3	741
923	52.7	1249	1353	12.1	94	1106	47.2	417
932	51.7	1277	900	40.5	2556	1148	49.5	236
963	55.5	757	992	50.3	841	1166	46.3	250
971	51.5	627	998	48.6	811	1215	43.3	171
977	55.1	546	1006	45.1	651	1280	44.0	104
993	52.9	512	1010	47.8	608	1292	41.5	87
1001	55.4	415	1020	53.4	583			
1038	54.3	293	1088	44.6	239			
			1130	45.2	139			

Table A.9. Measured ignition times for cyclohexane/air mixtures.

Mixture: 2.281% cyclohexane, 20.53% O_2, and 77.19% N_2; Φ = 1.0			Mixture: 1.154% cyclohexane, 20.77% O_2, and 78.08% N_2; Φ = 0.50			Mixture: 0.5802% cyclohexane, 20.89% O_2, and 78.53% N_2; Φ = 0.25		
T_5 [K]	P_5 [atm]	τ [μs]	T_5 [K]	P_5 [atm]	τ [μs]	T_5 [K]	P_5 [atm]	τ [μs]
964	14.7	1319	989	13.2	1918	1053	13.5	1281
994	14.9	1074	1068	13.0	592	1066	13.4	1090
1000	14.6	805	1123	13.1	338	1107	13.1	718
1018	13.8	766	1160	12.4	197	1132	11.0	515
1055	14.4	487	1224	12.1	112	1159	11.4	319
1055	15.0	379	1262	11.1	68	1175	11.6	264
1080	12.6	383	943	51.5	1555	1189	11.5	224
1107	12.0	252	961	49.7	1098	1202	11.5	216
1118	11.9	242	973	53.2	913	1248	11.7	136
1122	12.7	216	979	45.2	779	1270	12.0	131
1141	11.7	169	982	52.1	792	977	48.1	1723
1166	13.0	158	1012	44.4	531	1000	46.4	1043
847	58.8	1796	1055	47.0	328	1056	47.3	617
876	55.7	1282	1058	48.5	283	1092	40.7	410
878	55.4	1487	1078	42.6	220	1107	47.3	327
881	55.8	1365	1094	49.5	182	1176	45.3	141
891	58.9	1005	1124	46.5	122	1182	46.4	151
892	61.2	1104	1131	44.1	130	1264	51.3	71
895	56.4	1045	1142	46.6	120			
895	53.8	987						
898	56.0	1058						
906	55.7	877						
918	55.3	767						

Table A.10. Measured ignition times for methylcyclohexane (MCH) / air mixtures.

Mixture: 0.4977% MCH, 20.90% O_2, and 78.60% N_2; Φ = 0.25			Mixture: 0.9905% MCH, 20.80% O_2, and 78.21% N_2; Φ = 0.5			Mixture: 1.962% MCH, 20.60% O_2, and 78.21% N_2; Φ = 1.0		
T_5 [K]	P_5 [atm]	τ [μs]	T_5 [K]	P_5 [atm]	τ [μs]	T_5 [K]	P_5 [atm]	τ [μs]
1090	14.0	963	1042	14.2	770	973	15.3	1746
1107	15.3	772	1059	12.5	775	1009	15.3	1080
1122	14.0	712	1103	13.1	453	1013	14.0	1122
1174	14.3	373	1144	12.5	318	1027	15.0	946
1185	12.5	377	1184	11.8	198	1058	12.7	740
1238	12.0	210	1236	11.0	107	1069	13.9	612
1319	12.7	89	959	51.4	923	1095	12.5	415
916	41.9	1664	1025	52.2	414	1099	16.4	340
1001	46.4	869	1061	50.8	256	1141	14.2	212
1033	44.9	686	1106	49.6	194	1187	13.6	124
1104	46.4	394	1150	47.4	120	818	41.8	1627
1156	45.0	232				881	50.1	1218
1180	40.4	180				920	54.4	840
1230	37.1	116				940	57.6	730
1252	41.9	82				954	49.5	834
						956	46.9	778
						961	49.2	770
						962	51.2	724
						965	53.4	665
						997	51.9	412
						1043	52.7	219
						1078	51.9	143
						1119	66.3	52
						1156	69.5	29

Table A.11. Measured ignition times for ethylcyclohexane (ECH) / air mixtures.

Mixture: 0.4358% ECH, 20.92% O_2, and 78.65% N_2; Φ = 0.25			Mixture: 0.8603% ECH, 20.83% O_2, and 78.31% N_2; Φ = 0.5			Mixture: 1.721% ECH, 20.65% O_2, and 77.63% N_2; Φ = 1.0		
T_5 [K]	P_5 [atm]	τ [μs]	T_5 [K]	P_5 [atm]	τ [μs]	T_5 [K]	P_5 [atm]	τ [μs]
1042	12.2	1230	1032	10.8	1081	979	14.3	1478
1059	13.6	1004	1059	12.1	687	1023	15.1	788
1093	11.9	772	1077	14.0	551	1054	12.5	538
1166	12.2	338	1079	12.8	482	1068	11.3	518
1191	12.0	255	1169	12.8	174	1072	11.8	409
1210	11.6	205	1241	16.3	72	1082	12.6	379
961	48.2	1210	976	47.3	856	1142	13.1	177
1018	50.5	708	1007	43.4	546	1147	13.0	161
1067	45.1	461	1016	49.2	456	896	42.9	1103
1084	52.8	401	1035	44.7	376	966	45.1	634
1099	39.4	344	1068	48.2	255	989	44.0	447
1131	45.2	237	1074	47.2	227	999	42.8	317
1194	42.9	124	1123	49.8	139	1011	45.8	292
			1124	50.5	129	1018	43.9	296
			1187	51.5	60	1028	42.8	221

Table A.12. Measured ignition times for decalin/air mixtures.

decalin/air, Φ = 0.5			decalin/air, Φ = 1.0		
P_5 [atm]	T_5 [K]	τ [μs]	P_5 [atm]	T_5 [K]	τ [μs]
13.5	1100	837	15.2	1037	867
12.0	1130	567	13.5	1049	871
12.1	1137	505	12.5	1057	825
11.6	1182	321	13.9	1063	627
12.1	1192	294	12.2	1074	580
11.1	1208	287	14.1	1105	371
10.6	1263	161	10.5	1134	315
10.7	1305	113	11.4	1164	200
42.1	999	1186	9.3	1190	203
44.5	1033	717	34.6	993	793
41.4	1060	455	48.0	1008	654
37.2	1061	464	46.7	1028	509
37.0	1116	279	41.6	1049	340
35.8	1143	202	42.6	1060	305
			44.6	1096	197
			41.8	1105	160
			38.1	1135	103

Table A.13. Measured ignition times for toluene/air mixtures.

Mixture: 2.281(±0.01)% toluene, 20.53(±0.07)% O_2, and 77.19% N_2; Φ = 1.0			Mixture: 1.154(±0.005)% toluene, 20.77(±0.04)% O_2, and 78.08N_2; Φ = 0.50			Mixture: 0.5802(±0.003)% toluene, 20.89(±0.02)% O_2, and 78.53% N_2; Φ = 0.25		
T_5 [K]	P_5 [atm]	τ [μs]	T_5 [K]	P_5 [atm]	τ [μs]	T_5 [K]	P_5 [atm]	τ [μs]
1129	13.4	1380	1110	13.3	1244	1152	11.6	966
1164	13.5	934	1153	12.3	920	1169	12.4	600
1197	12.4	798	1186	14.7	480	1171	12.4	687
1235	11.3	483	1188	13.5	533	1191	13.5	639
1239	14.5	471	1200	14.0	508	1220	13.4	465
1290	11.2	281	1220	13.4	409	1230	13.5	398
1371	13.2	137	1226	13.3	400	1231	11.5	475
1021	53.8	1255	1299	12.5	205	1263	11.9	342
1041	47.6	1203	1320	12.1	159	1268	11.1	298
1082	46.9	757	1119	40.2	793	1291	10.8	233
1085	51.0	546	1128	46.7	619	1385	10.3	151
1116	49.5	492	1170	45.6	343	1400	12.1	94
1117	46.2	459	1171	45.2	353	1085	43.7	1280
1135	50.9	346	1179	47.1	339	1092	46.9	1181
1218	51.4	117	1251	50.9	149	1152	43.6	767
1232	57.5	97	1268	45.1	126	1153	46.7	662
1256	61.5	61	1277	45.7	127	1165	45.7	604
1305	60.7	44	1301	43.5	96	1171	42.8	559
						1190	41.5	399
						1241	43.8	280
						1261	41.7	224
						1302	40.7	171

Table A.14. Measured ignition times for C_8H_{10}/air mixtures. Mixtures for Φ = 0.5 are 0.9905% C_8H_{10}, 20.80% O_2, and 78.21% N_2 and for Φ = 1.0 are 1.962% C_8H_{10}, 20.60% O_2, and 77.44% N_2.

o-xylene / air, Φ = 0.5			m-xylene / air, Φ = 0.5			p-xylene / air, Φ = 0.5		
T_5 [K]	P_5 [atm]	τ [μs]	T_5 [K]	P_5 [atm]	τ [μs]	T_5 [K]	P_5 [atm]	τ [μs]
1126	12.4	1235	1200	11.6	560	1132	12.1	1310
1142	13.3	878	1249	10.2	424	1137	11.7	1316
1179	12.6	702	1253	10.8	382	1169	11.9	896
1191	13.7	594	1258	10.4	335	1190	11.2	681
1233	12.4	407	1292	10.2	257	1214	11.0	523
1264	11.6	327	1319	9.4	180	1272	11.4	371
1315	10.9	209	1399	12.3	93	1277	11.5	338
1359	11.5	134	1074	36.4	1037	1321	10.8	208
1403	11.9	94	1094	41.7	853	1359	10.5	152
1061	41.8	955	1116	36.6	657	1398	10.4	117
1073	40.9	826	1145	33.9	482	1056	38.4	1442
1087	39.9	688	1224	35.2	201	1082	36.5	1027
1121	37.7	513	1236	33.0	177	1118	33.6	770
1140	36.8	355	1243	34.8	170	1142	34.5	545
1181	36.3	260	1269	38.0	132	1189	35.3	360
1197	36.7	198				1213	34.2	270
1235	37.5	153				1282	35.3	141
o-xylene / air, Φ = 1.0			m-xylene / air, Φ = 1.0			p-xylene / air, Φ = 1.0		
T_5 [K]	P_5 [atm]	τ [μs]	T_5 [K]	P_5 [atm]	τ [μs]	T_5 [K]	P_5 [atm]	τ [μs]
1112	13.9	985	1153	9.4	1198	1160	10.8	1260
1137	13.5	769	1216	10.7	619	1179	11.3	982
1140	12.0	926	1255	9.8	365	1197	10.3	942
1174	12.7	490	1285	9.7	318	1258	10.0	445
1203	12.0	473	1339	9.0	171	1267	9.1	411
1242	12.5	305	1364	8.8	142	1310	9.0	260
1246	12.2	348	1408	9.0	102	1329	8.9	273
1303	12.9	167	1023	40.2	1374	1400	9.2	133
1309	12.2	164	1041	37.7	1213	1061	38.5	1093
996	43.5	1313	1076	35.7	715	1068	42.8	935
1039	44.4	821	1126	35.6	490	1121	33.7	692
1067	41.7	591	1130	35.1	453	1134	33.5	496
1099	38.8	365	1202	34.2	201	1203	35.5	256
1163	36.4	219				1294	38.7	90
1224	37.4	104						
ethylbenzene / air, Φ = 0.5			ethylbenzene / air, Φ = 1.0					
T_5 [K]	P_5 [atm]	τ [μs]	T_5 [K]	P_5 [atm]	τ [μs]			
1040	10.6	1302	1043	13.2	1079			
1057	12.9	1103	1044	10.0	1323			
1079	12.6	731	1083	10.2	637			
1168	12.5	246	1093	12.2	493			
1216	12.2	160	1097	9.9	582			
1251	11.2	93	1161	11.2	284			
1002	42.6	1511	1216	11.0	136			
1026	41.2	1125	941	45.3	1489			
1027	39.1	886	967	44.6	995			
1046	38.2	711	969	41.1	962			
1088	37.4	431	1013	41.6	554			
1119	38.5	233	1050	42.9	236			
1149	38.6	177						

Table A.15. Ignition time measurements for neat α-methylnaphthalene (AMN)/air mixtures.

AMN / air, Φ = 1.0; 1.53% AMN, 20.69% O_2, 77.78% N_2			AMN / air, Φ = 0.5; 0.778% AMN, 21.01% O_2, 78.99% N_2		
T_5 [K]	P_5 [bar]	τ [μs]	T_5 [K]	P_5 [bar]	τ [μs]
1101	11.6	1404	1108	12.8	1377
1119	11.6	1072	1109	12.1	1604
1161	14.5	676	1135	7.8	1674
1162	9.8	997	1193	10.1	735
1167	12.5	707	1215	10.9	609
1194	8.3	738	1259	12.0	366
1204	10.2	540	1277	9.9	362
1208	14.7	423	1283	14.7	256
1226	11.0	490	1308	10.7	216
1245	9.7	420	1323	10.1	200
1256	10.9	297	1379	11.0	120
1269	9.9	311	1445	8.4	98
1283	9.1	263			
1307	9.9	240	1105	43.1	790
1317	10.9	188	1118	40.0	673
1327	11.4	160	1120	39.8	738
1336	11.7	145	1143	36.6	528
1362	12.4	103	1157	27.9	554
1400	13.2	76	1158	36.7	414
			1177	26.2	428
1061	31.9	1170	1179	35.1	323
1116	37.1	431	1190	31.6	364
1148	41.2	248	1226	37.7	197
1157	30.4	333	1252	38.3	147
1168	39.1	229	1257	39.3	141
1182	41.1	200	1286	37.6	101
1182	44.5	178	1339	31.4	76
1207	40.5	141			
1224	35.5	146			
1225	38.7	142			
1226	42.9	130			
1248	35.4	116			
1251	37.0	95			
1265	35.8	84			
1273	40.4	78			

Table A.16. Ignition time measurements for AMN/n-decane/air mixtures.

30%-molar AMN / 70%-molar n-decane / air, Φ = 1.0; 0.417% AMN, 0.973% n-decane, 20.72% O_2, 77.89% N_2						70%-molar AMN / 30%-molar n-decane / air, Φ = 1.0; 1.03% AMN, 0.440% n-decane, 20.70% O_2, 77.83% N_2		
T_5 [K]	P_5 [bar]	τ [μs]	T_5 [K]	P_5 [bar]	τ [μs]	T_5 [K]	P_5 [bar]	τ [μs]
968	17.4	1105	887	28.1	1074	1016	16.8	1077
985	19.2	1191	915	32.6	998	1031	14.8	1185
991	19.5	917	943	38.6	793	1067	20.5	625
997	19.9	943	980	41.4	646	1082	18.7	614
1040	19.3	588	1002	43.8	424	1086	17.5	676
1054	21.8	503	1032	43.1	425	1102	20.1	548
1056	19.5	546	1034	43.8	421	1111	20.1	453
1061	19.2	500	1093	55.7	187	1164	16.2	367
1062	13.8	791	1111	54.4	141	1184	17.0	290
1069	20.0	521	1120	55.4	123	1219	15.6	245
1071	18.9	561	1154	61.1	92	1247	16.5	187
1094	20.0	425	1175	61.8	72	1264	16.2	154
1102	18.6	420	1181	60.9	64	1349	16.3	57
1102	19.7	349	1195	54.9	65			
1103	19.7	405	1214	62.4	55	848	33.5	1089
1107	18.6	350				879	33.7	1384
1109	18.6	330				886	34.1	1250
1117	20.2	368				911	42.4	1047
1135	18.3	327				935	44.5	905
1136	18.0	373				960	46.0	890
1141	18.6	262				971	44.8	886
1141	20.8	254				1016	47.3	586
1146	18.6	257				1032	57.3	417
1164	20.7	242				1042	53.3	456
1180	20.0	182				1053	57.6	321
1182	19.3	172				1065	54.1	316
1190	19.3	162				1071	53.3	364
1198	17.8	161				1083	48.8	292
1205	18.0	148				1088	51.4	272
1211	19.7	128				1095	48.6	276
1213	19.4	148				1117	49.0	196
1215	20.0	116				1127	50.2	204
1215	20.7	128				1148	50.7	143
1218	19.5	143				1179	44.8	110
1227	16.1	126						
1228	18.0	126						
1229	19.5	114						
1235	17.4	106						
1249	17.2	113						
1254	16.9	94						
1264	17.8	88						
1283	17.9	72						
1284	17.2	73						
1293	18.7	73						
1294	16.9	70						
1319	20.1	54						
1329	17.7	45						

Table A.17. Ignition time measurement for Jet-A (POSF 4658)/air and POSF 4658 with JP-8 additives.

POSF 4658 Φ = 1.0 in air 1.368/20.72/77.92 fuel/O_2/N_2 by moles			POSF 4658 with additives Φ = 1.0 in air 1.368/20.72/77.92 fuel/O_2/N_2 by moles		
P_5 [atm]	T_5 [K]	Ignition time [μs]	P_5 [atm]	T_5 [K]	Ignition time [μs]
20.8	674	8974	20.5	906	2453
21.8	680	6703	21.1	928	1729
21.3	681	5821	21.4	960	1513
23.5	700	3887	20.3	962	1437
23.7	703	4216	22.1	970	1261
23.4	704	3204	22.5	991	1097
24.3	717	2737	22.8	991	1086
20.0	723	2287	22.6	1003	1013
23.7	737	1871	18.5	1010	900
20.9	750	1842	22.7	1030	737
20.8	753	1894	19.0	1041	567
21.2	755	1788	19.4	1064	469
20.5	757	1757	20.4	1089	390
23.0	797	1618	19.5	1107	319
24.8	797	1618	19.4	1132	227
21.5	802	1616	19.8	1152	181
23.2	803	1625	18.5	1165	153
22.1	815	1742	18.0	1193	95
19.1	820	2102	18.1	1201	106
21.2	826	1896	19.1	1204	96
21.7	831	1789	17.9	1214	91
20.5	836	2038	16.2	1217	84
20.9	845	2138	17.4	1238	77
21.2	849	2059	18.6	1243	57
22.1	849	1897	18.4	1254	53
21.8	851	1908			
22.8	871	1843			
21.6	882	2032			
21.5	904	2031			
20.9	931	1749			
22.7	940	1675			
21.1	955	1354			
21.7	973	1236			
19.9	984	1140			
18.9	991	1050			
19.2	1025	816			
16.7	1043	706			
21.6	1046	563			
21.0	1050	458			
19.3	1072	464			
19.1	1083	375			
18.4	1092	318			
16.9	1100	355			
18.2	1106	261			
18.1	1109	249			
17.7	1117	225			
19.2	1126	185			
18.7	1138	181			
18.1	1143	176			
17.2	1145	184			
18.1	1177	104			
16.3	1187	116			
16.5	1197	95			
16.8	1222	77			

Table A.18. Ignition time measurement for Princeton-MURI surrogate 1/air mixtures.

Princeton-MURI surrogate 1 Φ = 1.0 in air		
P_5[atm]	T_5 [K]	Ignition time [μs]
22.5	666	8764
21.8	672	8650
21.4	683	5895
20.9	685	5292
20.9	687	4794
19.7	709	3134
19.8	709	3295
21.1	709	2856
18.0	727	2414
17.7	747	2284
19.5	754	1712
22.9	798	1373
20.0	833	1788
21.7	840	1870
19.0	850	2011
18.8	875	2326
18.1	890	2500
18.9	926	2456
20.8	942	2009
21.2	971	1393
20.5	990	1163
20.4	1023	728
19.9	1028	760
22.3	1044	538
18.5	1068	453
21.3	1074	422
20.4	1105	290
18.9	1128	210
21.2	1165	113
19.2	1207	69

Table A.19. Ignition time measurements for RPI surrogate 1/air mixtures.

RPI surrogate 1 Φ = 1.0 in air		
P_5 [atm]	T_5 [K]	Ignition time [μs]
18.9	704	4854
18.4	710	4070
17.4	725	3226
19.9	762	2708
19.3	767	2149
21.7	769	2112
19.2	774	2390
18.5	797	2289
19.7	803	2409
20.9	827	2565
19.7	857	2740
21.6	896	2433
21.6	896	2433
19.8	911	2350
19.8	911	2350
23.1	927	1956
23.1	927	1956
21.9	929	2048
21.4	938	1585
17.9	943	1883
17.9	943	1883
20.3	963	1799
20.8	970	1386
20.8	990	1418
22.0	997	1097
21.2	1034	677
21.9	1043	516
21.8	1052	570
20.9	1064	389
21.9	1069	502
18.3	1071	491
21.5	1076	405
20.5	1091	281
20.3	1092	248
20.3	1107	253
20.0	1118	200
20.0	1141	212
19.6	1162	115
21.3	1192	121
17.7	1210	68